CHAPTER 2 TDIP SURVEY

2-1 Objectives

The TDIP (Time Domain Induced Polarization) survey was carried out in order to extract mineralized zones in the potential area delineated by geological and airborne magnetic survey in Phase I of this project.

2-2 Survey Locations and Specifications

The survey areas were Mogoin gol area and the Under/Shand area located respectively to the northwest and south of the Erdenet Mine. The distance from the Erdenet Mine is about 30km to the Mogoin gol area and about 25km to the Under/Shand area. In the Under/Shand area, the potential area was narrowed down to three small areas(Under/Shand 1, 2 and 3 areas) based on the result of airborne magnetic survey. Table II-2-1 shows the coordinates of the survey areas.

Table II-2-1 Coordinate of the survey area

Area	UTM coordinate of the corners		Area	UTM coordinate of the corners	
	East	North		East	North
Mogoin gol	408387	5444792	Under/Shand 2	438517	5405312
	411387	5444792		441117	5405312
	411387	5451792		441117	5407062
	408387	5451792		438517	5407062
Under/Shand 1	441450	5406900	Under/Shand 3	440450	5401284
	443450	5406900		443450	5401284
	443450	5408400		443450	5403034
	444450	5408400		440450	5403034
	444450	5409650			
	441450	5409650			

The IP data were taken along lines spaced every 250m by keeping a potential dipole of 200m with a separation factor from 1 to 5. Table II-2-2 shows amounts of TDIP survey.

Table II-2-2 Amounts of TDIP survey

Area	Number of lines	Total length	Number of points
Mogoin gol	7.0km × 13 lines	91.0km	2015
Under/Shand 1	3.0km × 6 lines	30.0km	510
Under/Shand 2	2.6km × 8 lines	20.8km	360
Under/Shand 3	3.0km × 8 lines	24.0km	440
Total	41 lines	165.8km	3325

Resistivity as well as chargeability values of rocks and core samples were also measured in the laboratory

2-3 Survey Method

2-3-1 Procedures

The Induced Polarization survey was carried out using a time-domain method with a dipole-dipole electrode configuration. The electrode configuration was arranged so that the survey lines were spaced 250m and the measurements were taken every 200m along the lines using a separation factor from 1 to 5. In the measurement, the current was injected into the earth through current electrodes and the resulting voltage was measured across potential electrodes. Fig. Ⅱ-2-1 shows the array utilized as well as the location of the plotting points.

In the TDIP surveys, the current is turned on for a certain length of time (on-time) then turned off (off-time). The transmitted waveform is then repeated with current flow in opposite direction. The pair of positive and negative on-off waveforms constitutes a cycle, which in this survey lasted 8 seconds, as indicated in Fig. Ⅱ-2-2. According to Fig. Ⅱ-2-3, the polarization of the target creates a transient decay voltage and its corresponding changing response is observed in the received waveform.

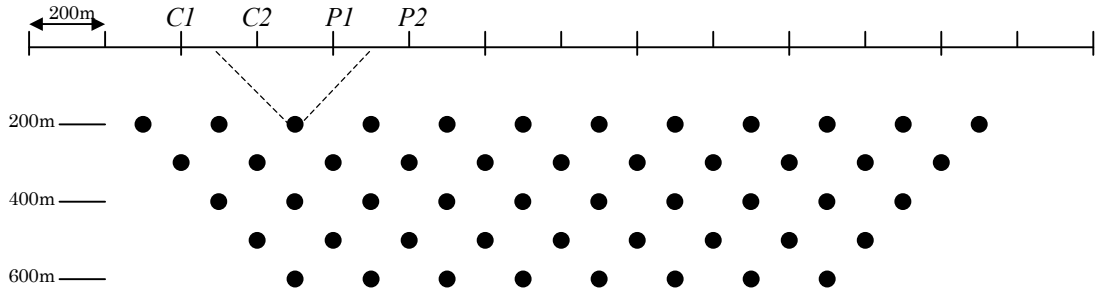

Fig. II-2-1 Dipole-dipole array and plotting procedure

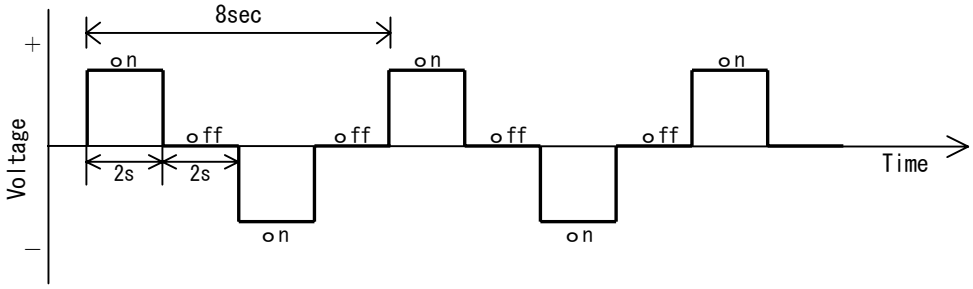

Fig. II-2-2 Waveform produced by the transmitter

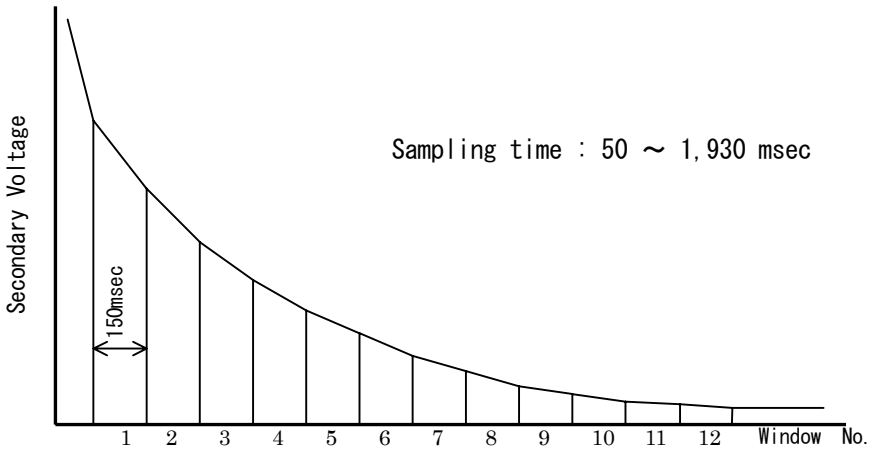

Fig. II-2-3 Sampling interval of the TDIP receiver

2-3-2 Instrumentation

The instrumentation used for the time-domain IP survey is described in the Table Ⅱ - 2-3.

Table II-2-3 Specifications of TDIP survey instruments

Receiver	**Zonge GDP-16**	**Scintrex IPR-12**
Frequency range	DC to 8KHz	1,2,4,8,16,32 seconds
Number of channels	3	8
Maximum input voltage	±32V	±14V
Detectable signal	1μV	10μV
Transmitter	**CH-95A**	**CH-97**
Output Power	2Kw,800v,12A	4.5kw
Maximum Current	10A	10A
Generator	**Geonics GPU2000**	**Honda ET4500**
Maximum output	2Kw	4.5Kw
Output Voltage	200V	200V
Output Frequency	400Hz	50Hz

2-4 Analysis Method

2-4-1 Data processing

The TDIP data processing involves the determination of 3 parameters, i.e., apparent resistivity, chargeability as well as metal factor. The first 2 parameters are calculated directly by the receiver unit during data acquisition. The third one is calculated as a simple relation between the first 2 parameters. These 3 parameters are calculated as follows:

a) Apparent resistivity (ρ)

$$\rho = K\frac{V_P}{I},$$

where $\boldsymbol{K} = \pi\boldsymbol{an}(\boldsymbol{n}+1)(\boldsymbol{n}+2)$, $\boldsymbol{Vp}$ is the received voltage in volts, $\boldsymbol{a}$ is the A-spacing in meters, $\boldsymbol{n}$ is the separation factor and $\boldsymbol{I}$ is the transmitted current in amperes.

b) Chargeability (M)

$$M = \frac{1.87}{V_P}\int_{t_1}^{t_2} V_s dt,$$

where $\boldsymbol{Vp}$ is the primary voltage in volts and $\boldsymbol{Vs}$ is the secondary voltage in millivolts. Here, the secondary voltage is calculated from 450msec. to 1,100msec.

c) Metal factor (MF)

$$MF = \frac{M}{\rho}\times 100,$$

where $\boldsymbol{M}$ is the chargeability (mV/V) and ρ the apparent resistivity (Ωm)

2-4-2 Topographic corrections

Since the apparent resistivity is calculated here as a function of the location of the current and potential electrodes on a half-infinite plane, and is affected by topography depending on the location of the electrodes. For the case of a dipole-dipole configuration, the apparent resistivity appears to be high beneath a hill and low beneath a valley. On the other hand, the chargeability values are less affected by topography.

In order to make the appropriate corrections for the present survey, the topographic correction is calculated for each survey line using 2D finite element method (FEM). The corrected apparent resistivity values are then used to construct the related sections and plane maps.

2-4-3 Pseudo-sections and plane maps

After topographic corrections, apparent resistivity, chargeability and metal factor pseudo-sections are made for every line of the survey. Plane maps of the above mentioned 3 parameters are also made for every separation factor.

It is normal to plot the measured results as conventional pseudo-sections so that preliminary interpretations can be made. This is also important for assessing data quality. Anomalies having high chargeability are easily observed but caution should be taken to directly infer the location and depth by simple inspection of the pseudo-section.

2-4-4 Two-dimensional analysis

The pseudo-sections do not show the real image of subsurface structure. In order to estimate the subsurface structure from TDIP data, we applied a 2-D quantitative analysis method to the measured data, consisting of forward calculations using FEM and inversion calculations using non-linear least square method.

In order to make the model calculations, the subsurface structure is divided into many small blocks, each of them having initially assigned their own chargeability and resistivity value. The size of the blocks are relatively small at the shallower part, but large at the deeper part.

Theoretical values are calculated from the block models using FEM, and the parameter of each block is made to change until the difference between the theoretical value and measured value is sufficiently small.

2-5 Survey Results

2-5-1 Under/Shand 1 area

(1) Lines location

Fig.II-2-4 shows the location of the TDIP lines in the Under/Shand 1 area. This area is located in the north of the Under/Shand area. 12 lines of 2.0km long each were planned along N90°E. As the result of the measurement, a part of remarkable chargeability anomaly was detected at the northeastern edge of the survey area, therefore 6 lines in the north side were extended 1km each on the east side and additional measurement was carried out.

(2) Results

Figs.II-2-5 to II-2-7 show the pseudo-sections, while Figs.II-2-8 to II-2-10 indicate the plane maps from n=1 to 5.

In this area, the apparent resistivity value ranges between 140 to 5200Ωm and average is 1200Ωm.

Relatively low resistivity zone under 1000Ωm is distributed along the direction of NW-SE on the plane map for n=1. In this low resistivity zone, andesitic to rhyolitic tuff or porphyritic monzonite are distributed. The area underlain by andesitic to rhyolitic tuff shows minimum resistivity value in this zone. The plane maps for n=2 and 3 show almost the same distribution as n=1.

High resistivity zones are detected in the northeast and southwest of the area. These correspond to the area underlain by granodiorite or porphyritic granodiorite.

The chargeability value ranges between 1.1 and 21mV/V and average is 5.8mV/V. It shows maximum value 21mV/V at the station 18 to 20 on the line-I.

The pseudo-sections show typical pants-legs shape of the chargeability at the station 18 to 20 on the

lines H to L. The depth of this chargeability anomaly is shallowest on the line-I, and becomes deeper northward and southward.

The chargeability anomaly zone shows high apparent resistivity value over 1000Ωm. It is possible to reflect weak mineralization.

Metal factor value is almost under 3, and no remarkable anomaly is recognized.

(3) 2-D analysis

Figs.II-2-11 to II.2-16 show the 2-D analysis sections and plane maps.

The analyzed resistivity value ranges between 24 to 310kΩm and average is 2300Ωm.

Continuous low resistivity zone below 500Ωm is detected at the shallower part, and it seems to continue to deeper part. This anomaly zone has northwestern trending at shallower part. Below the depth of 250m, its scale becomes smaller and the trending turns northward.

High resistivity zone above 1000Ωm corresponds to the area underlain by granodiorite or porphyritic granodiorite. This high resistivity zone continues to deeper part widely.

The analyzed chargeability value ranges between 1 to 32mV/V and average is 6.3mV/V. High chargeability anomaly zone is distributed in the northeast of the survey area. Maximum value 32mV/V is detected at the station 18 to 20 on the line-I. This anomaly zone extends about 300m from east to west and about 500m from north to south. It is possible to reflect mineralization but its intensity is considered to be weak because resistivity shows high value.

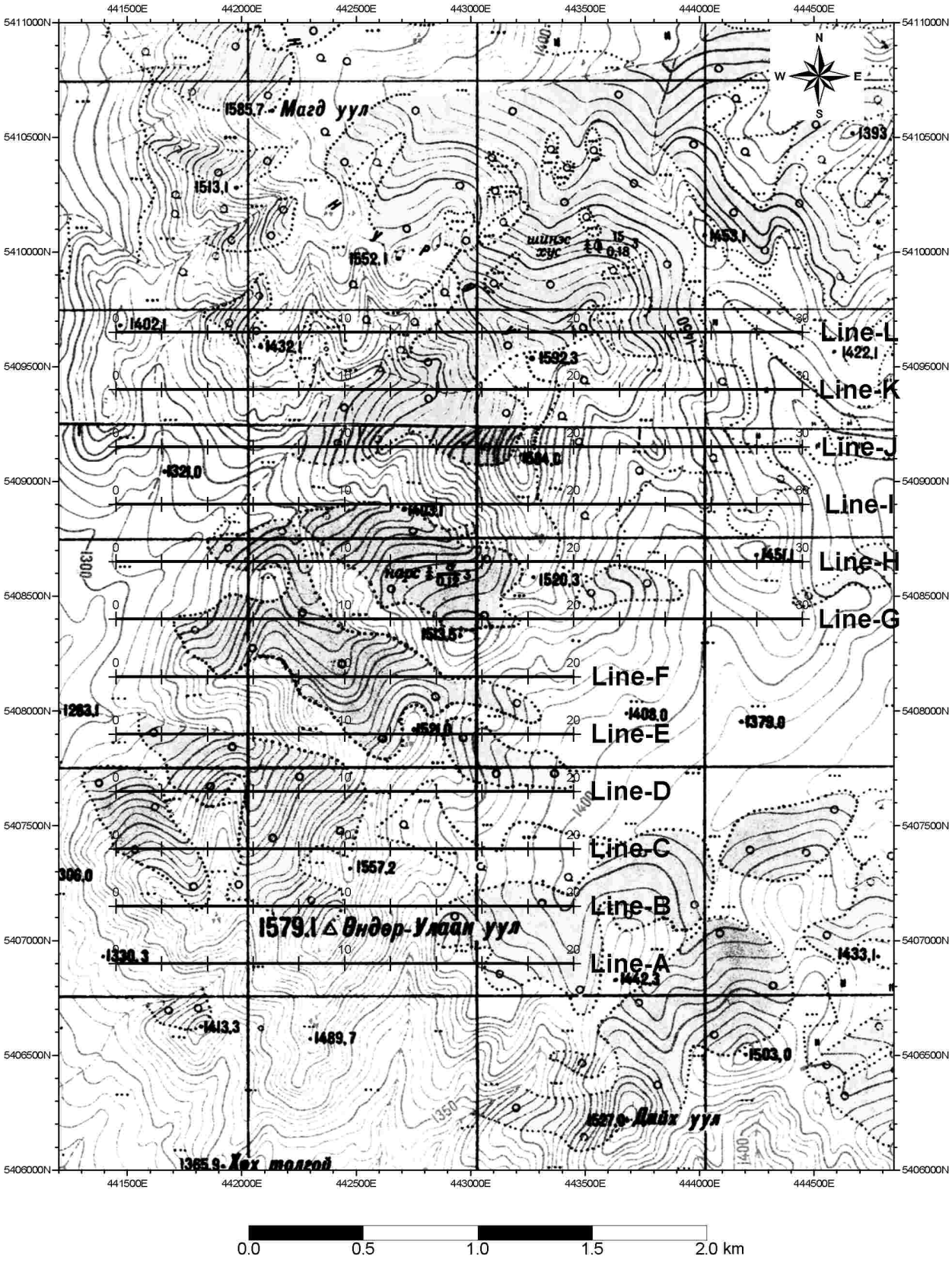

Fig.II-2-4 Geophysical survey location in Under/Shand_1 area

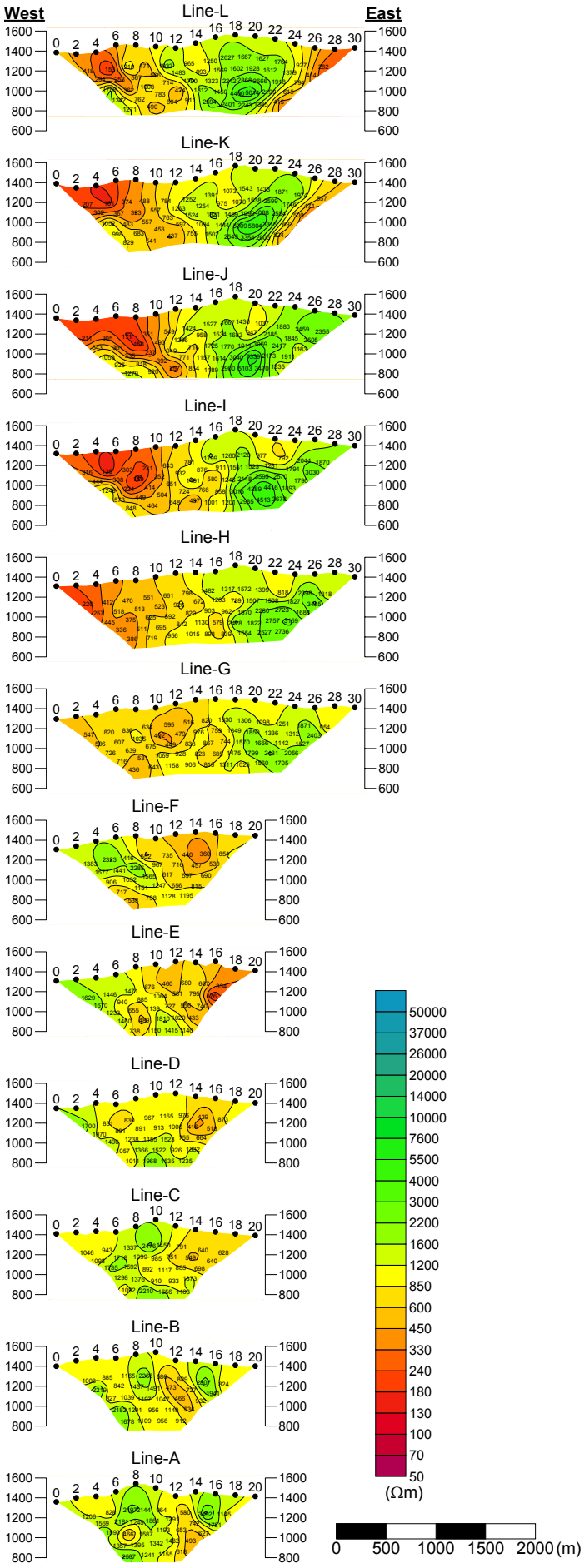

Fig.II-2-5 Apparent resistivity pseudo-sections in Under/Shand_1 area

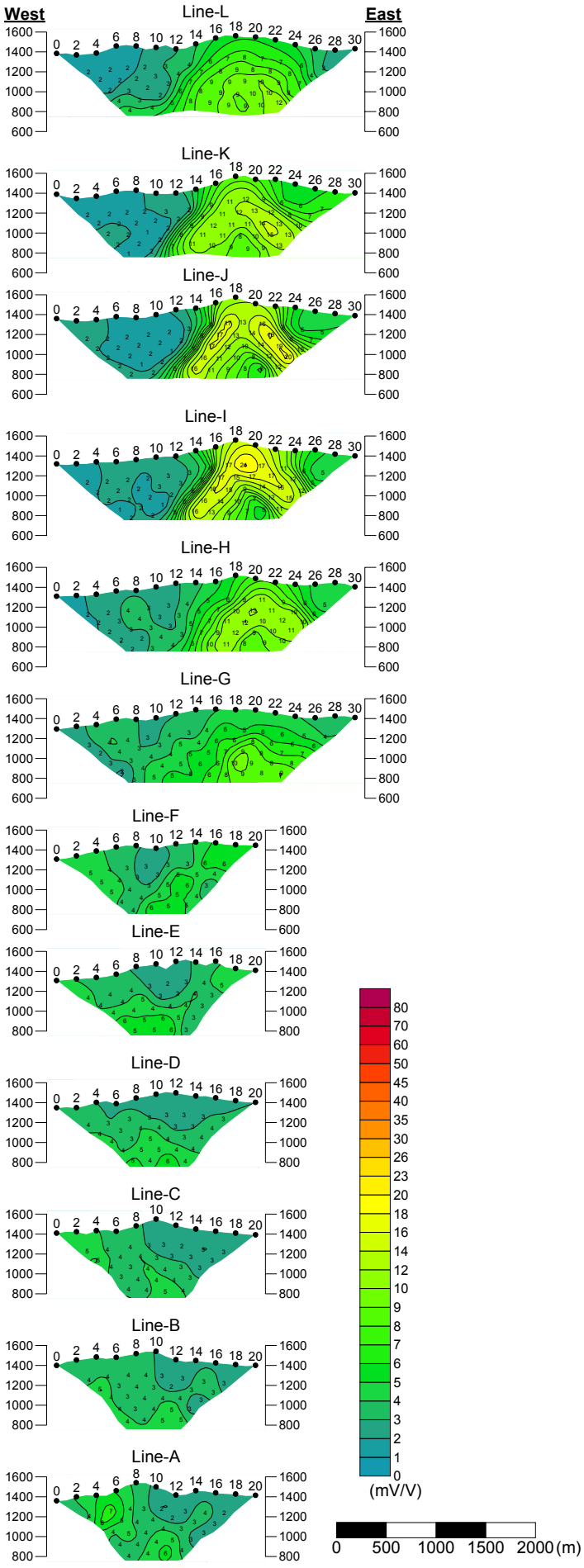

Fig.II-2-6 Chargeability pseudo-sections in Under/Shand_1 area

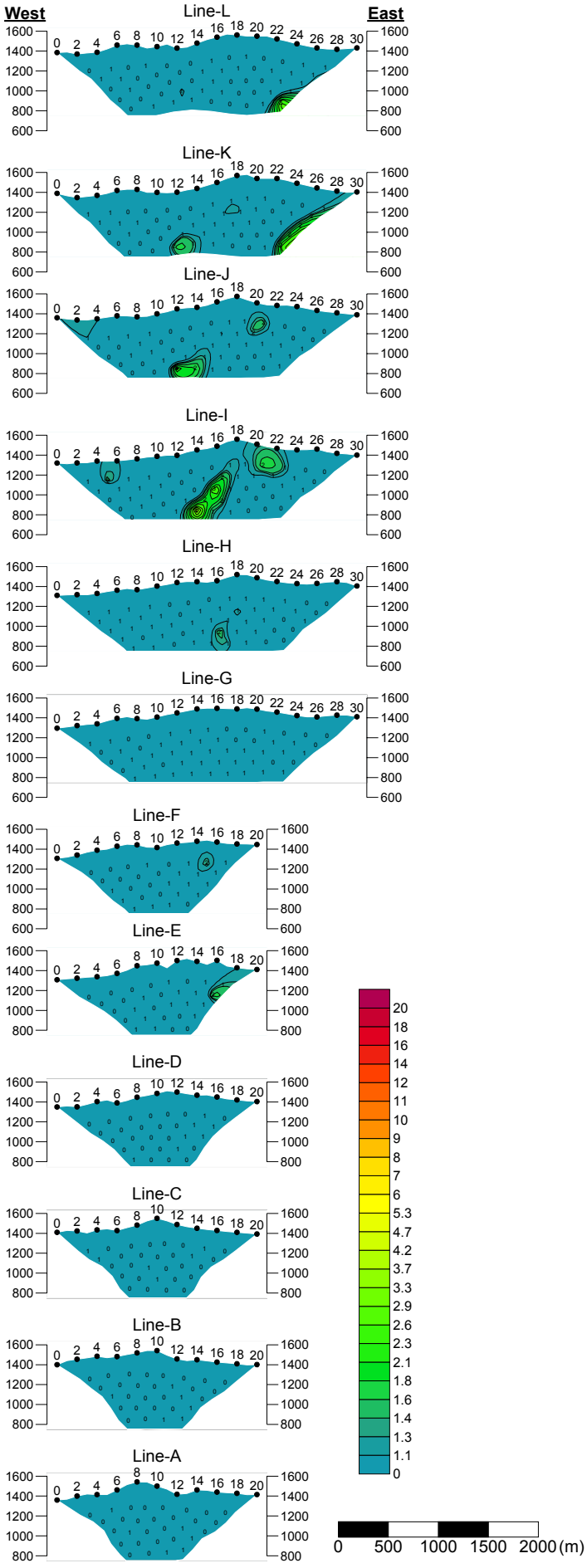

Fig.II-2-7　Metal factor pseudo-sections in Under/Shand_1 area

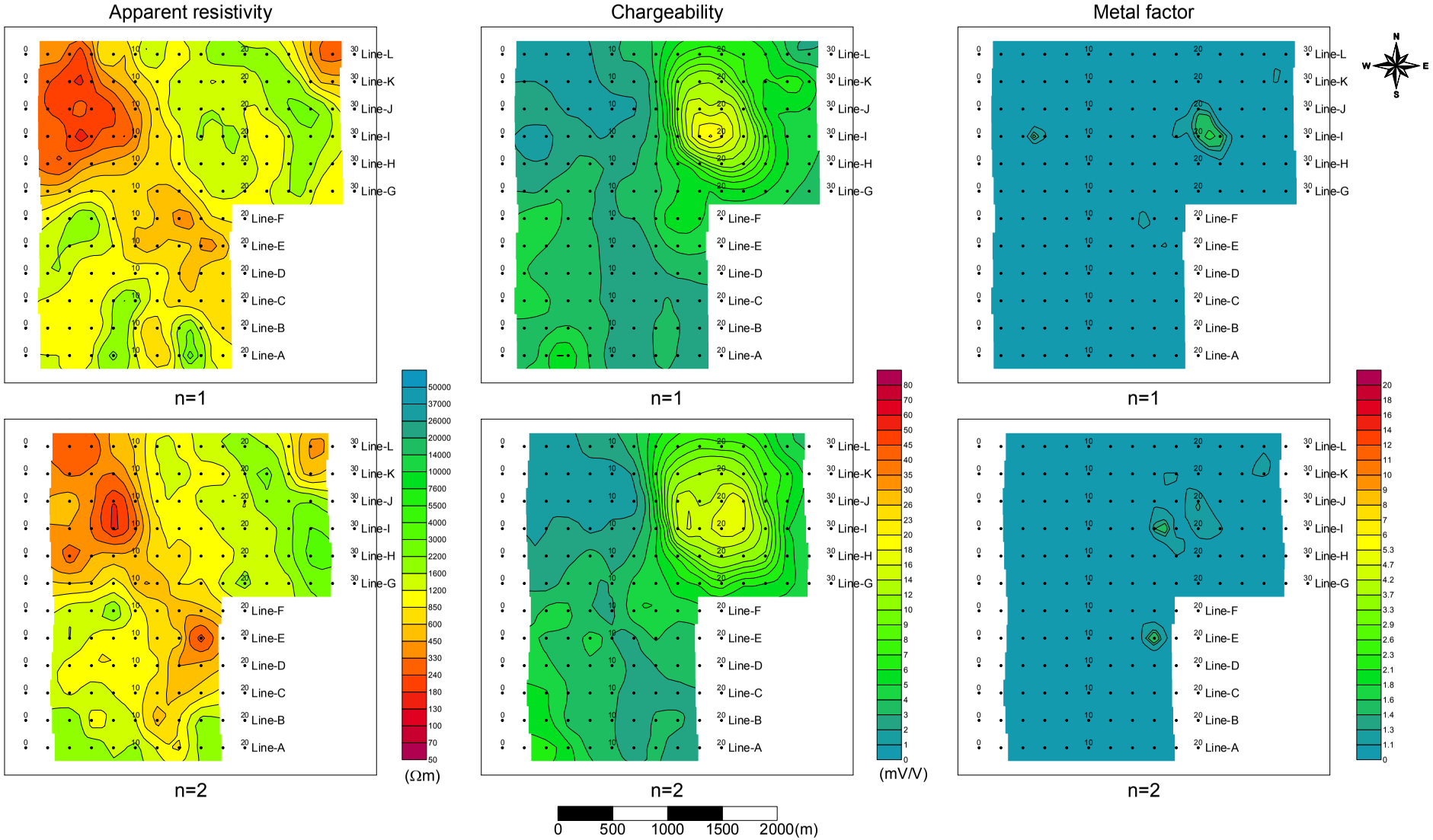

Fig.II-2-8 TDIP plane map for n=1 and 2 in Under/Shand_1 area

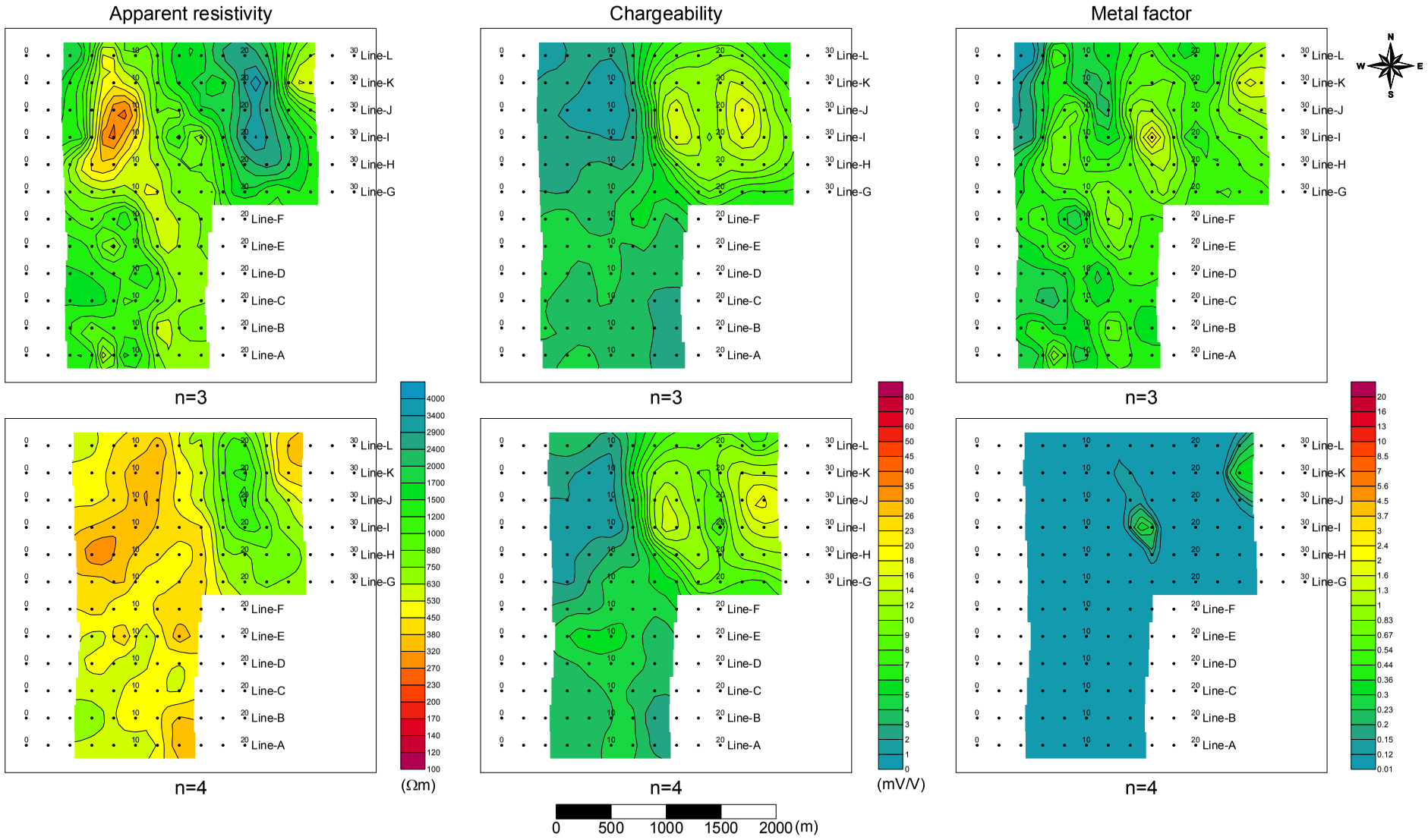

Fig.II-2-9 TDIP plane map for n=3 and 4 in Under/Shand_1 area

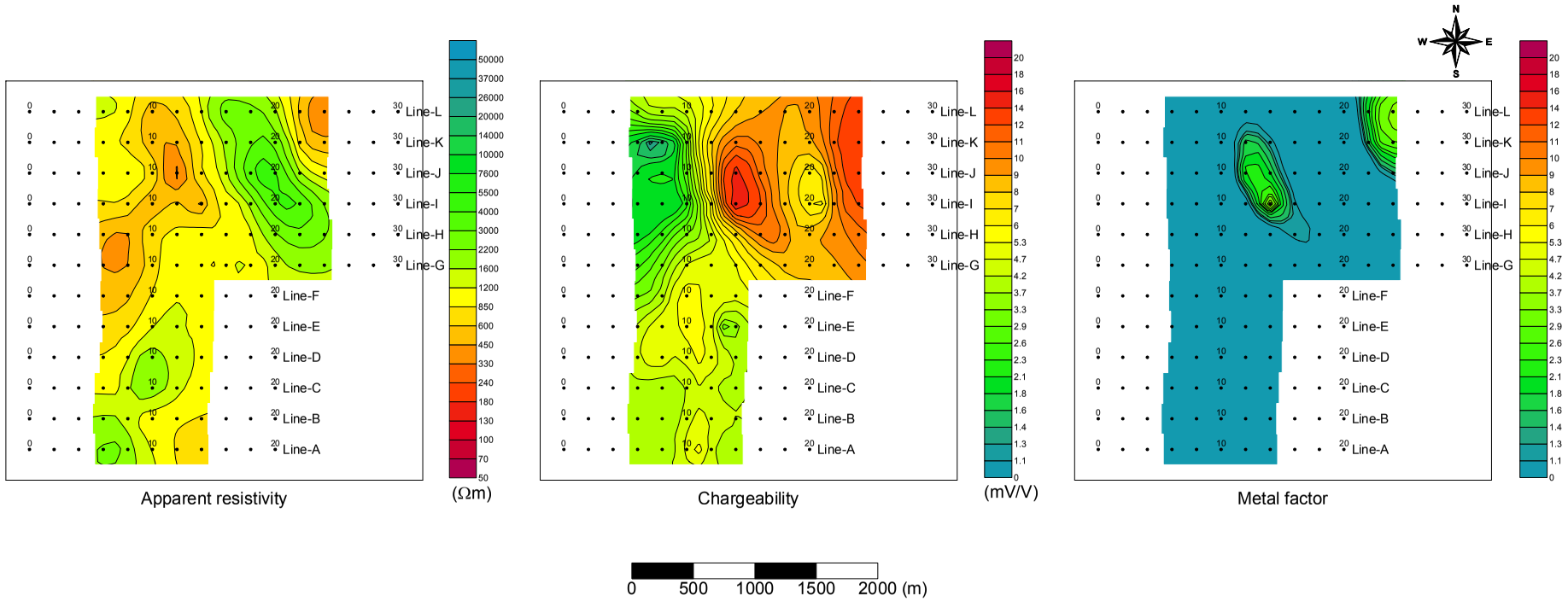

Fig.II-2-10 TDIP plane map for n=5 in Under/Shand_1 area

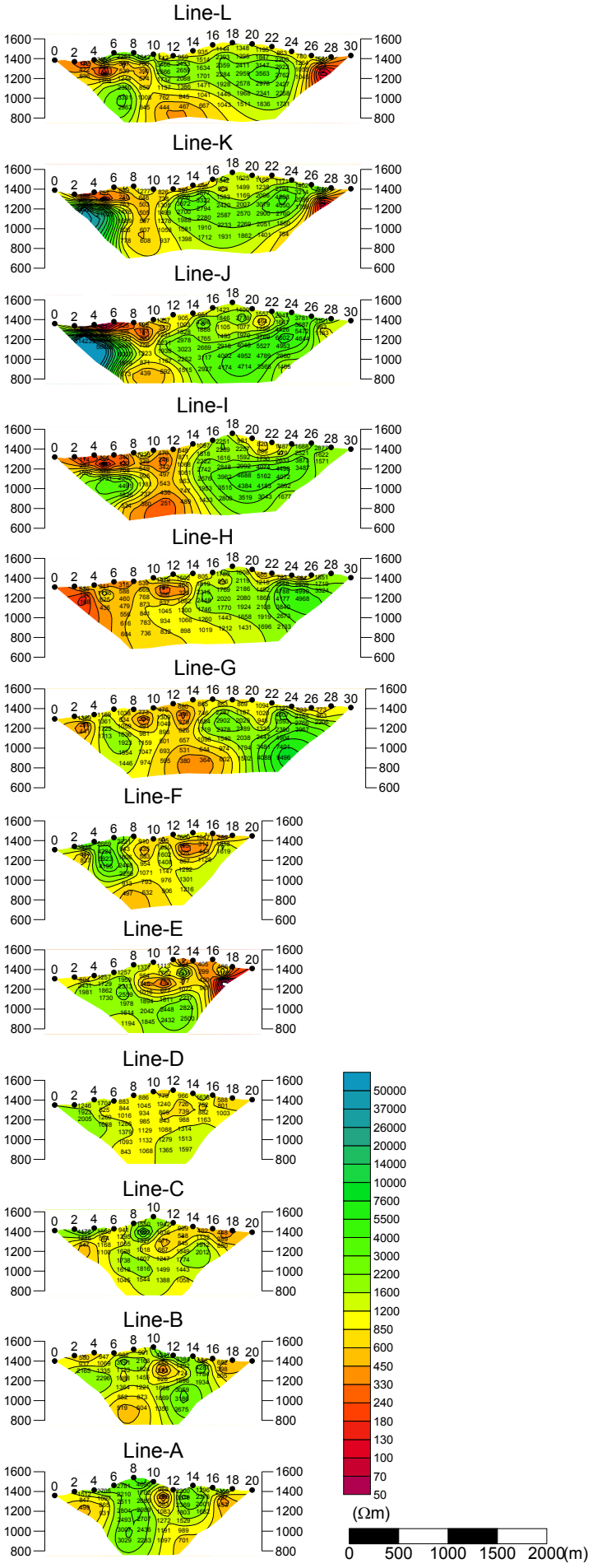

Fig.II-2-11　2D analysis sections for resistivity in Under/Shand_1 area

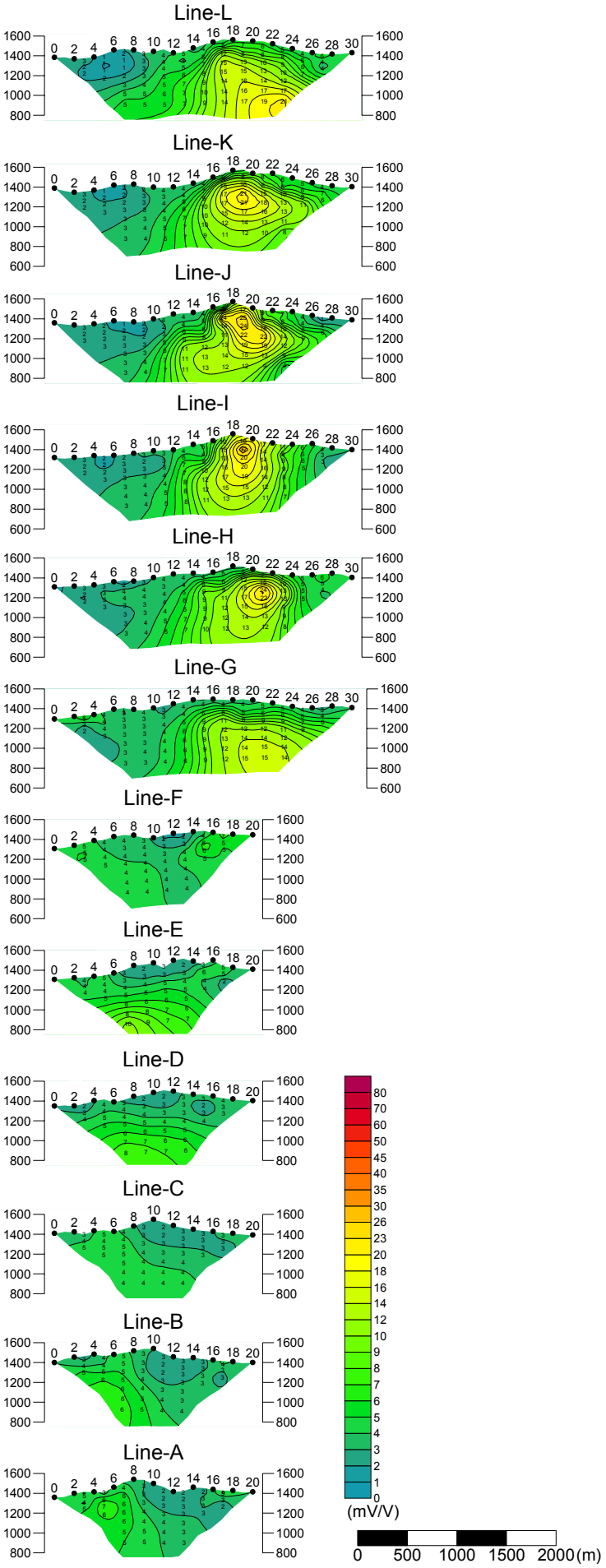

Fig.II-2-12　2D analysis sections for chargeability in Under/Shand_1 area

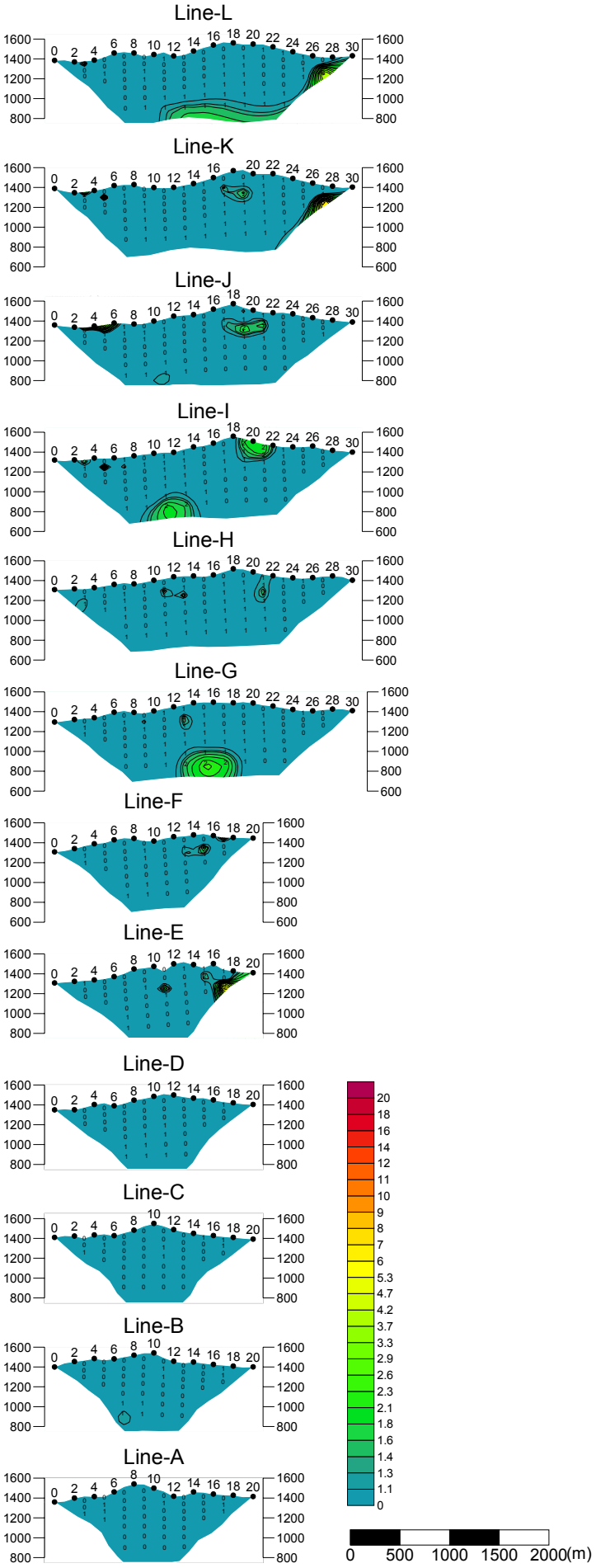

Fig. II-2-13 2D analysis sections for metal factor in Under/S

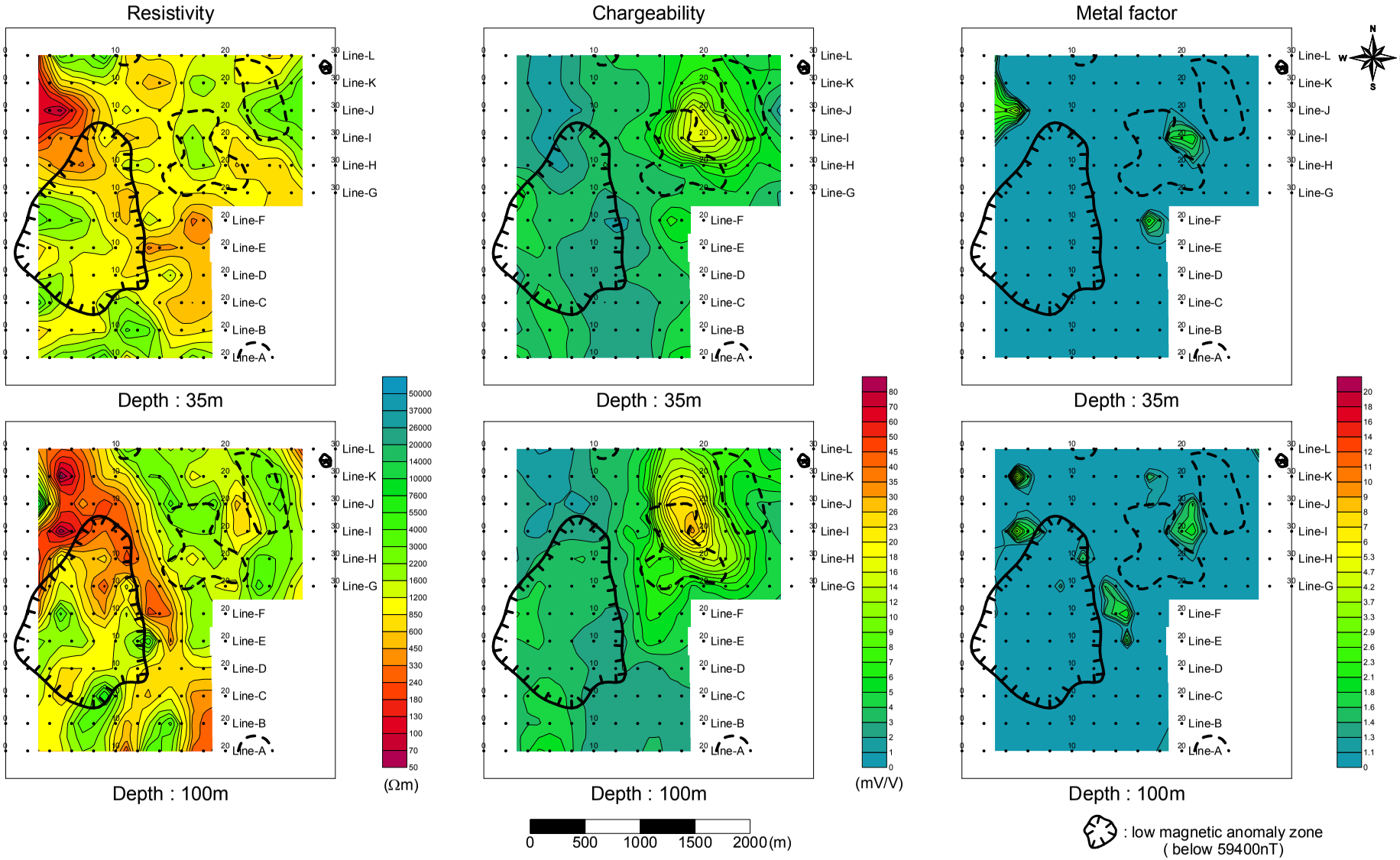

Fig.II-2-14　2D analysis plane map at the depth of 35m and 100m in Under/Shand_1 area

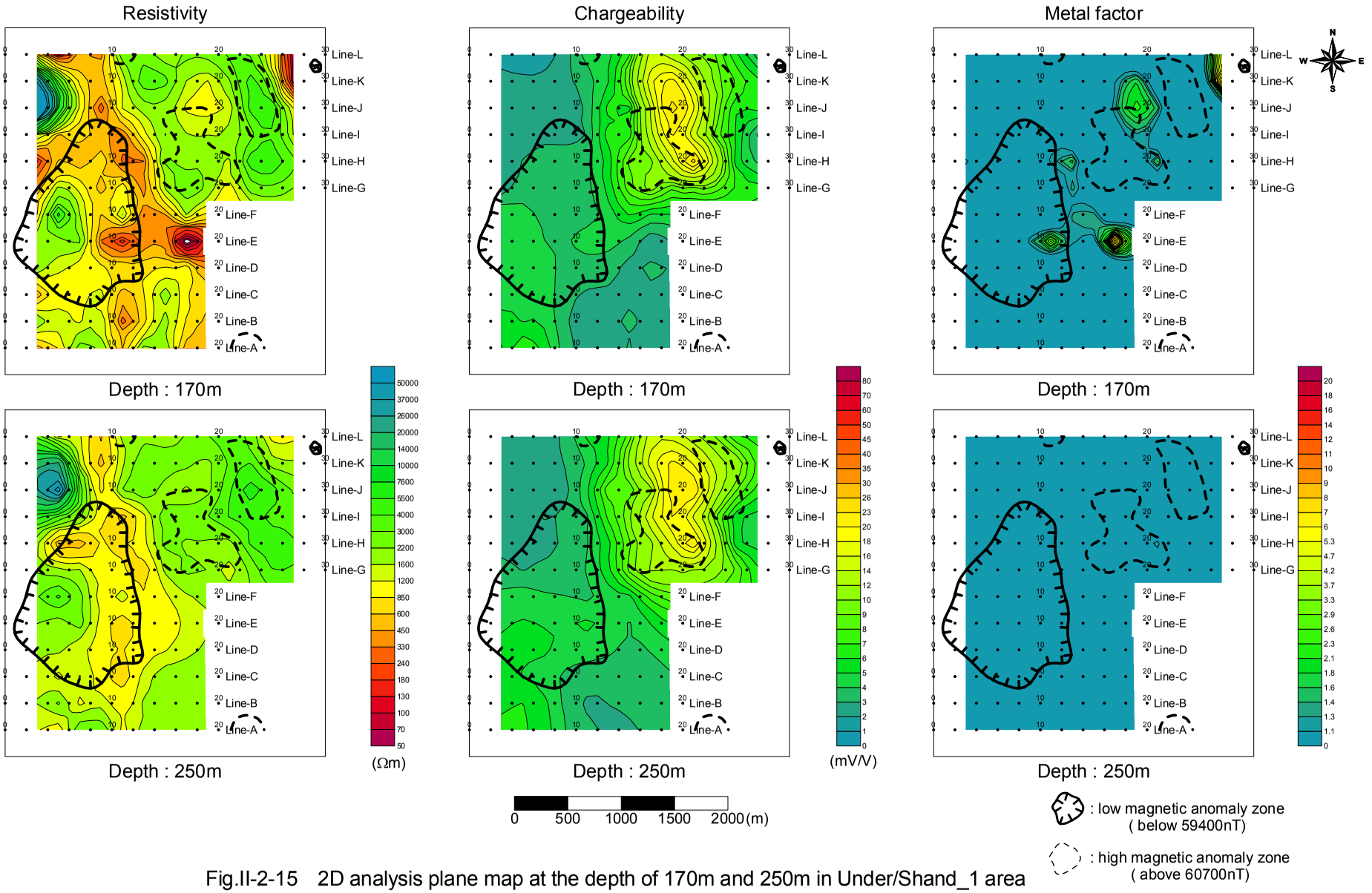

Fig.II-2-15 2D analysis plane map at the depth of 170m and 250m in Under/Shand_1 area

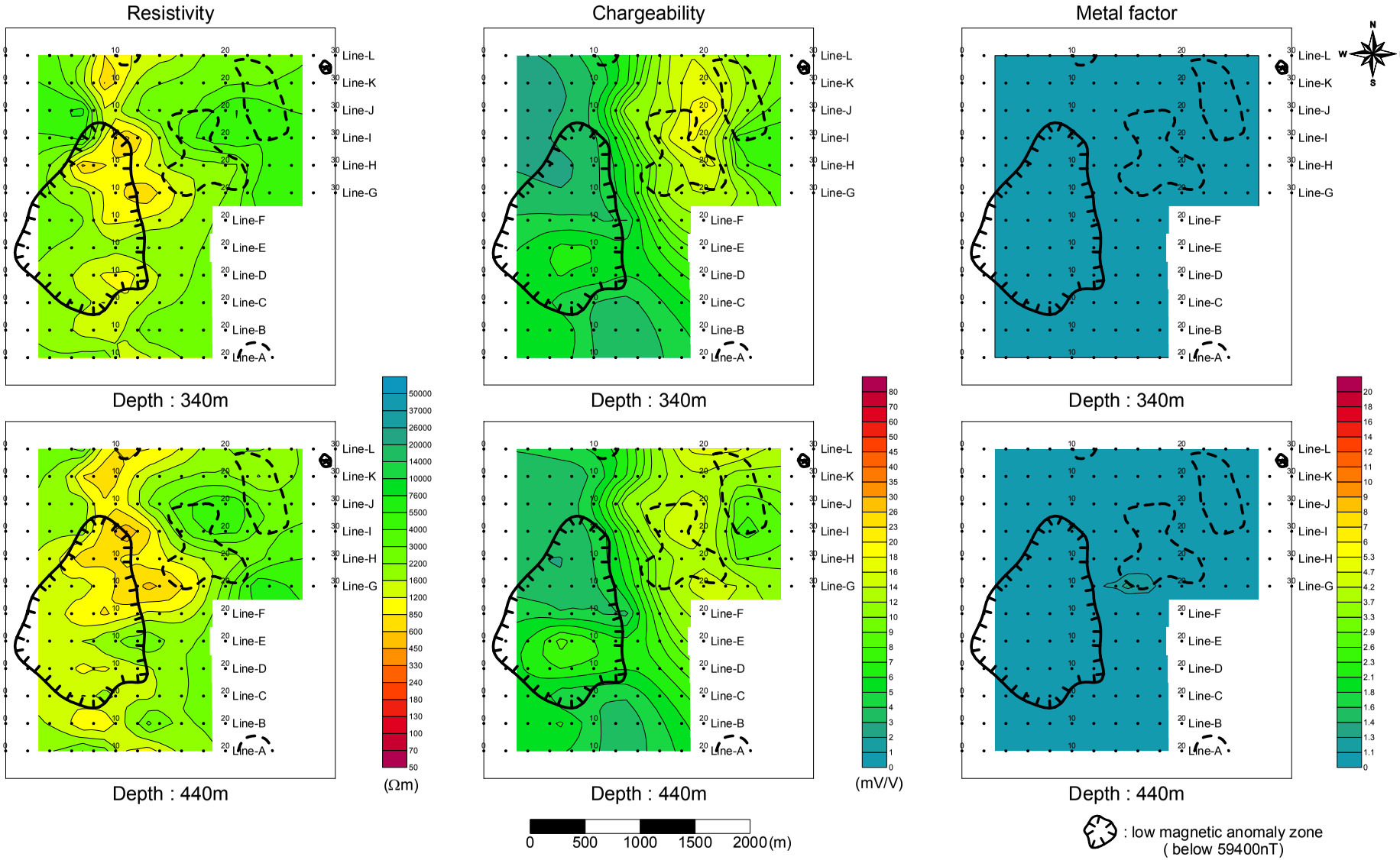

Fig.II-2-16　2D analysis plane map at the depth of 340m and 440m in Under/Shand_1 area

2-5-2 Under/Shand 2 area

(1) Lines location

Fig.II-2-17 shows the location of TDIP lines. This area is located in the center of the Under/Shand area. 8 lines of 2.6km each were set up along N90°E.

(2) Results

Figs.II-2-18 to II-2-20 show the pseudo-sections, while Figs.II-2-21 and II-2-22 indicate the plane maps from n=1 to 5.

In this area, the apparent resistivity value ranges between 105 to 3200Ωm and average is 630Ωm. According to the plane map for n=1, low resistivity is widely distributed and its distribution area corresponds to the area underlain by Quaternary sediments. In the center of north side, high resistivity above 1000Ωm is detected and corresponds to the area underlain by granodiorite

The chargeability value ranges between 2.1 to 10mV/V and average is 4.4mV/V. No remarkable high chargeability anomaly is detected.

(3) 2-D analysis

Figs.II-2-23 to II.2-27 show the 2-D analysis sections and 2-D analysis plane maps.

The analyzed resistivity value ranges between 40 to 30kΩm and average is 1300Ωm.

At the shallower part, high resistivity zone above 500Ωm corresponds to granodiorite and low resistivity zone below 500Ωm to Quaternary sediments.

The low resistivity zone shows north trending above 100m depth and east to southeast trending at the deeper part. Taking account of the thickness of Quaternary sediments, it is considered that the resistivity of Quaternary sediments is below 200Ωm and that of granodiorite underlying below Quaternary sediments is 200 to 500Ωm. Such a low resistivity of granodiorite is considered to reflect development of fracturing or alteration.

The analyzed chargeability value ranges between 1.8 to 23mV/V and average is 5.6mV/V. The chargeability shows generally low value, and no remarkable anomaly is detected.

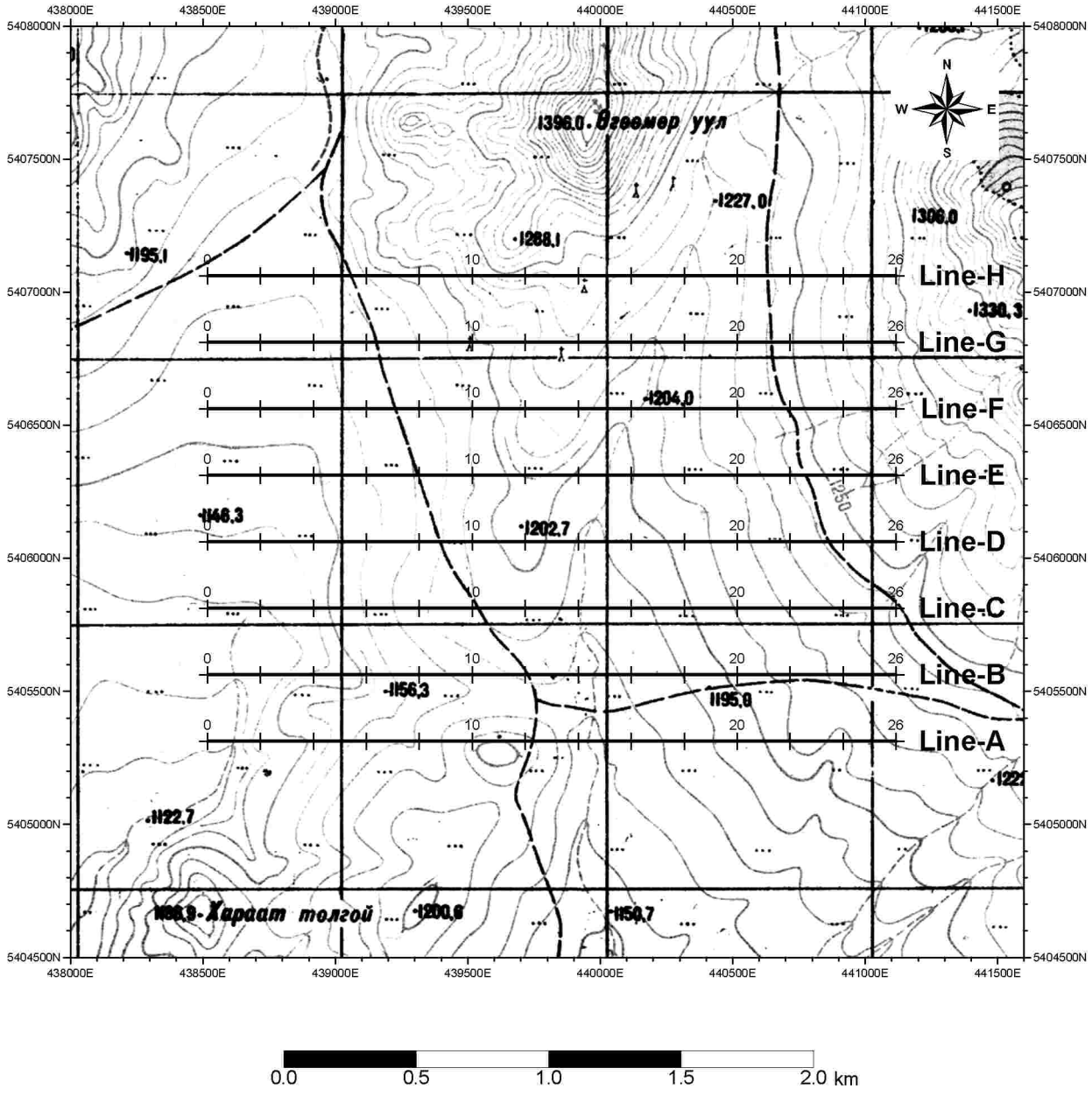

Fig.II-2-17　Geophysical survey location in Under/Shand_2 area

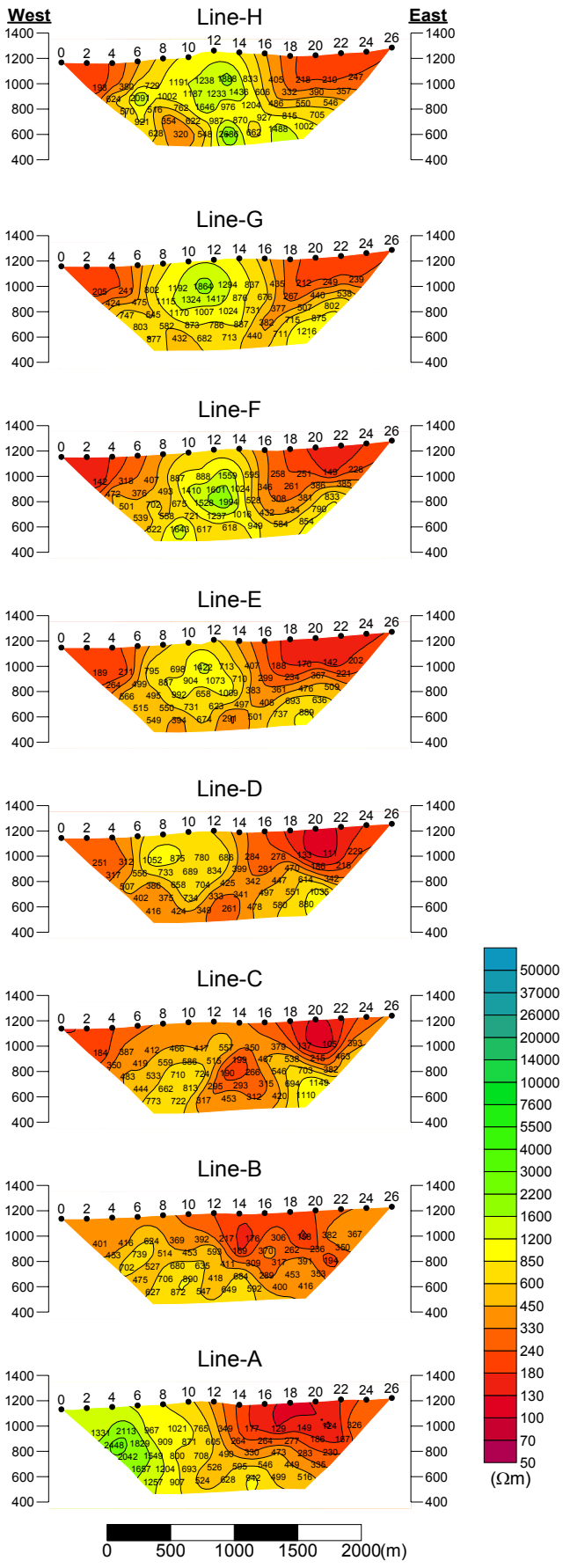

Fig.II-2-18 Apparent resistivity pseudo-sections in Under/Shand_2 area

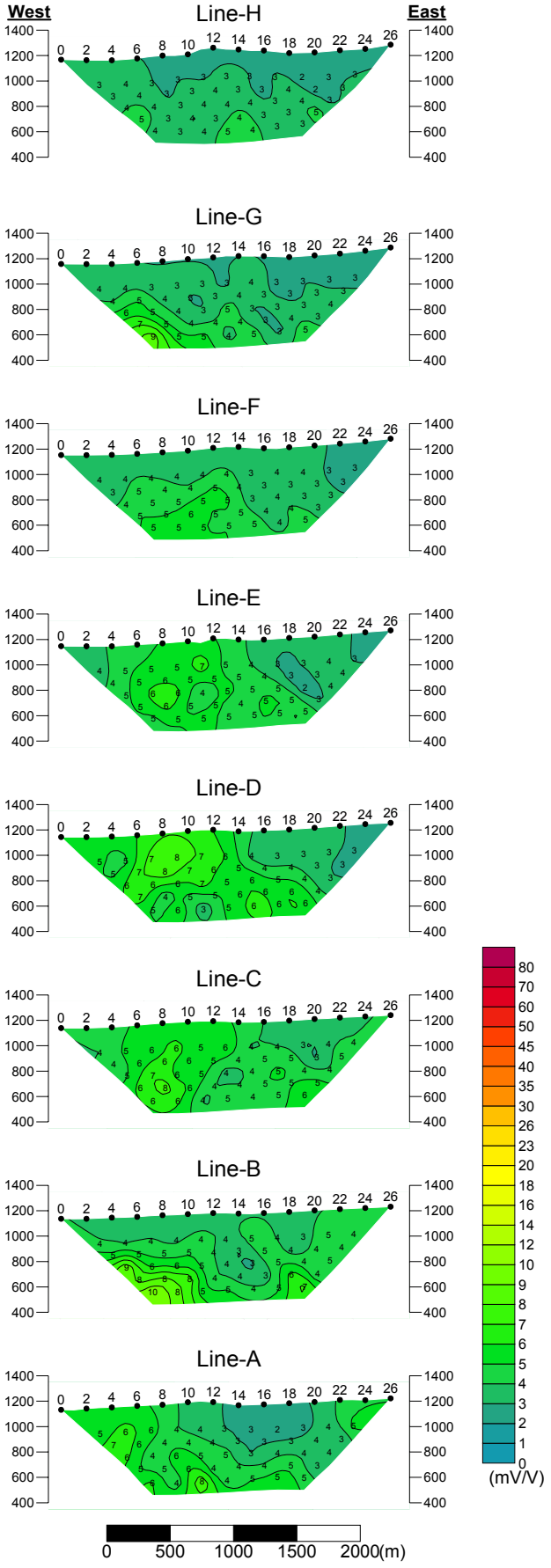

Fig.II-2-19 Chargeability pseudo-sections in Under/Shand_2 area

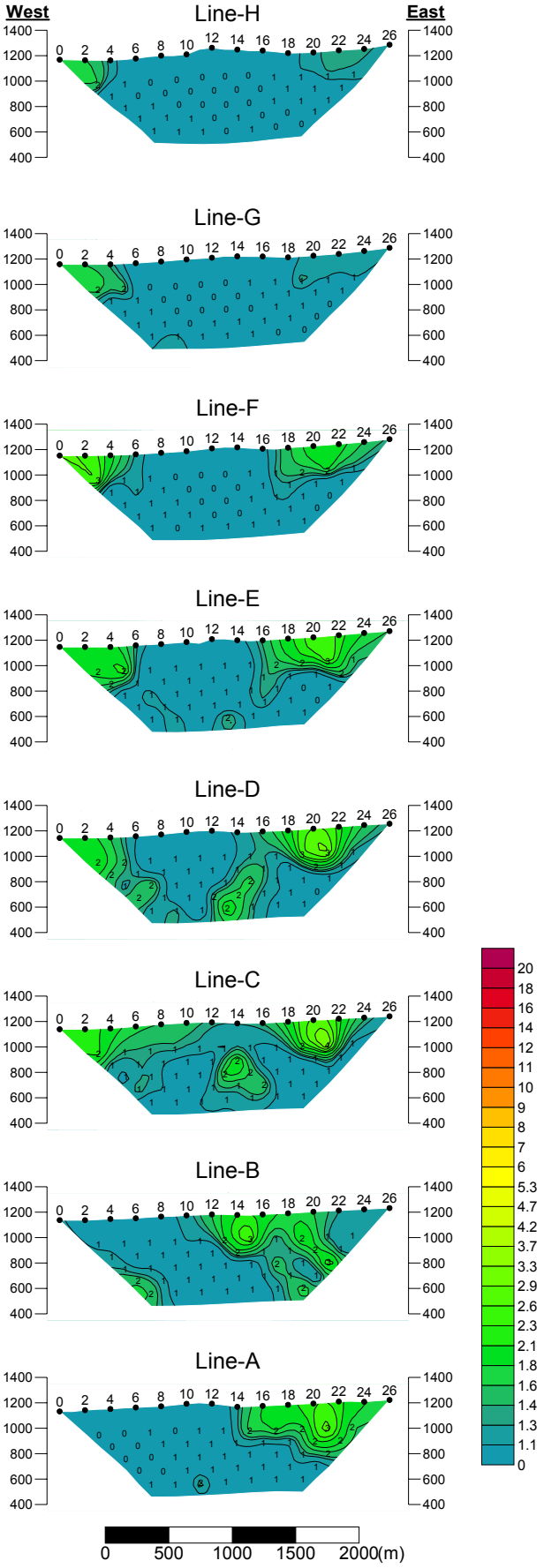

Fig.II-2-20 Metal factor pseudo-sections in Under/Shand_2 area

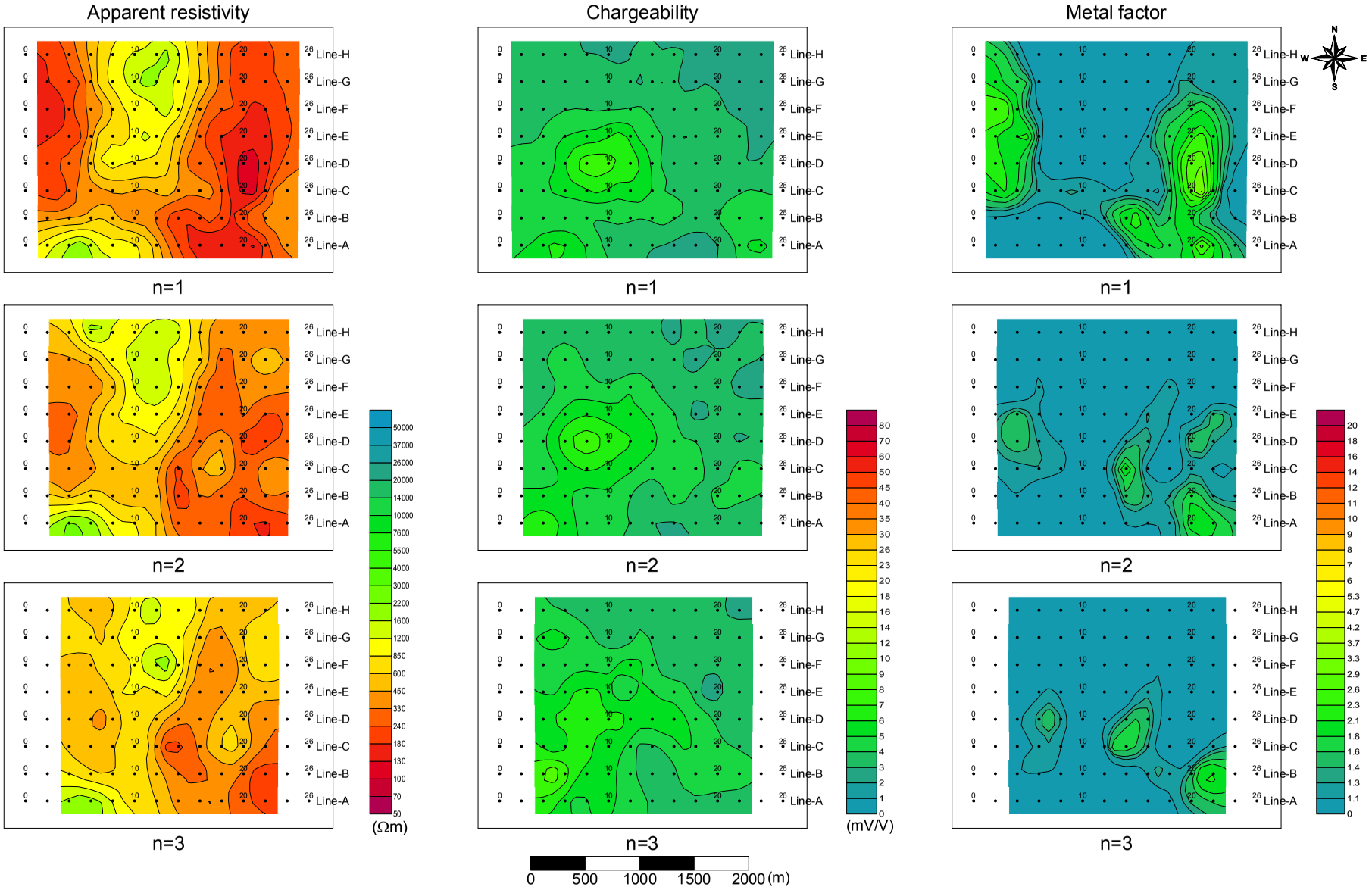

Fig.II-2-21 TDIP plane map for n=1, 2 and 3 in Under/Shand_2 area

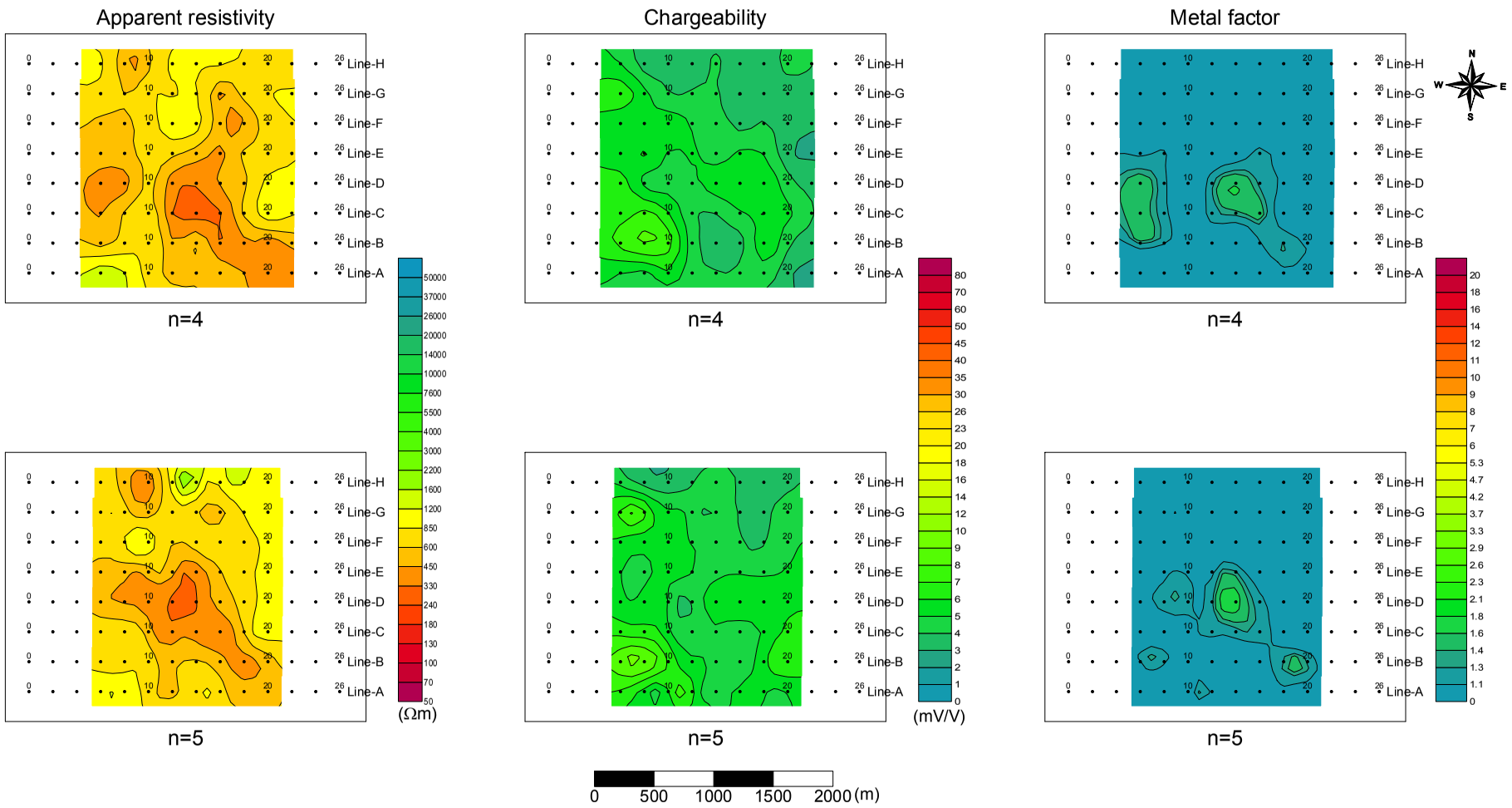

Fig.II-2-22　TDIP plane map for n=4 and 5 in Under/Shand_2 area

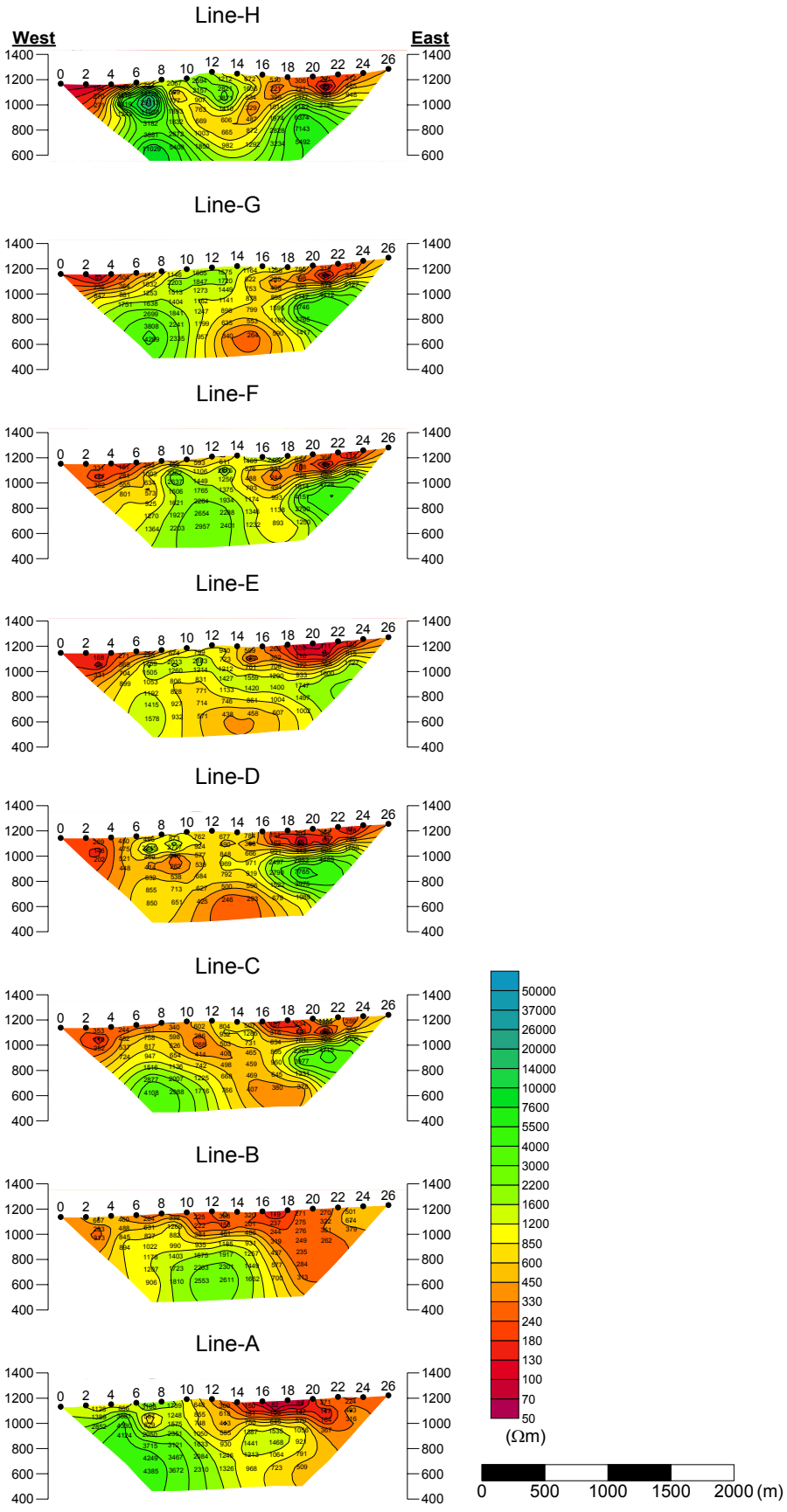

Fig.II-2-23　2D analysis sections for resistivity in Under/Shand_2 area

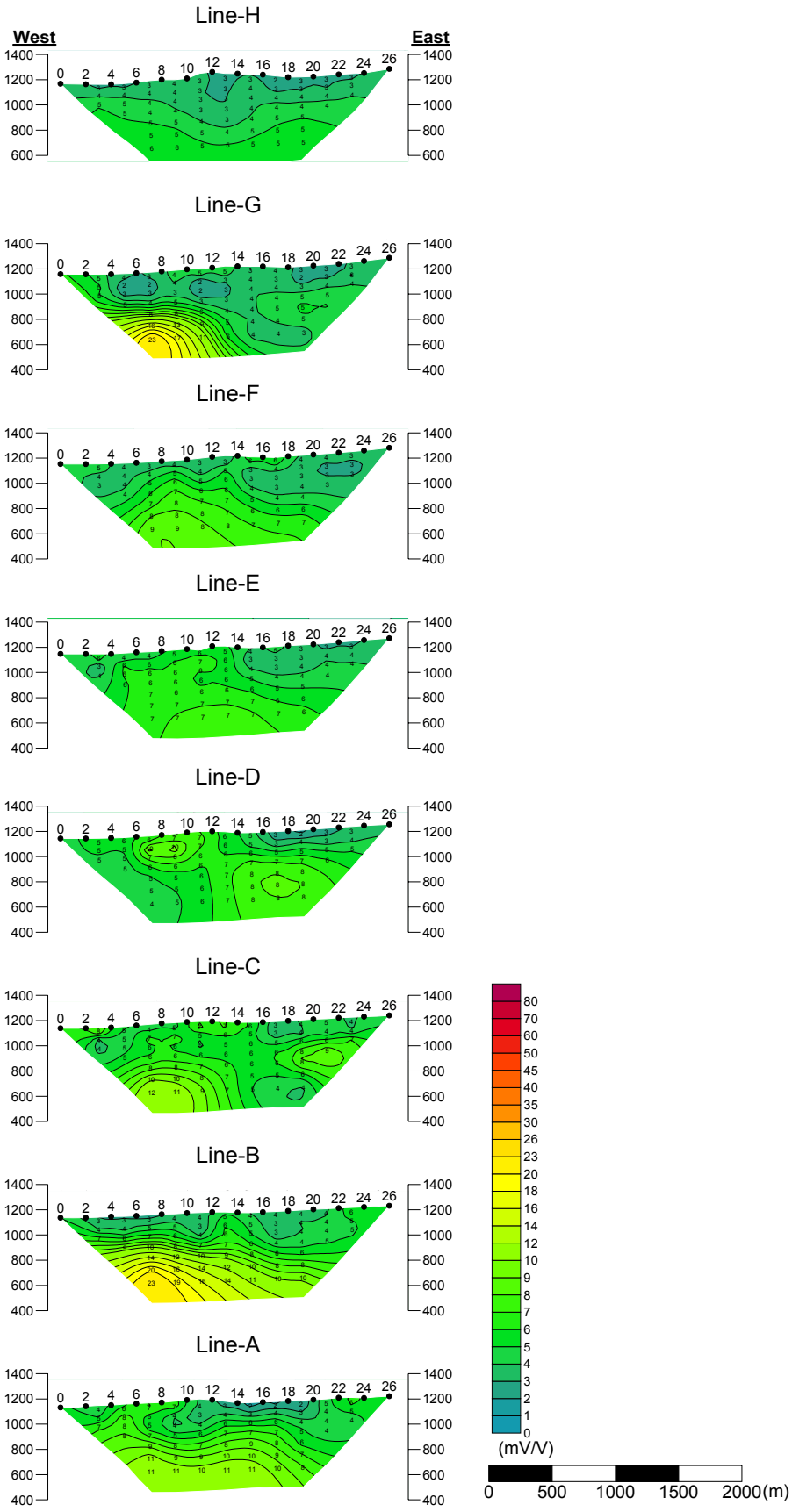

Fig.II-2-24　2D analysis sections for chargeability in Under/Shand_2 area

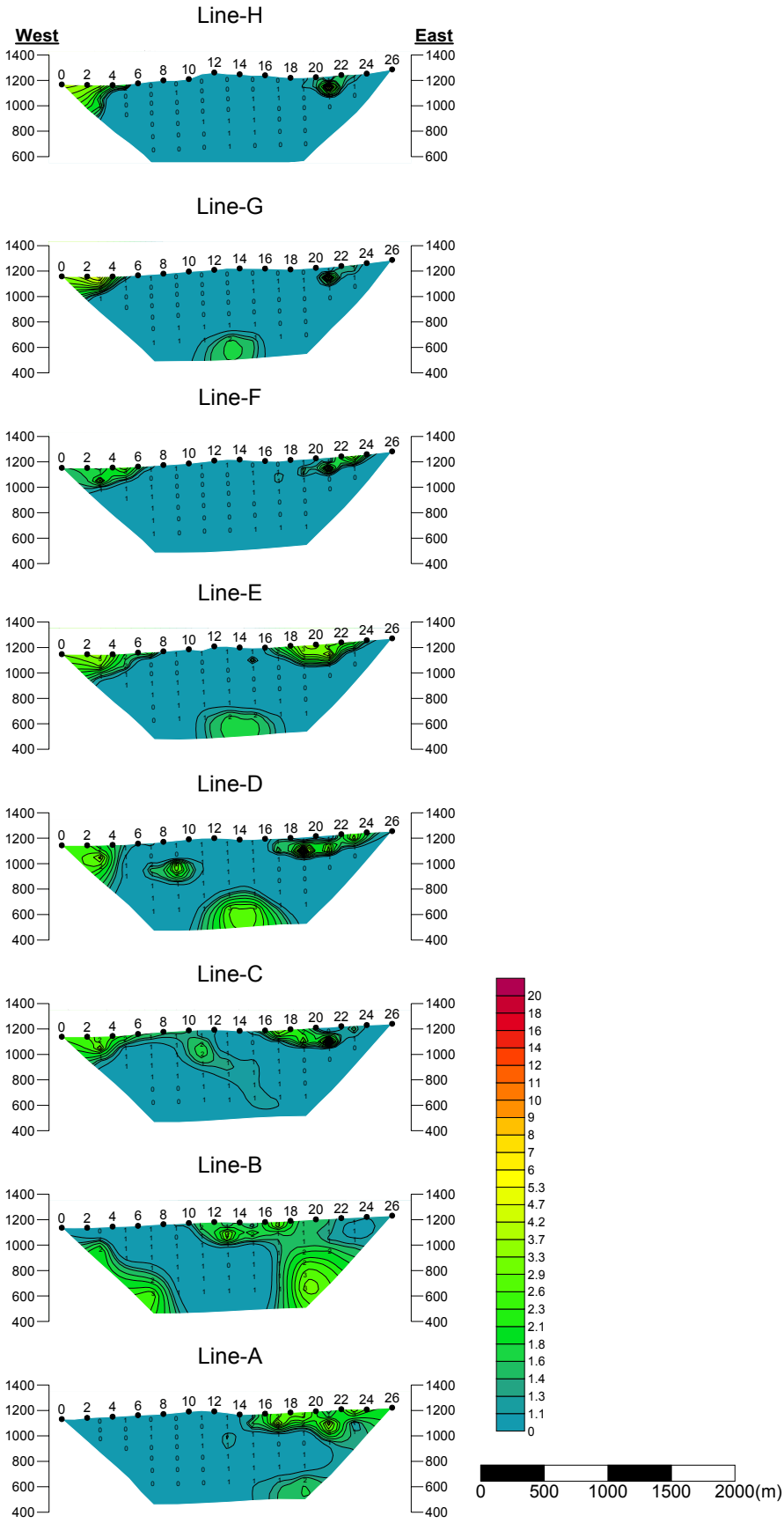

Fig.II-2-25　2D analysis sections for metal factor in Under/Shand_2 area

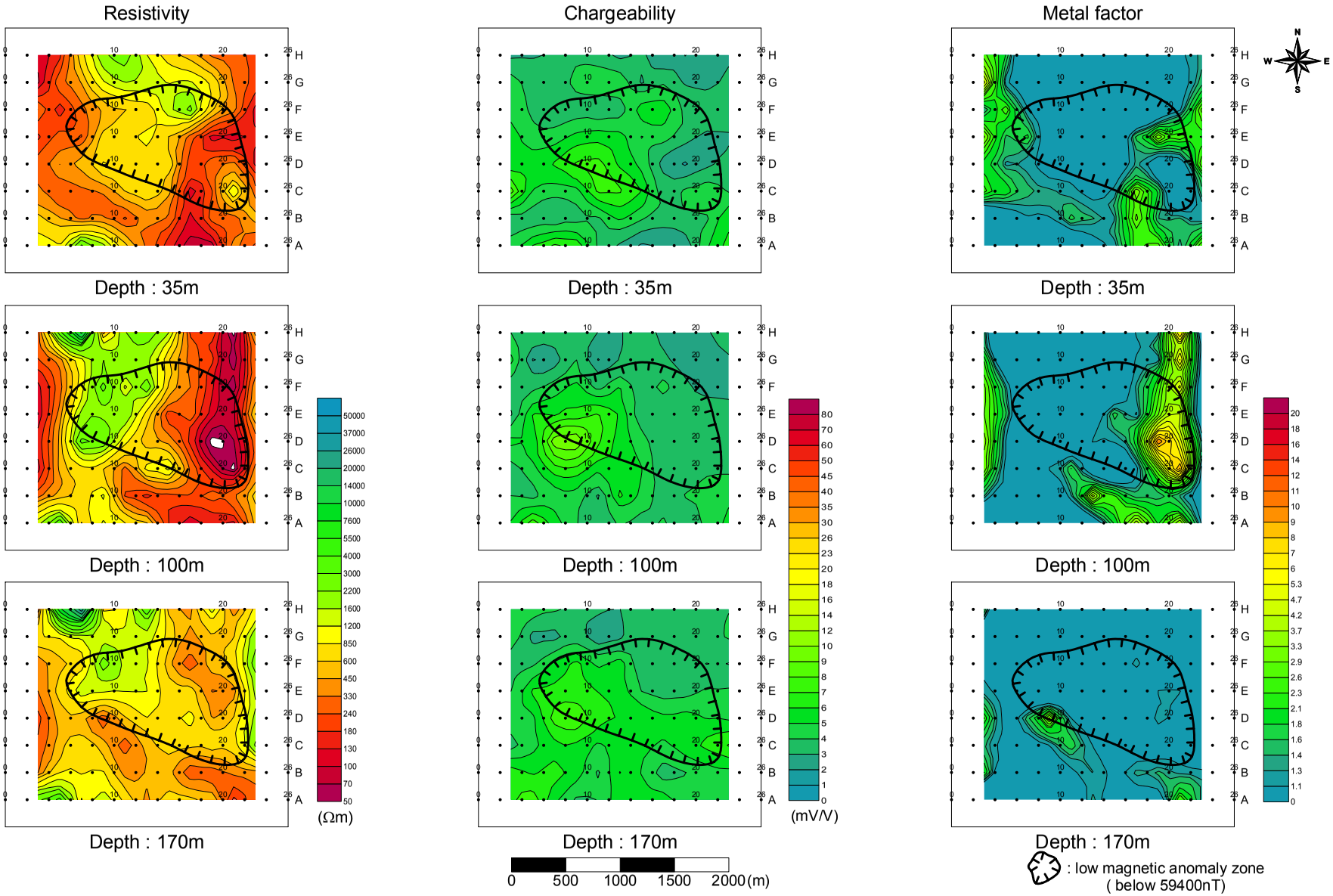

Fig.II-2-26 2D analysis plane map at the depth of 35m,100m and 170m in Under/Shand_2 area

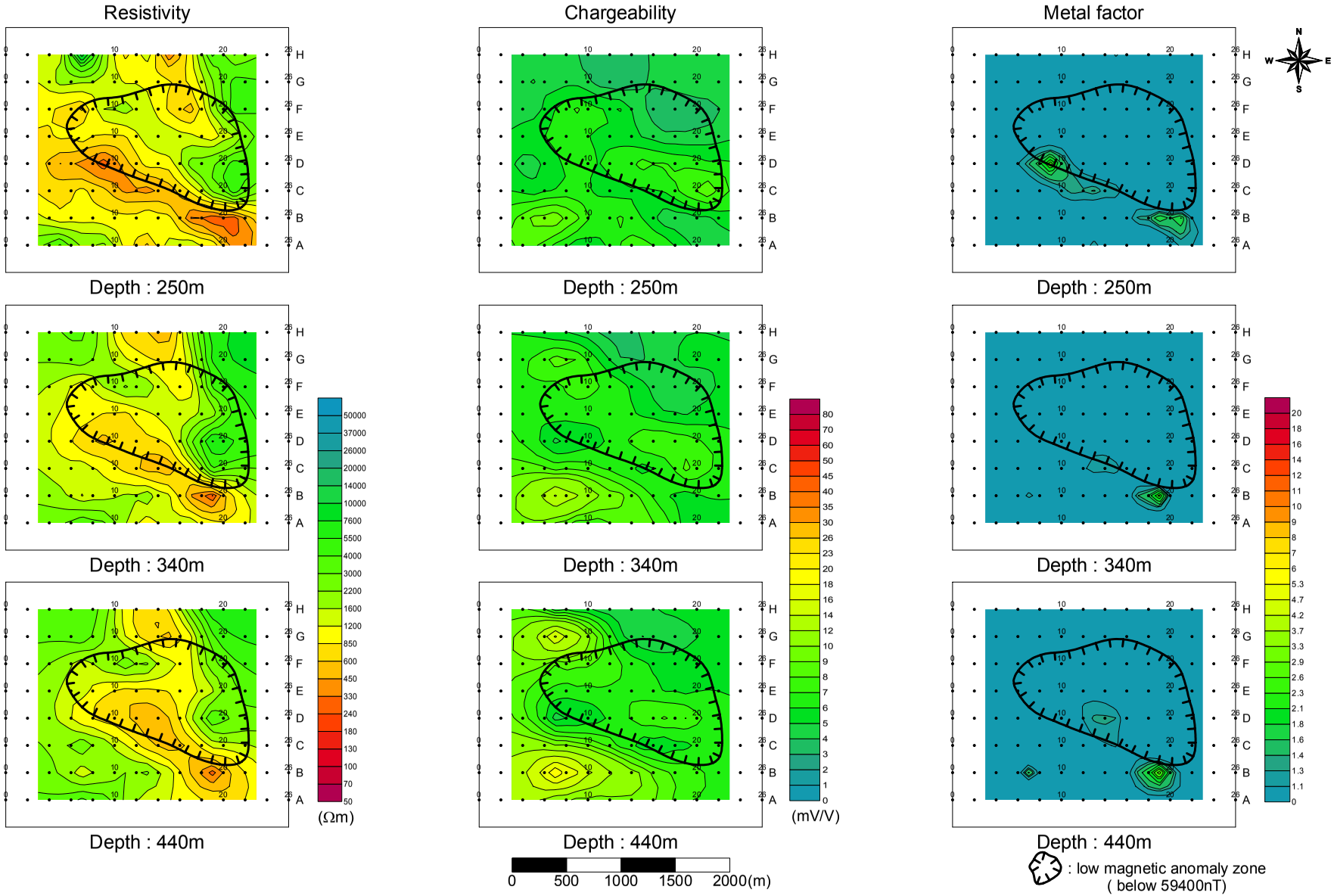

Fig.II-2-27 2D analysis plane map at the depth of 250m,340m and 440m in Under/Shand_2 area

2-5-3 Under/Shand 3 area

(1) Lines location

Fig.II-2-28 shows the location of TDIP lines. This area is located in the south of the Under/Shand area. 8 lines of 3.0km each were set up along N90°E.

(2) Results

Figs.II-2-29 to II-2-31 show the pseudo-sections, while Figs.II-2-32 and II-2-33 indicate the plane maps from n=1 to 5.

In this area, the apparent resistivity value ranges between 80 to 12kΩm and average is 1200Ωm.

According to the plane map for n=1, low resistivity zone below 500Ωm is detected and corresponds to the area underlain by Quaternary sediments. High resistivity zones are distributed at the area underlain by granodiorite or porphyritic granodiorite. The map for n=2 to 5 show similar distribution of resistivity as n=1.

The chargeability value ranges between 1.0 to 38mV/V and average is 8.8mV/V.

Remarkable high chargeability anomaly is recognized at northwestern part on the plane map for n=1. Its center is located at the station 8 to 10 on the line-F. This anomaly continues to deeper part(n=5).

The maximum value of the metal factor is 12. The feature of distribution is similar to that of the chargeability and forms remarkable anomaly.

(3) 2-D analysis

Figs.II-2-34 to II.2-38 show the 2-D analysis sections and 2-D analysis plane maps.

The analyzed resistivity value ranges between 47 to 40kΩm and average is 2600Ωm.

According to the plane maps above 100m depth, low resistivity is recognized widely and corresponds to Quaternary sediments. On the maps below 170m depth, low resistivity zone is concentrated to the northern part and corresponds to the low magnetic anomaly zone detected by airborne magnetic survey in Phase I.

The analyzed chargeability value ranges between 0.5 to 90mV/V and average is 13.3mV/V. Remarkable high chargeability zone is recognized in the north of the area. On the plane maps above 170m depth, the ring-shaped high chargeability zone is formed along the magnetic contour of 59400nT. Below the depth of 250m, high chargeability zone is detected not only along the magnetic contour of 59400nT but also inside the contour line. High chargeability zone extends 1200m from east to west and 1000m from north to south on the plane map of 250m depth.

The metal factor has similar feature of distribution to the chargeability. The maximum value of the metal factor is 38. This value is considered to reflect intense mineralization.

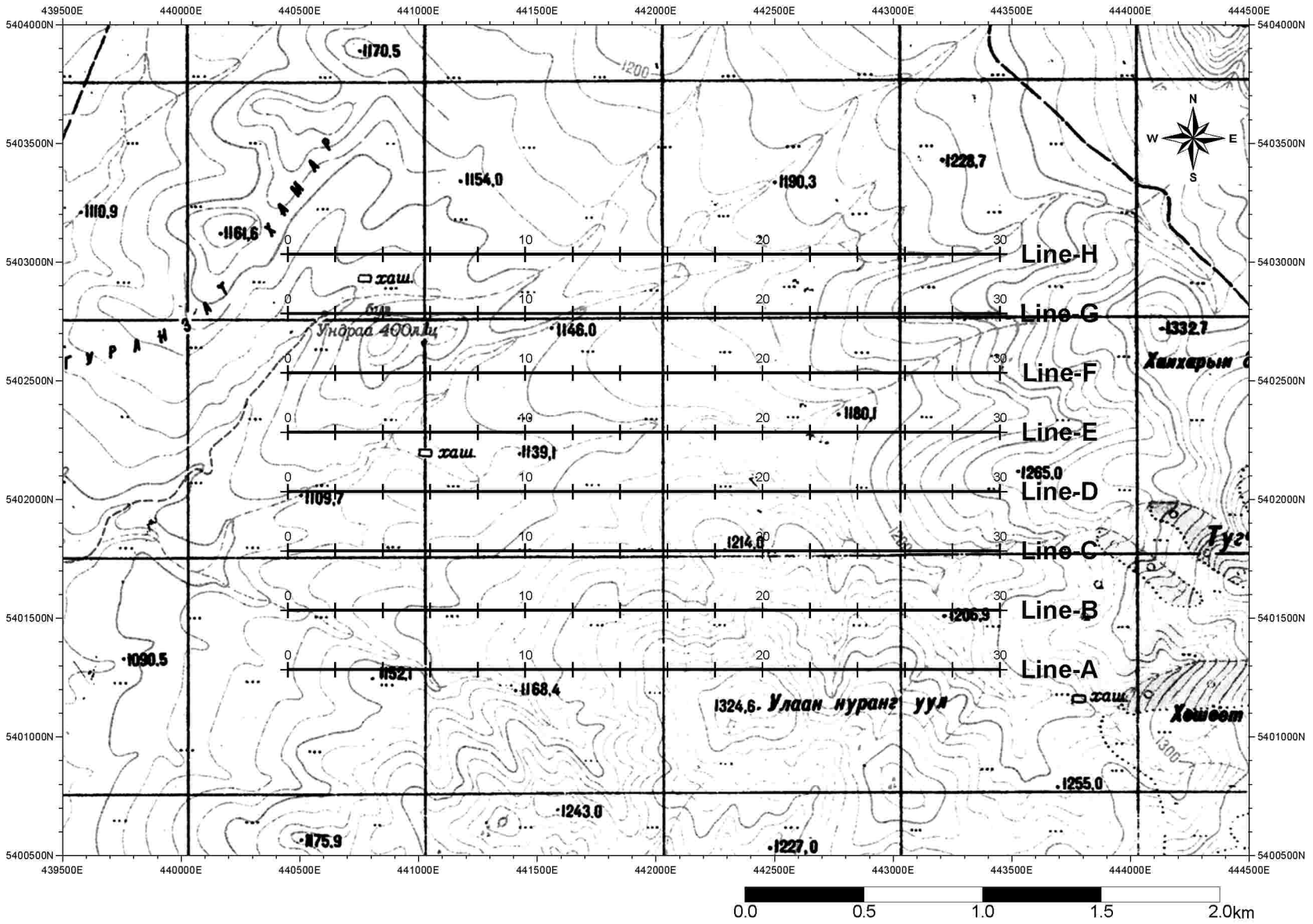

Fig.II-2-28 Geophysical survey location in Under/Shand_3 area

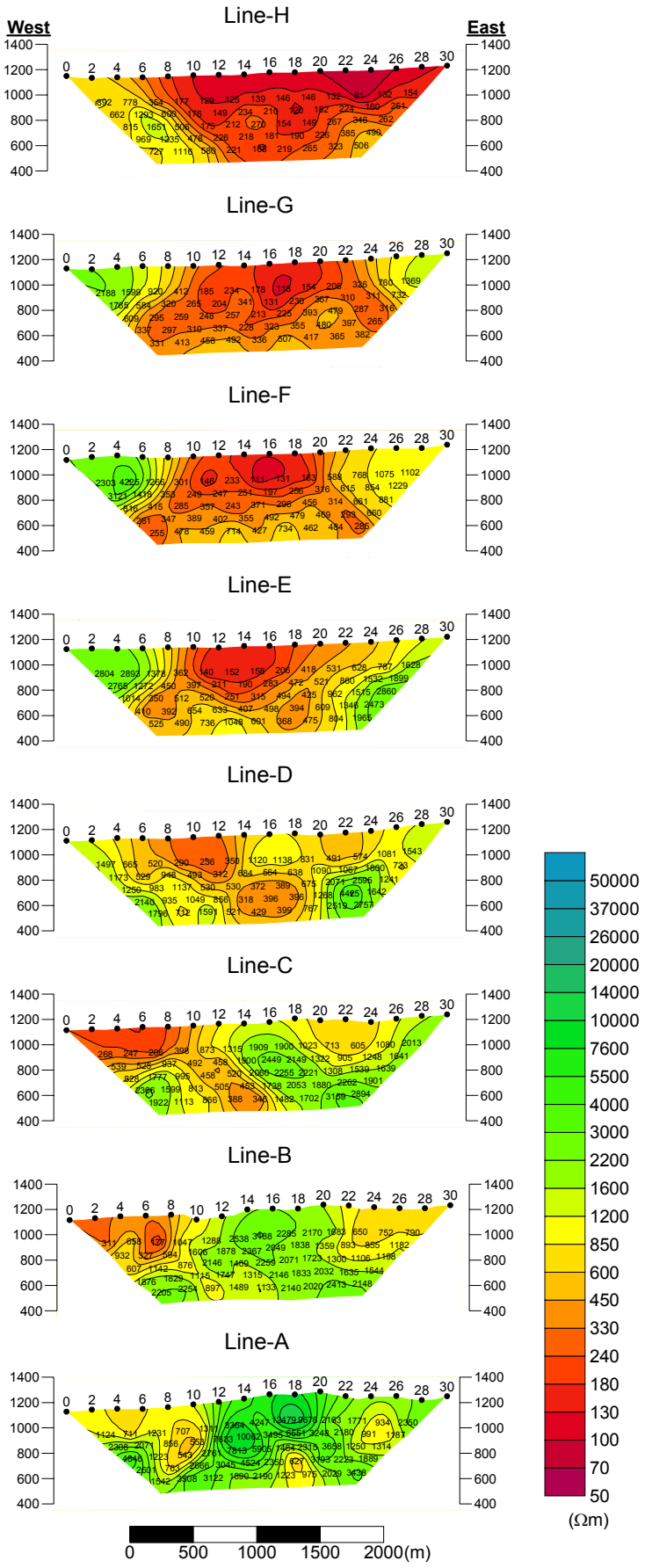

Fig.II-2-29 Apparent resistivity pseudo-sections in Under/Shand_3 area

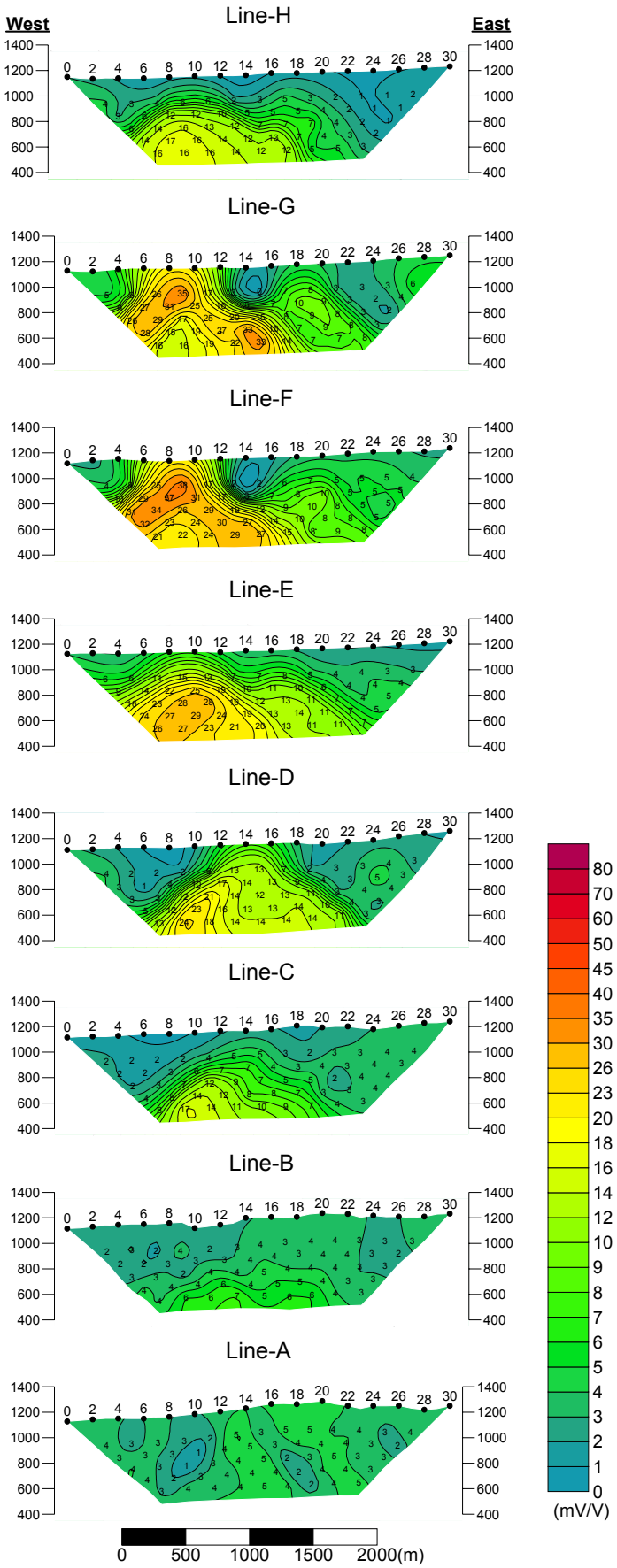

Fig.II-2-30 Chargeability pseudo-sections in Under/Shand_3 area

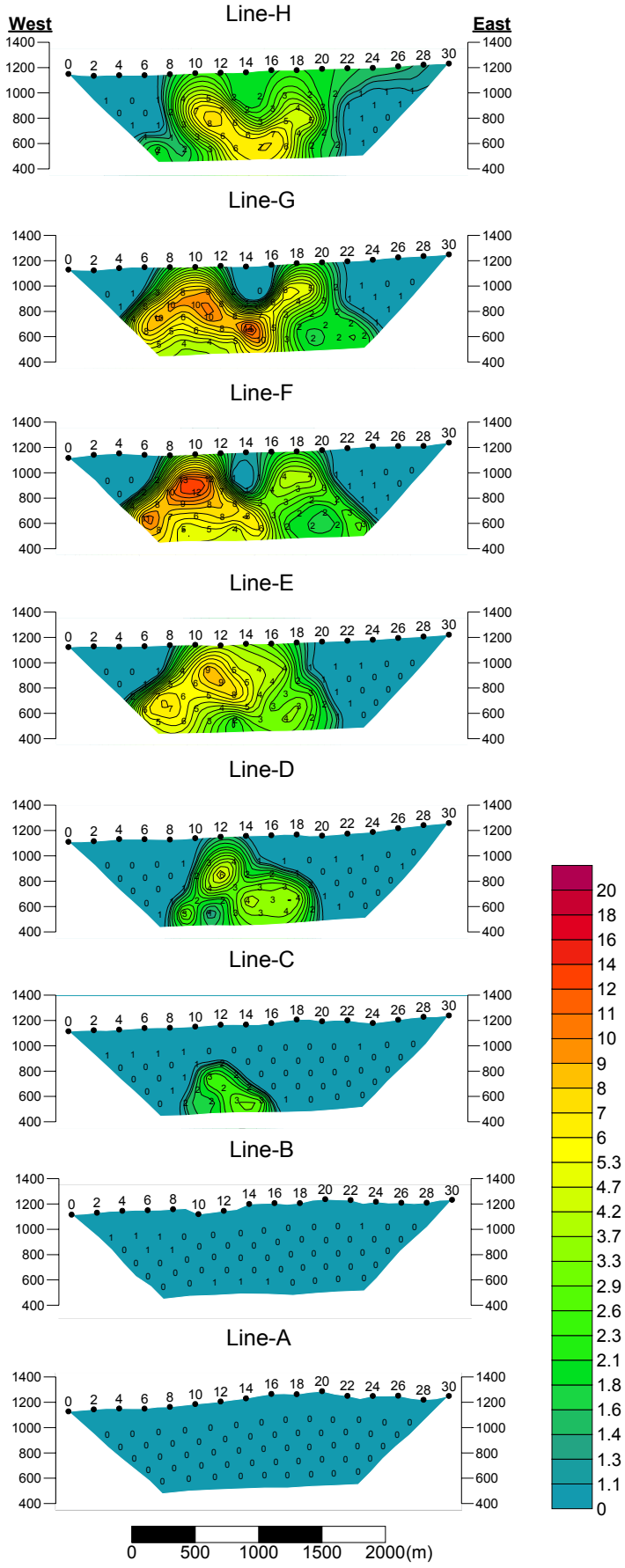

Fig.II-2-31　Metal factor pseudo-sections in Under/Shand_3 area

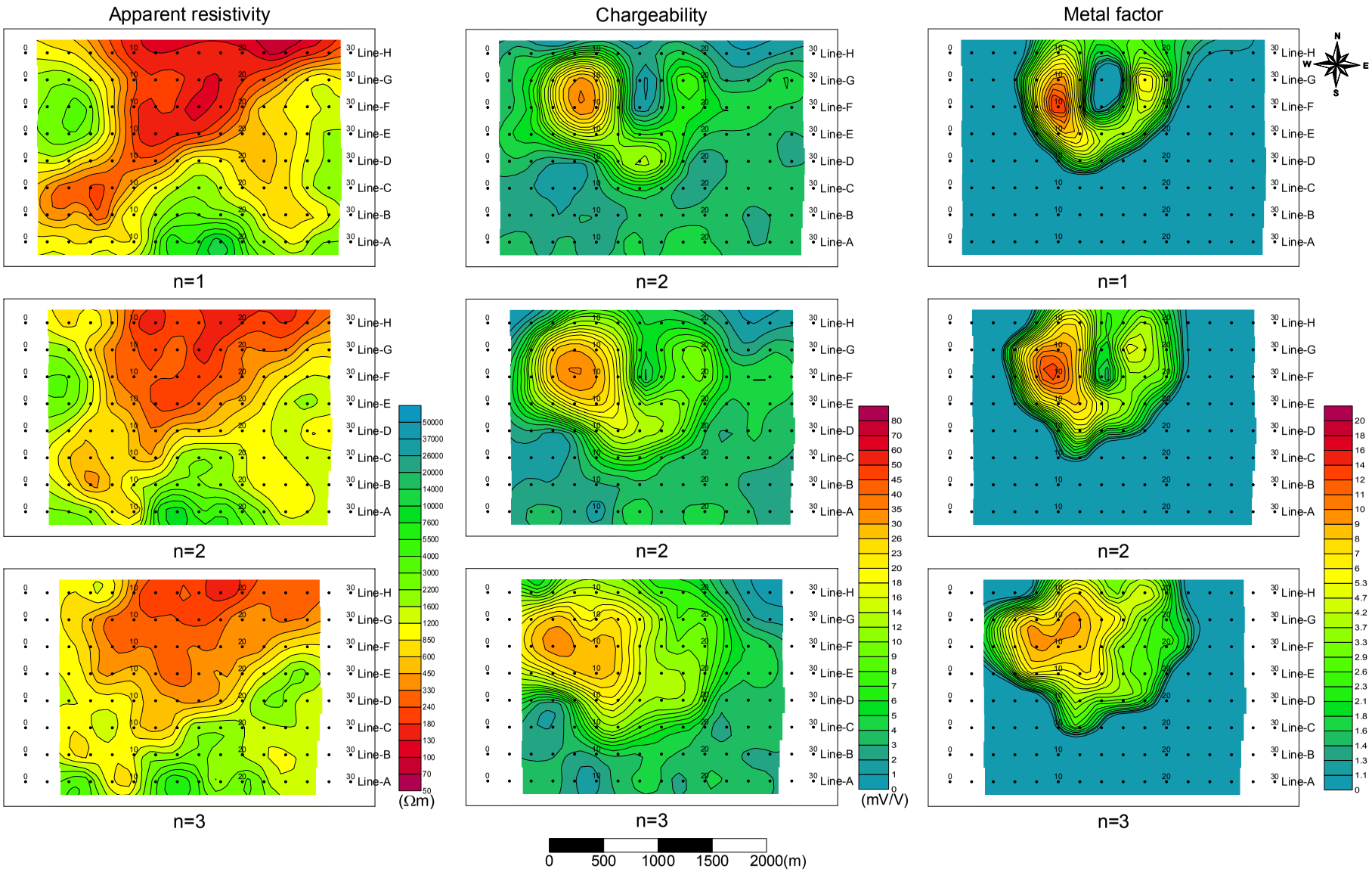

Fig.II-2-32 TDIP plane map for n=1, 2 and 3 in Under/Shand_3 area

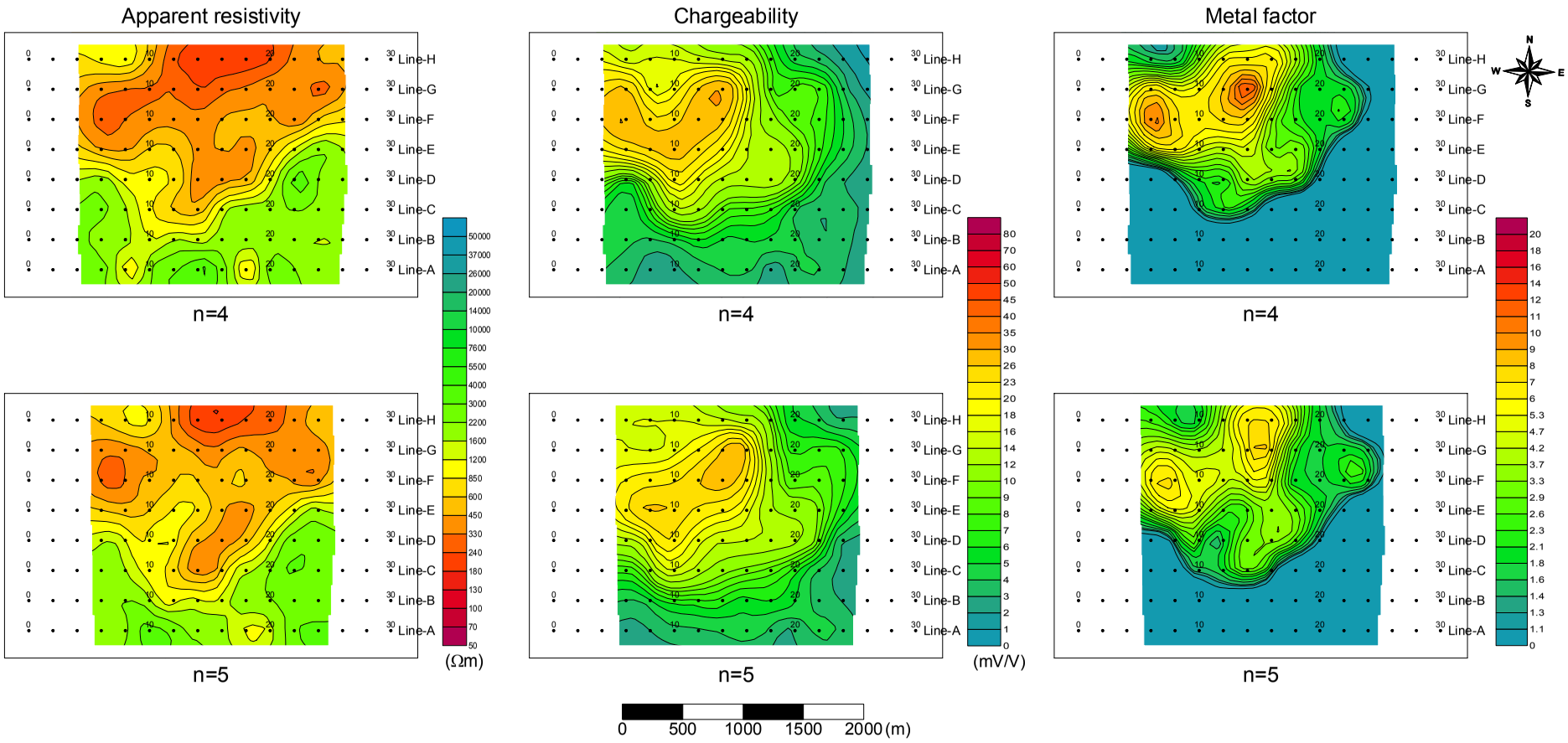

Fig.II-2-33 TDIP plane map for n=4 and 5 in Under/Shand_3 area

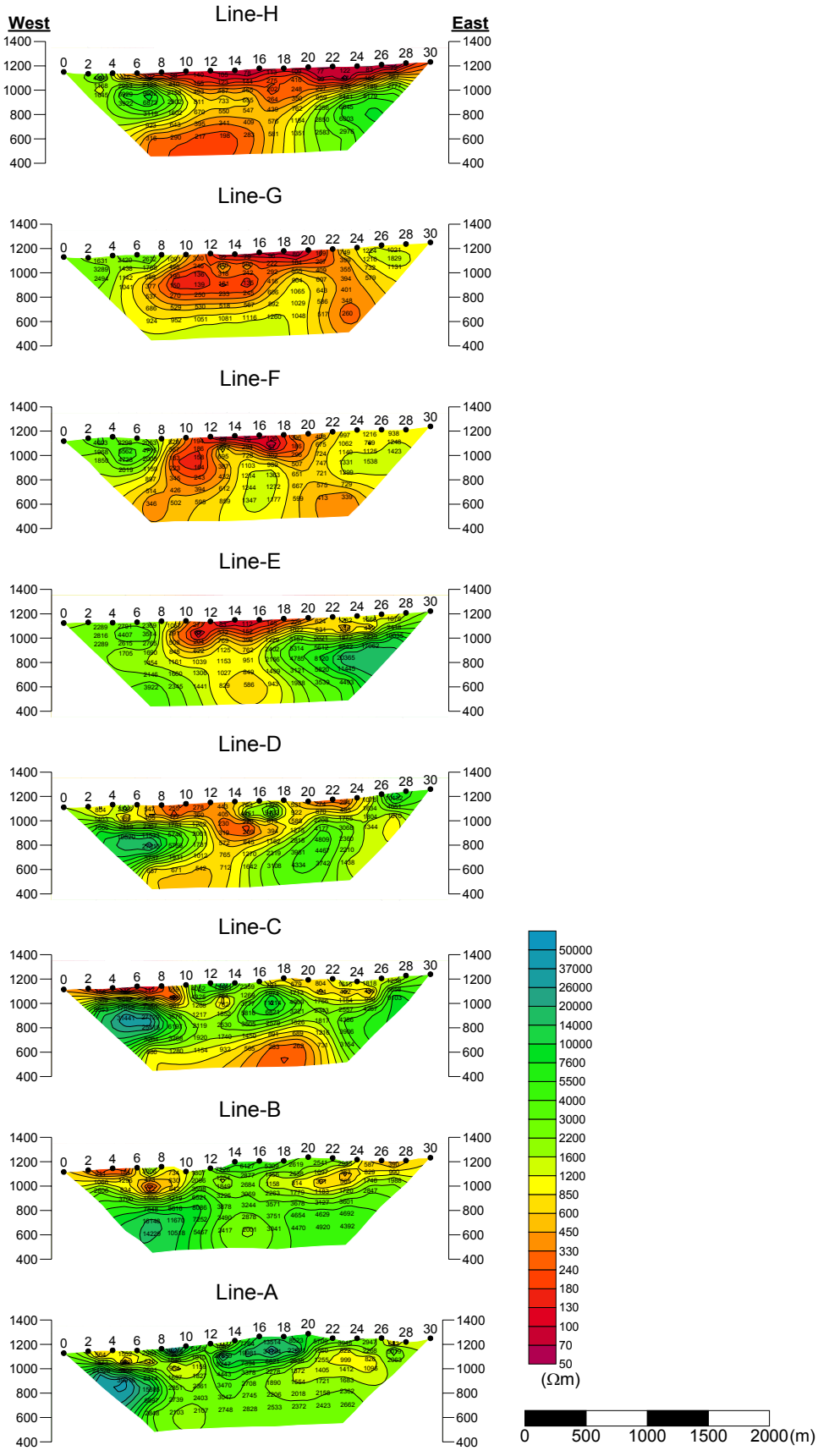

Fig.II-2-34　2D analysis sections for resistivity in Under/Shand_3 area

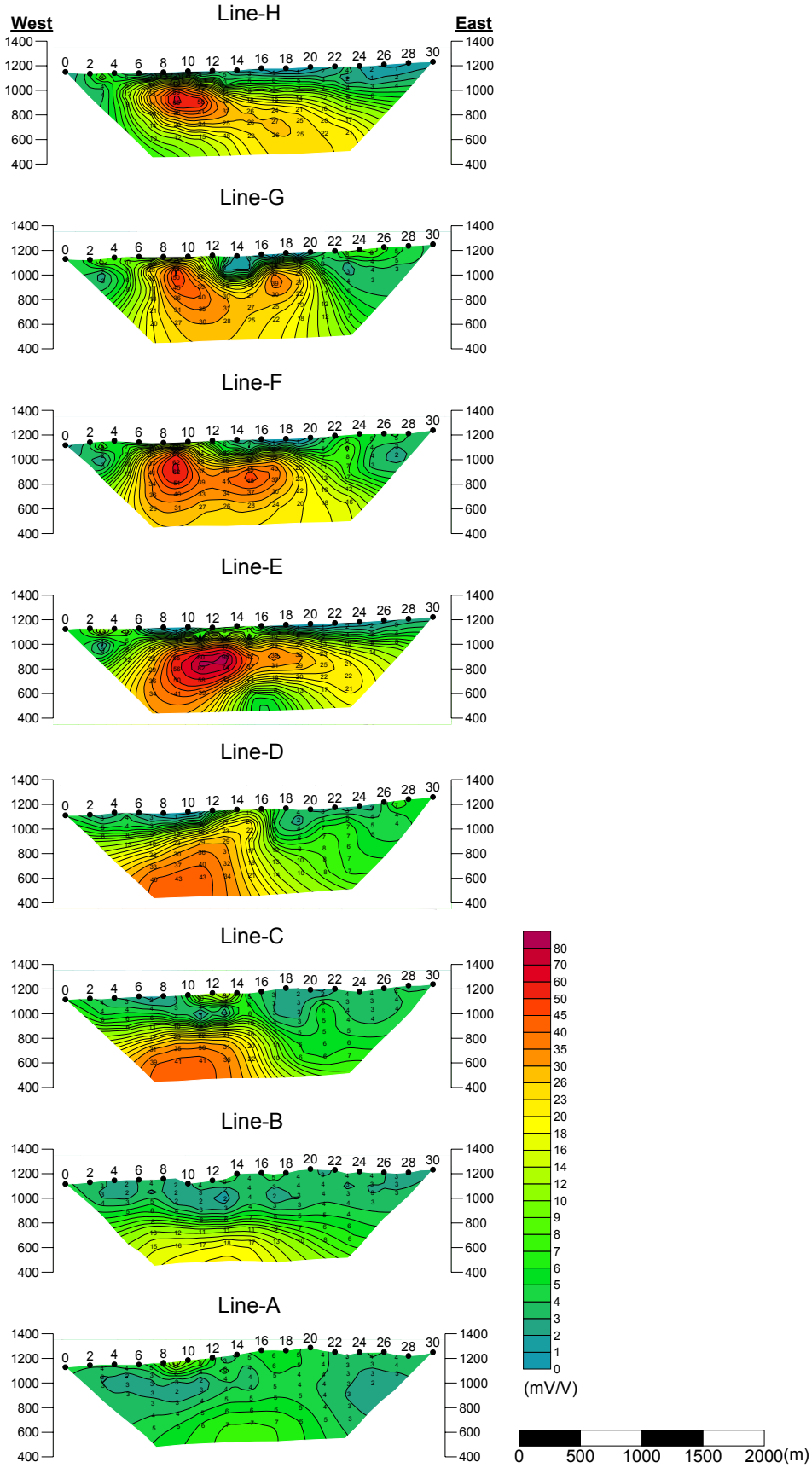

Fig.II-2-35　2D analysis sections for chargeability in Under/Shand_3 area

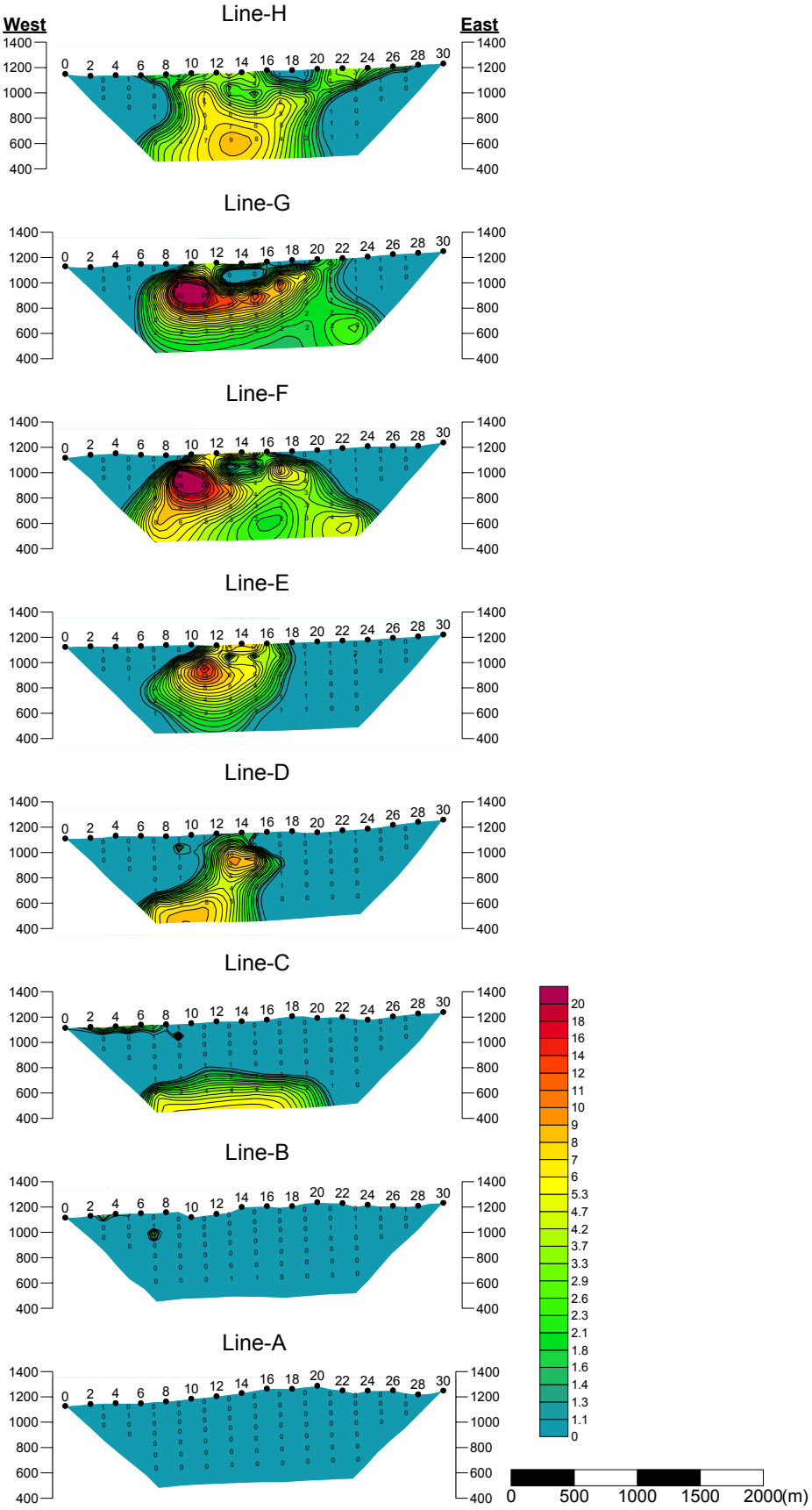

Fig.II-2-36　2D analysis sections for metal factor in Under/Shand_3 area

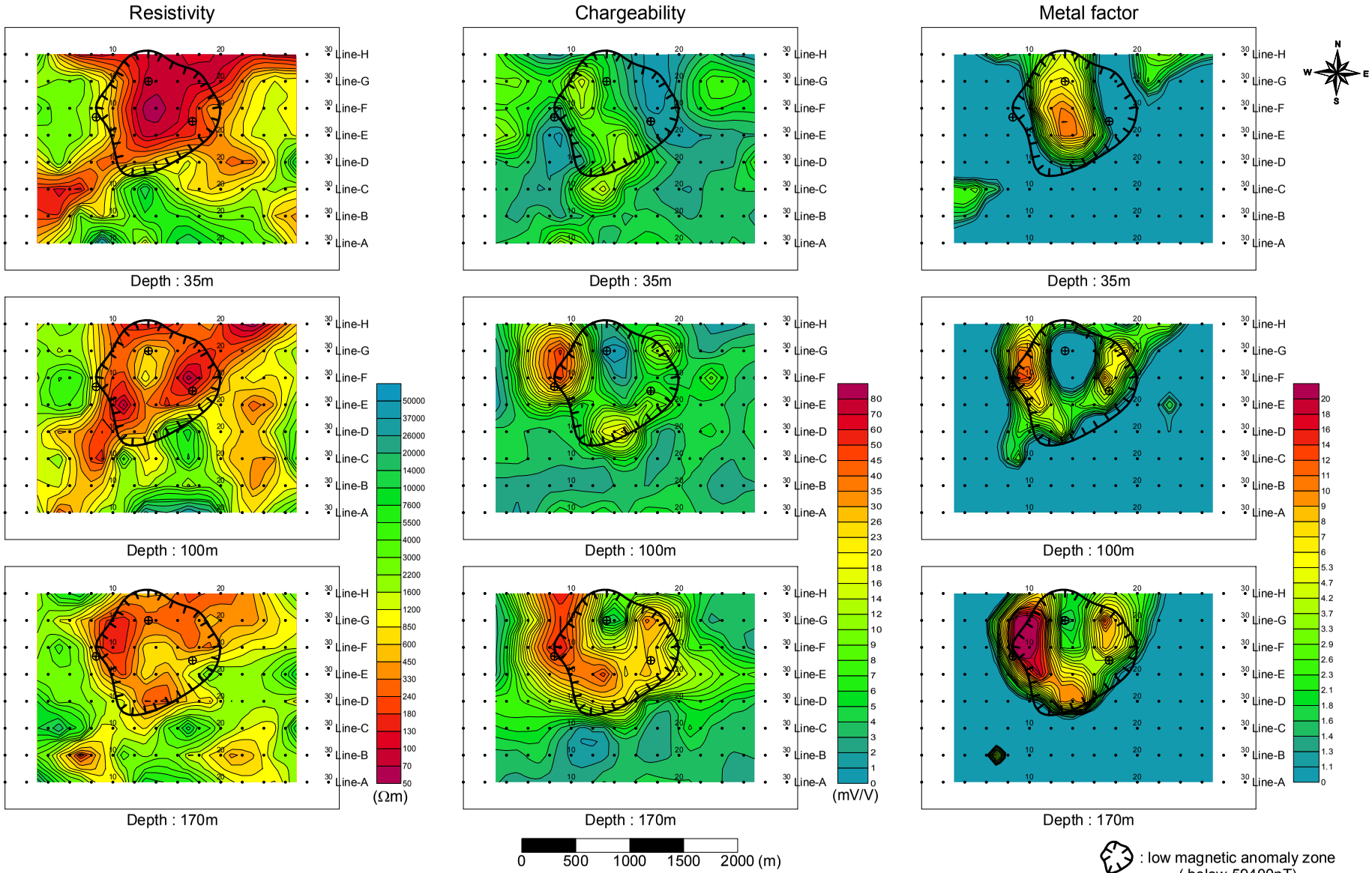

Fig.II-2-37 2D analysis plane map at the depth of 35m, 100m and 170m in Under/Shand_3 area

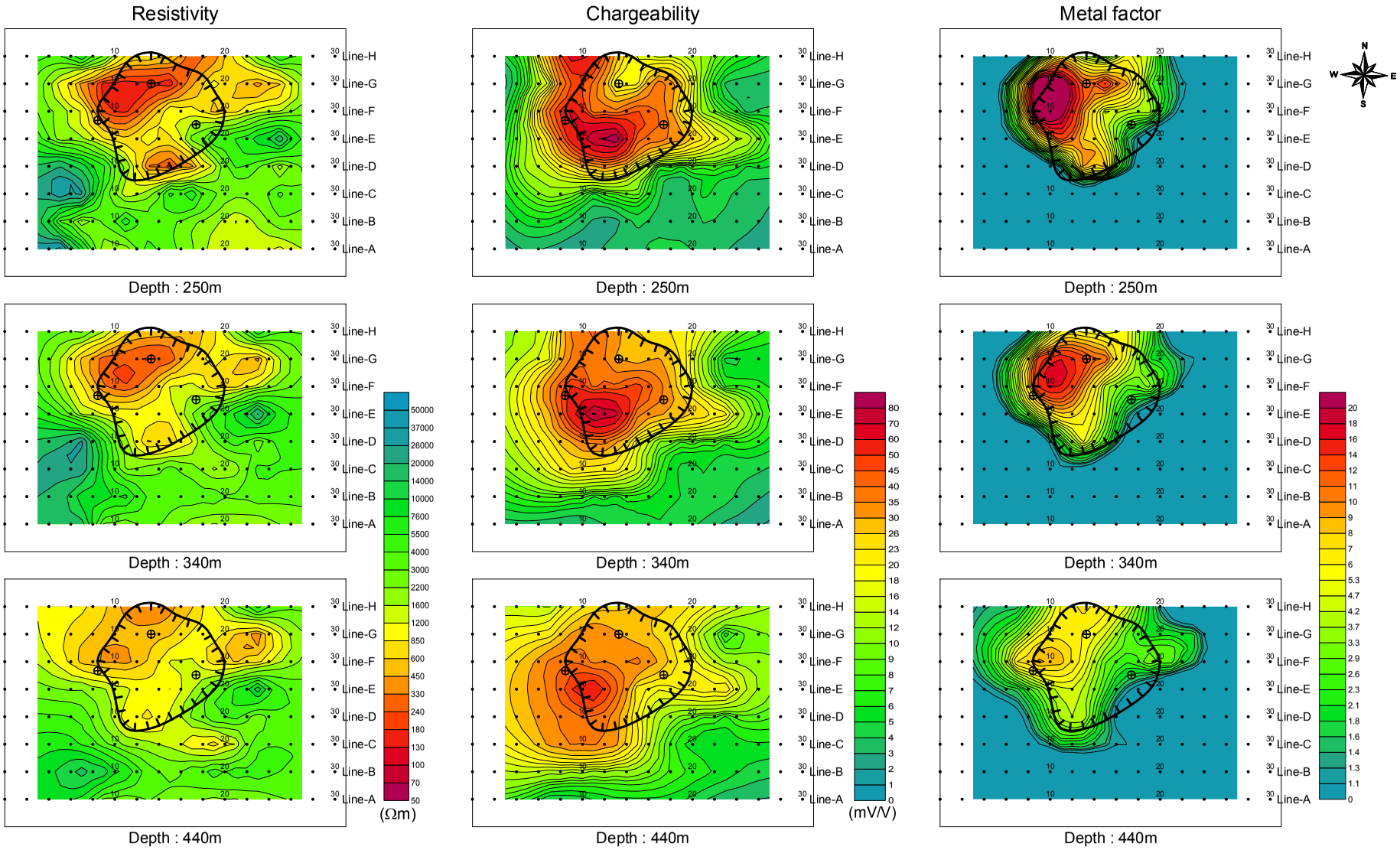

Fig.II-2-38 2D analysis plane map at the depth of 250m, 340m and 440m in Under/Shand_3 area

2-5-4 Mogoin gol area

(1) Lines location

Fig.II-2-39 shows the location of TDIP lines. In this area, 8 lines of 5.0km each were set up along N0°E. The survey area includes two white silicified alteration zones and low magnetic anomaly zone detected by geological survey and airborne magnetic survey respectively. As a result of the measurements, remarkable IP anomaly zone continuing to the east and the west was detected in the north edge of the survey area. Therefore, the survey area was extended to the north, east and west, and total amount is 13 lines of 7.0km each.

(2) Results

Figs.II-2-40 to II-2-42 show the pseudo-sections, while Figs.II-2-43 to II-2-47 indicate the plane maps from n=1 to 5.

In this area, the apparent resistivity value ranges between 115 to 16,655Ωm, and average is about 1,100Ωm. According to the plane map for n=1, the area underlain by Quaternary sediments shows low resistivity below 500Ωm. This low resistivity is caused by large amount of ground water contained in unconsolidated sediments. In the mountain area, high resistivity above 1,000Ωm is generally distributed, while two alteration zones shows low to middle resistivity between 300 and 1,500Ωm. On the plane maps for n=2 and 3, the feature of distribution of resistivity is similar to that of n=1. At the deeper part(n=4 and 5), low resistivity is widely distributed. This low resistivity is almost artifacts affected by the low resistivity which exists in near surface. Excepting the artifacts, low resistivity anomaly at the deep part is as follows. Deep parts below the stations 46 to 48 on the line MG-0, the stations 45 to 56 on the line MG-11 and the station 58 on the lines MG-11 and MG-12.

The chargeability value ranges between 0.5 to 42.8mV/V, and average is about 12.6mV/V. According to the plane map for n=1, high chargeability zones over 10mV/V are recognized around the alteration zones. Especially, at the northern alteration zone, the chargeability shows high value over 20mV/V. The chargeability anomalies over 10mV/V are also recognized at the stations 44 to 50 on the lines MG-0 to MG-3, the stations 28 to 36 on the lines MG-1 to MG-4 and the stations 30 to 34 on the lines MG-7 to MG-10. The chargeability anomaly distributed widely at the deeper part is almost the artifacts caused by the high chargeability located in near surface. In general, the chargeability value of the artifacts is smaller at the deeper part. Around the northern alteration zone, the chargeability shows high value over 30mV/V even at the deep part, therefore it is inferred that this high chargeability is not the artifacts but showing existing of some body having good polarizable property.

The metal factor shows high value over 10 around the alteration zones. Especially, at the northern alteration zone, high metal factor distributed continuously from shallow to deep part.

(3) 2-D analysis

Figs.II-2-48 to II.2-56 show the 2-D analysis sections and 2-D analysis plane maps.

The analyzed resistivity value ranges between 49.5 to 223k□m and average is 1940□m. According to the plane maps of 35m, 100m and 170m depth, the low resistivity zones below 500□m are recognized at the area underlain by Quaternary sediments. The plane maps of the depth below 250m show low to middle resistivity around the alteration zones. The distribution area of low resistivity at the southern alteration zone becomes smaller below 340m depth, while the low resistivity continues to deeper part at the northern alteration zone. Therefore, it is inferred that large scale conductive body exists under the northern alteration zone. Except for the area underlain by Quaternary sediments and the alteration zones, the resistivity shows high value over 1500□m, and distribution pattern is same at all levels.

The analyzed chargeability value ranges between 0.04 to 121mV/V and average is 17mV/V. According to the plane map of 35m depth, The high chargeability over 10mV/V around the alteration zones, the small scale high anomaly at the stations 42 to 46 on the lines MG-0 to MG-2 and the high anomaly extending eastward and southeastward from the station 30 on the line MG-1 are recognized. The second anomaly corresponds to the area intruded by rhyolite porphyry. The area of the last one is almost underlain by Quaternary sediments and intruded diorite is recognized at the center of the anomaly. According to the plane maps of 100m and 170m depth, high chargeability at the alteration zones become to be distributed in larger area and to show higher value over 30mV/V. At the northern alteration zone, high chargeability recognized continuously at the deeper part below 170m, while at the southern alteration zone, the center of the anomaly shifts eastward at the deeper part and is located at the stations 10 to 20 on the lines MG-8 to MG-9 below the depth of 250m. High chargeability zones are also recognized at the stations 32 to 46 on the line MG-6 and the stations 24 to 36 on the line MG-12. These anomalies are considered as artifacts caused by failure of assumption of 2 dimensional structure, and does not reflect real structure.

The metal factor shows high value around the alteration zones. The plane maps of 35m to 170m depth show the ring-shaped anomaly around the northern alteration zone. At the deeper part, the anomaly concentrates to the center of the alteration zone. At the southern alteration zone, the metal factor anomaly shows same distribution pattern as that of the northern alteration zone, but the peak of the anomaly concentrate to the center of the alteration zone at the depth of 170, and the anomaly disappear below the depth of 340m.

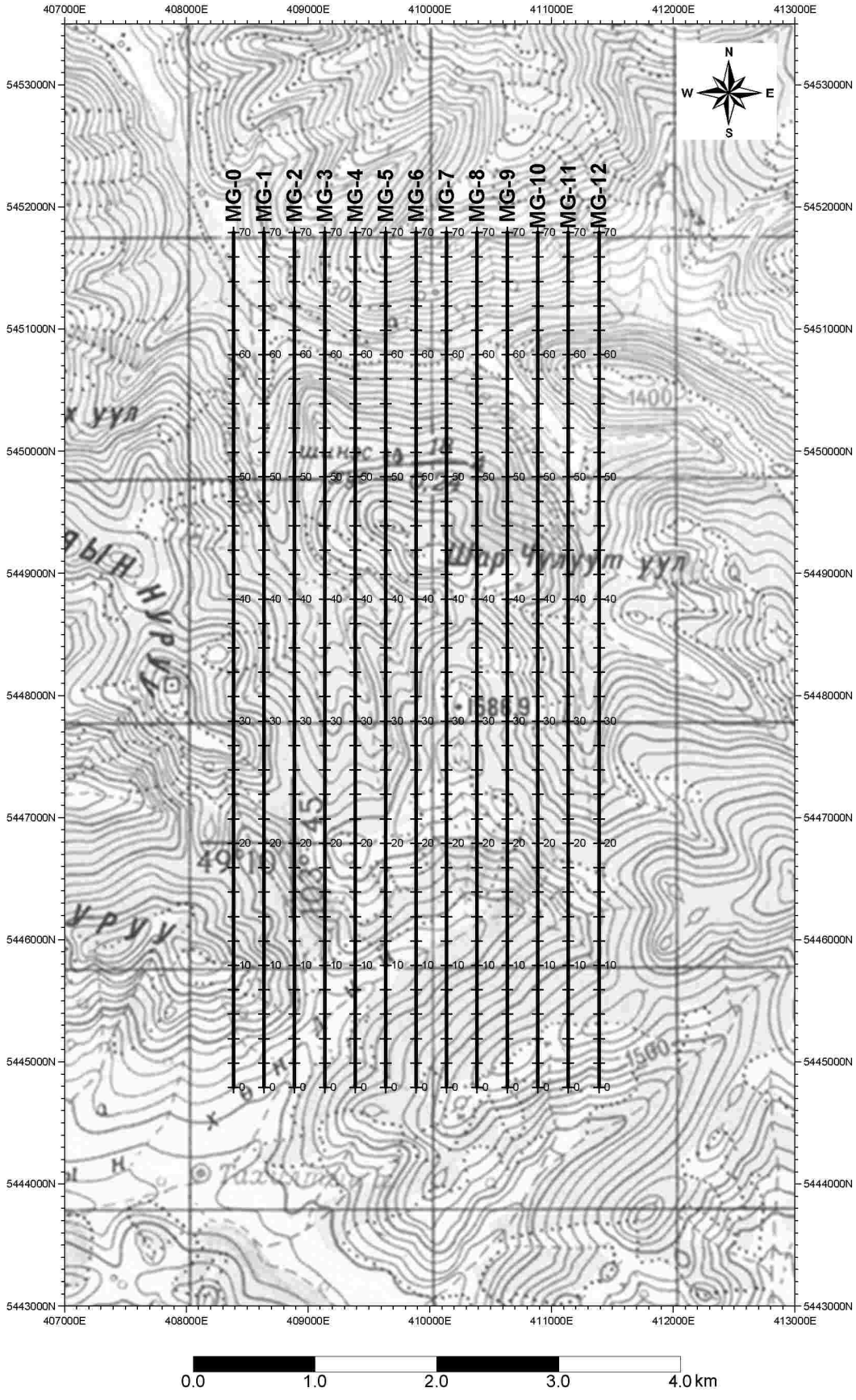

Fig.II-2-39 Geophysical survey location in Mogoin gol area

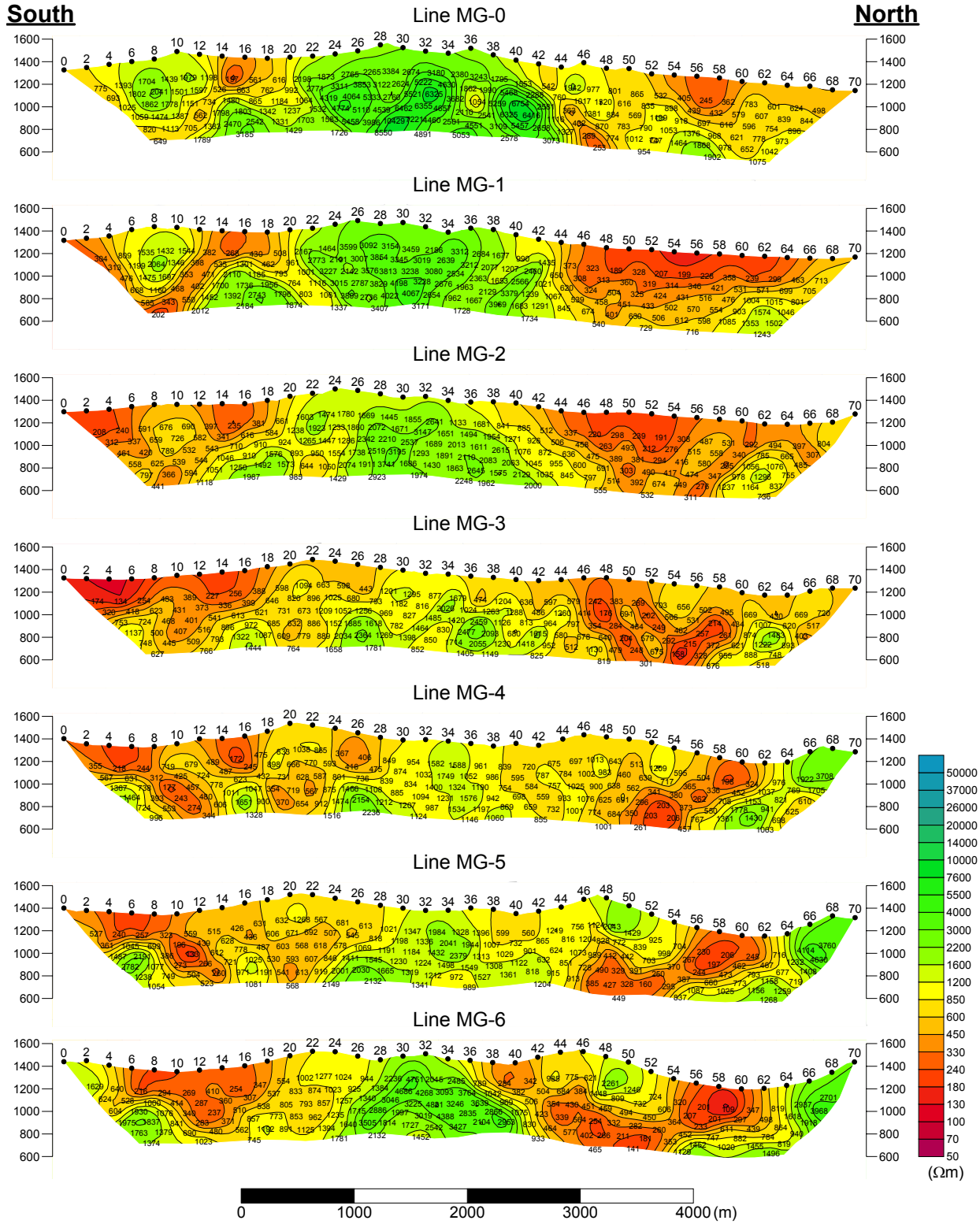

Fig.II-2-40(1)　Apparent resistivity pseudo-seciotns in Mogoin gol area (MG-0 ~ MG-6)

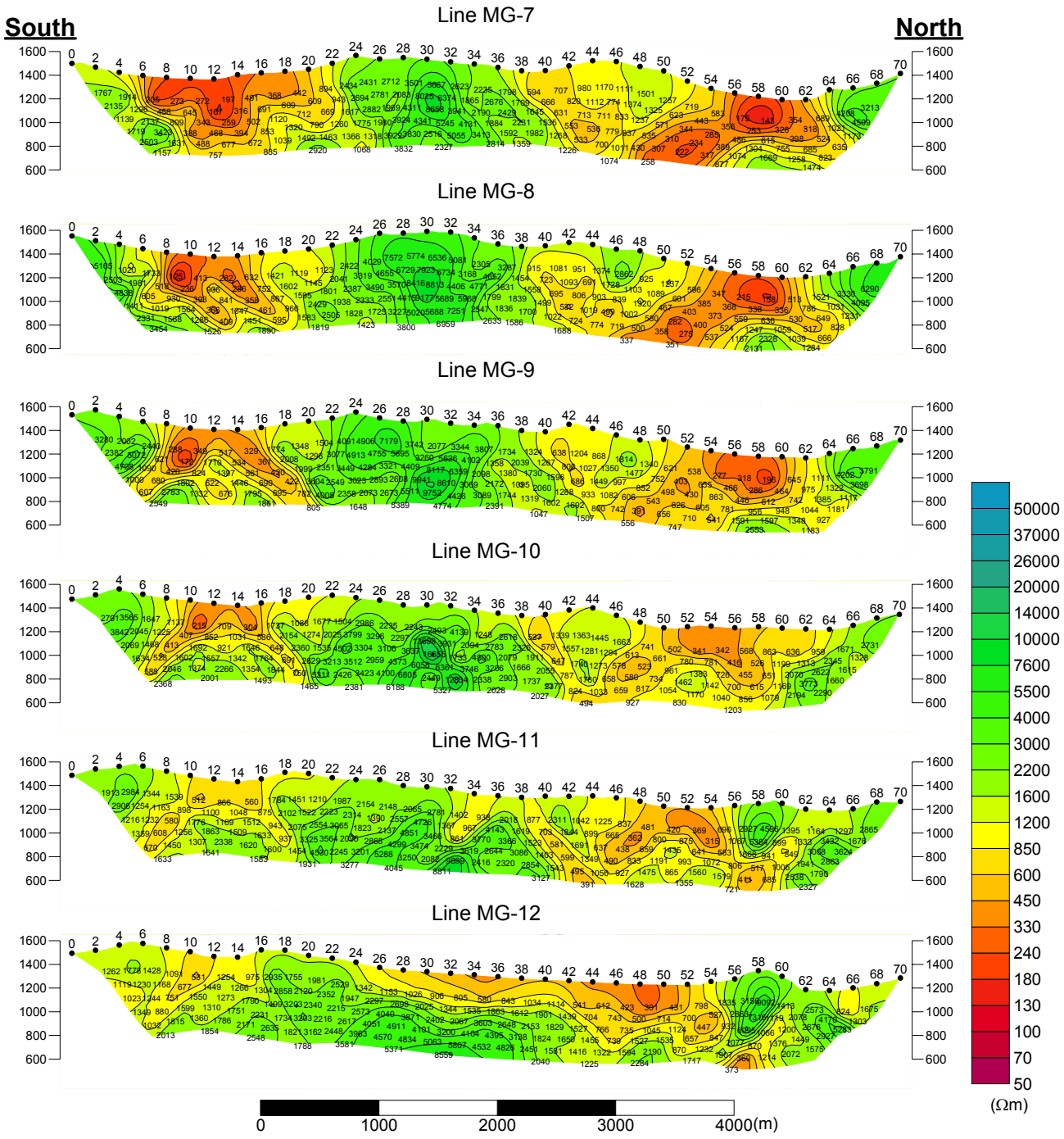

Fig.II-2-40(2) Apparent resistivity pseudo-seciotns in Mogoin gol area (MG-7 ~ MG-12)

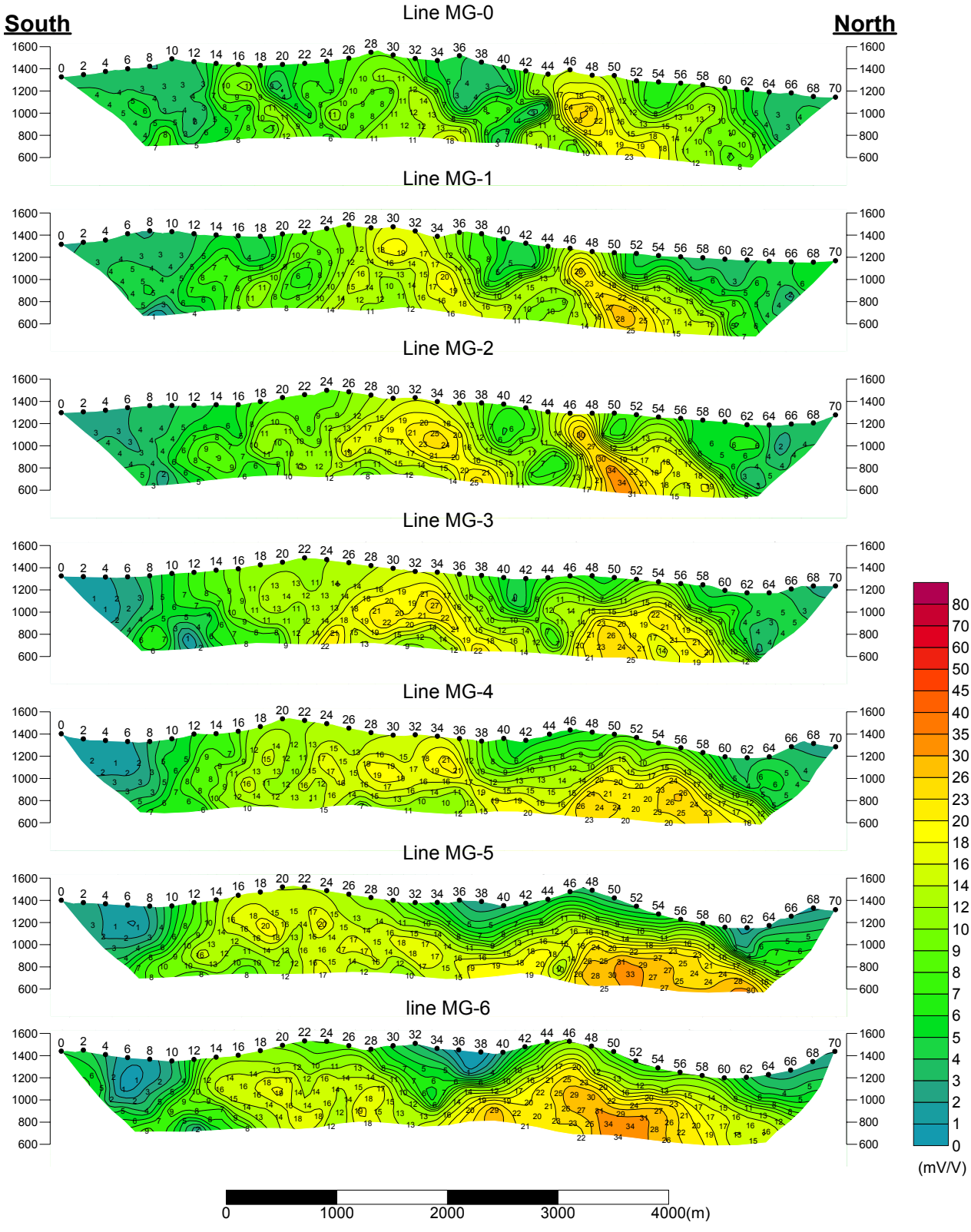

Fig.II-2-41(1)　Chargeability pseudo-seciotns in Mogoin gol area (MG-0 ~ MG-6)

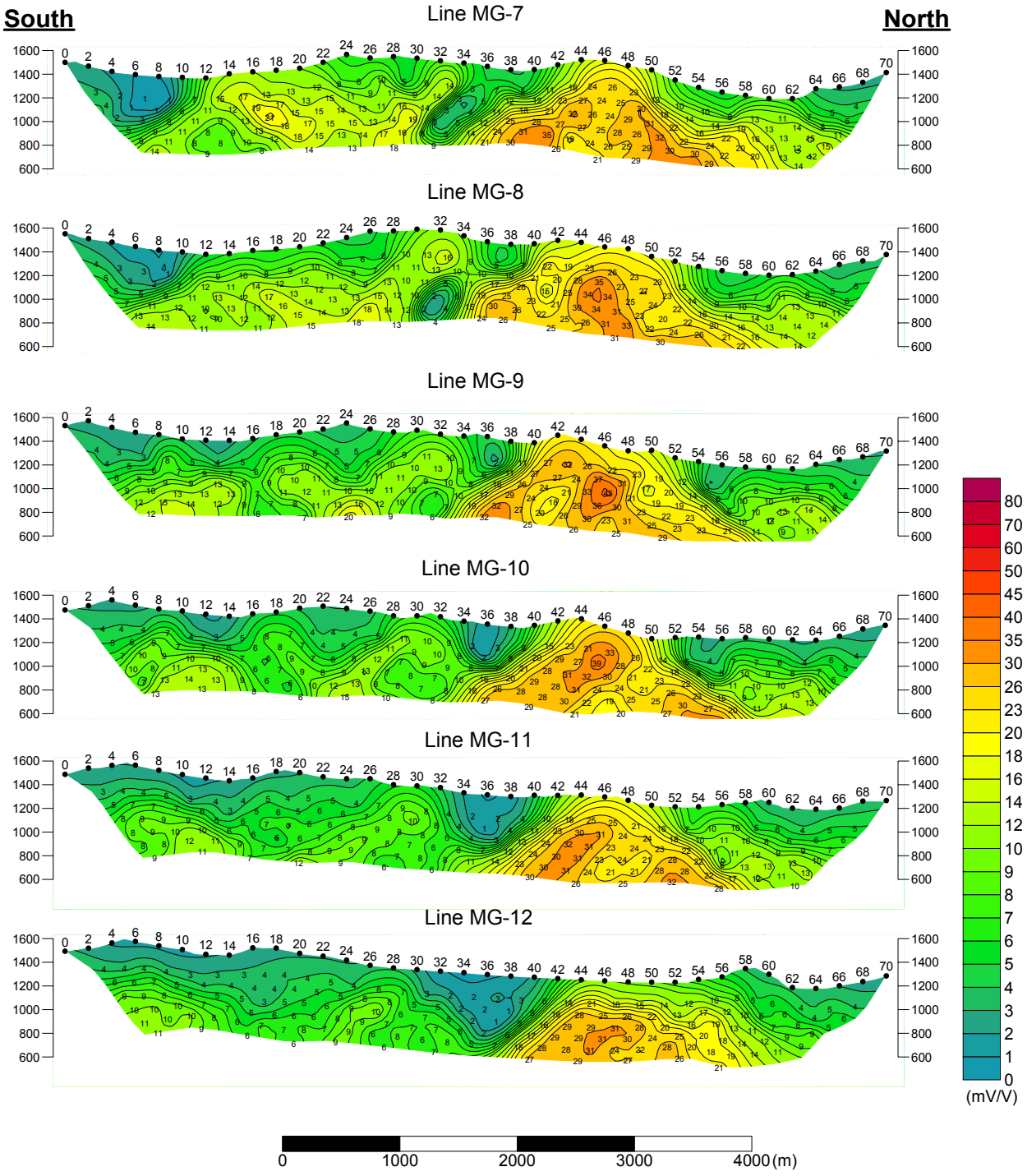

Fig.II-2-41(2)　Chargeability pseudo-seciotns in Mogoin gol area (MG-7 ~ MG-12)

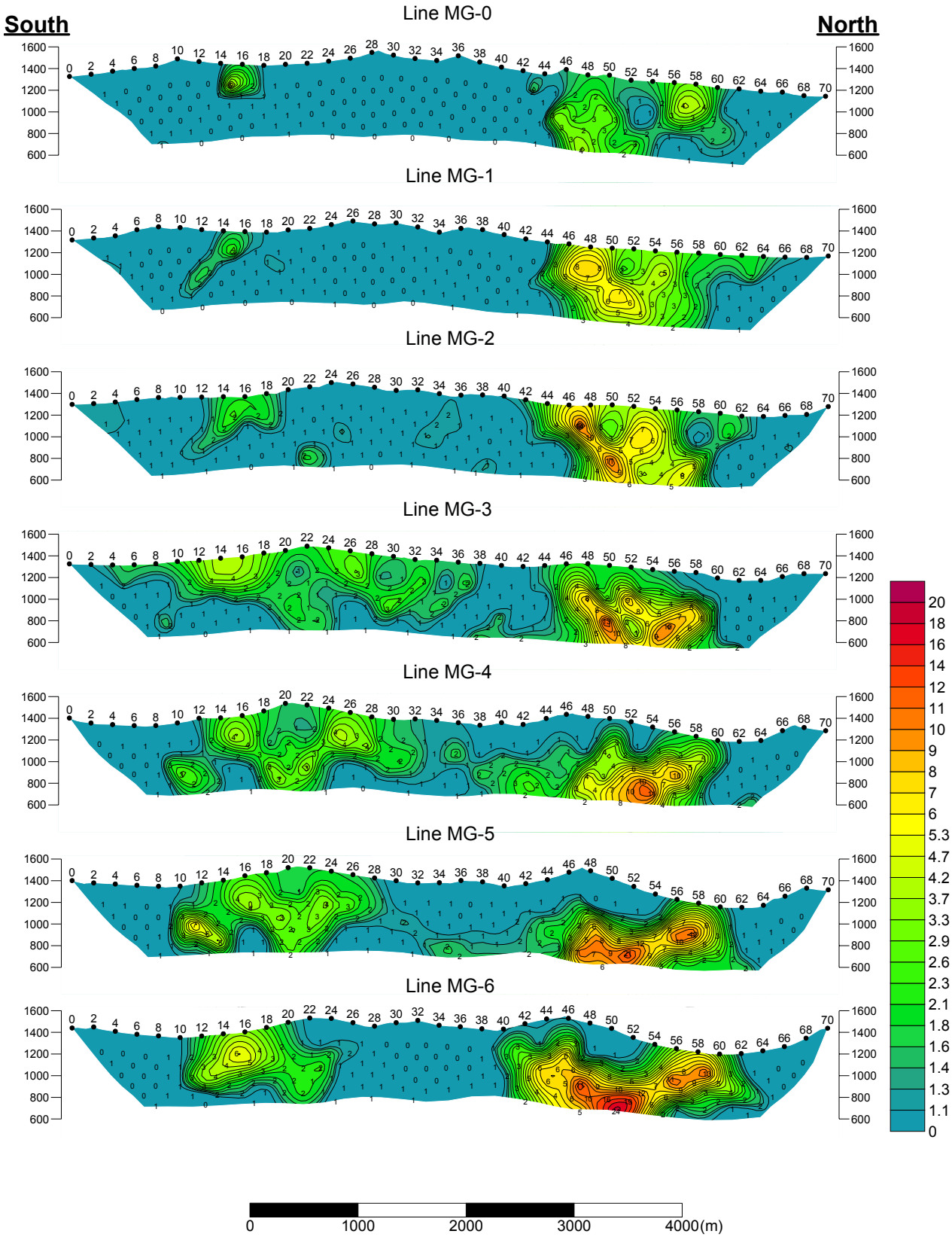

Fig.II-2-42(1)　Metal factor pseudo-seciotns in Mogoin gol area (MG-0 ~ MG-6)

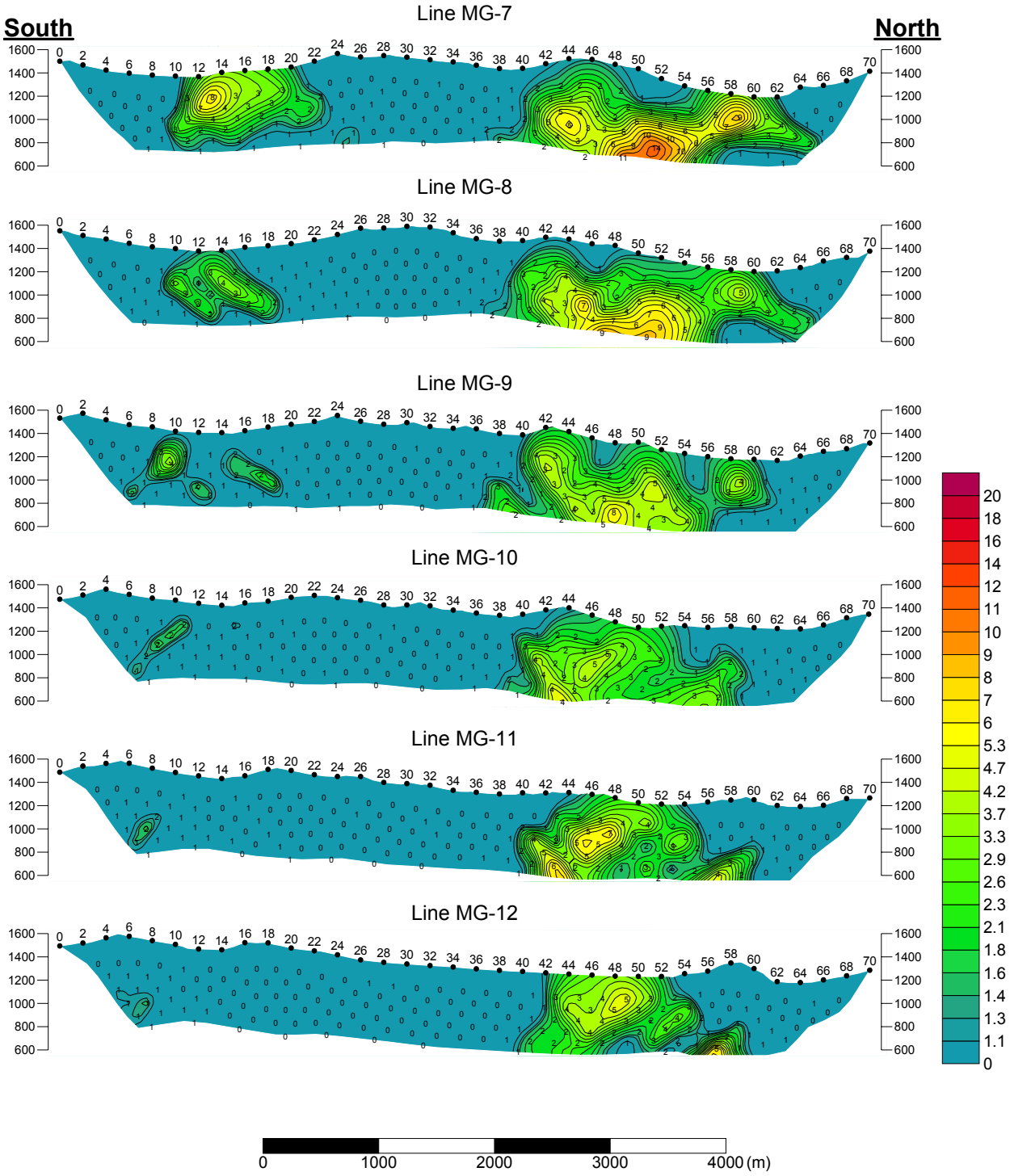

Fig.II-2-42(2)　Metal factor pseudo-seciotns in Mogoin gol area (MG-7 ~ MG-12)

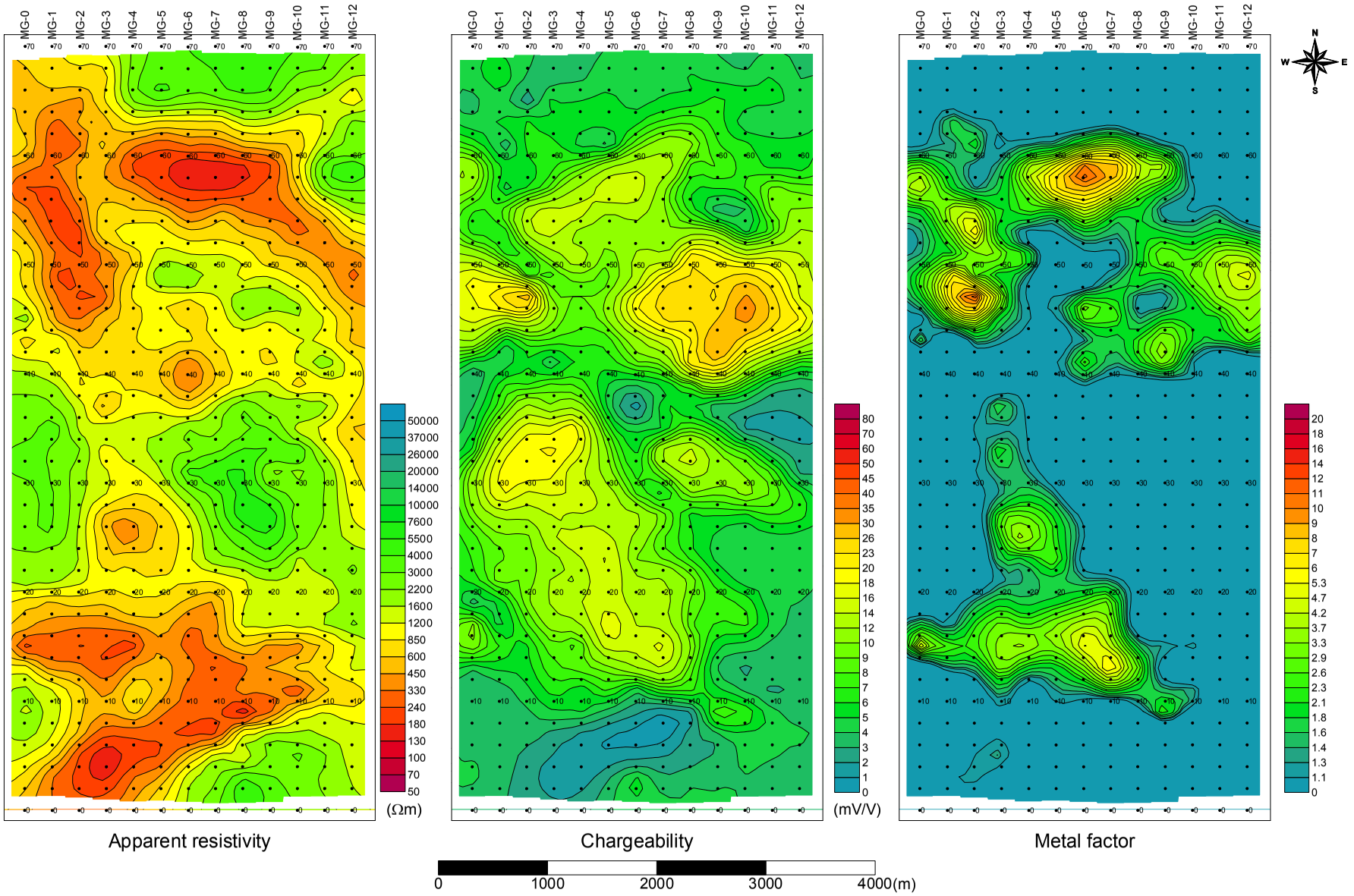

Fig.II-2-43 TDIP plane map for n=1 in Mogoin gol area

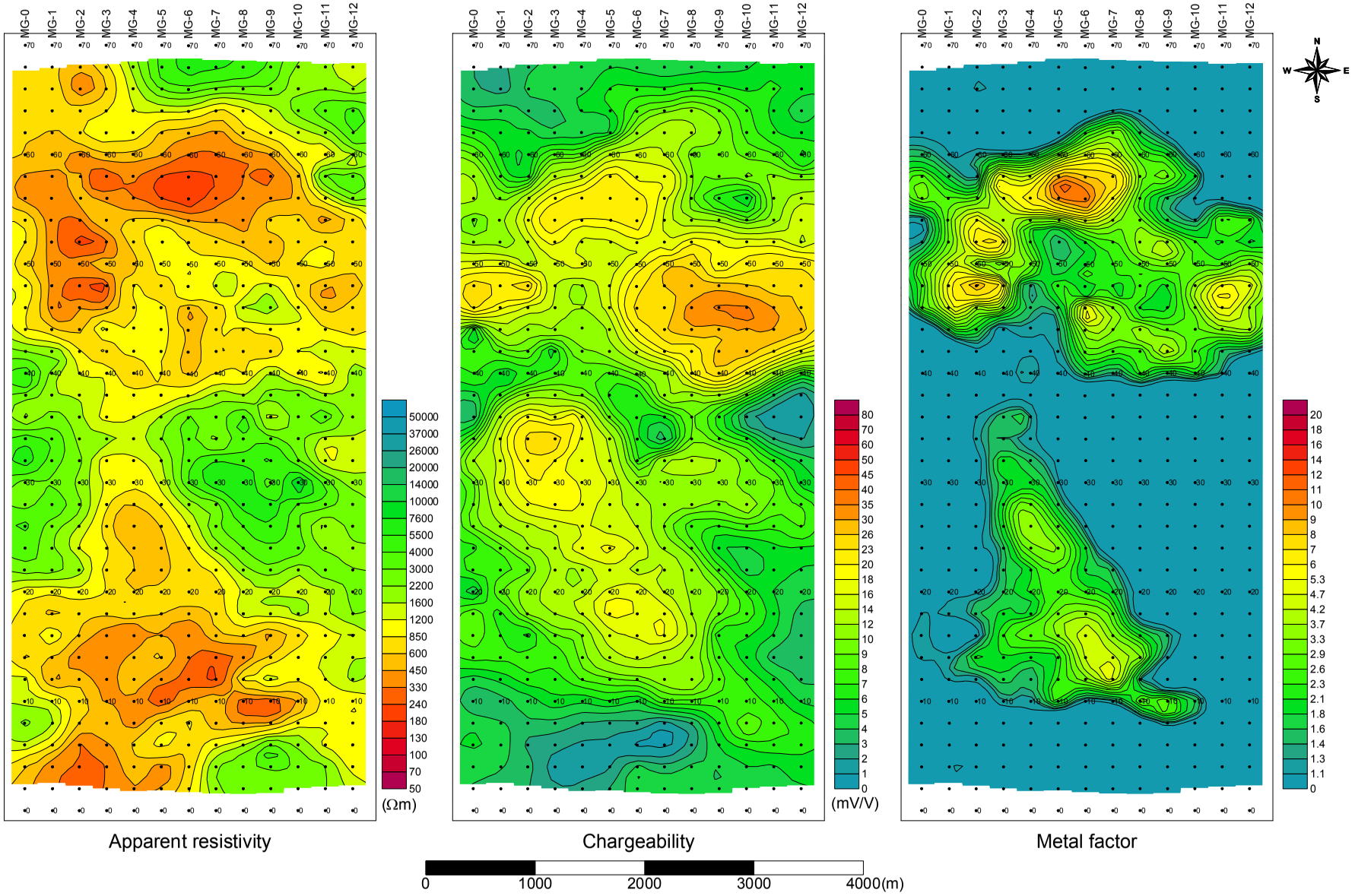

Fig.II-2-44 TDIP plane map for n=2 in Mogoin gol area

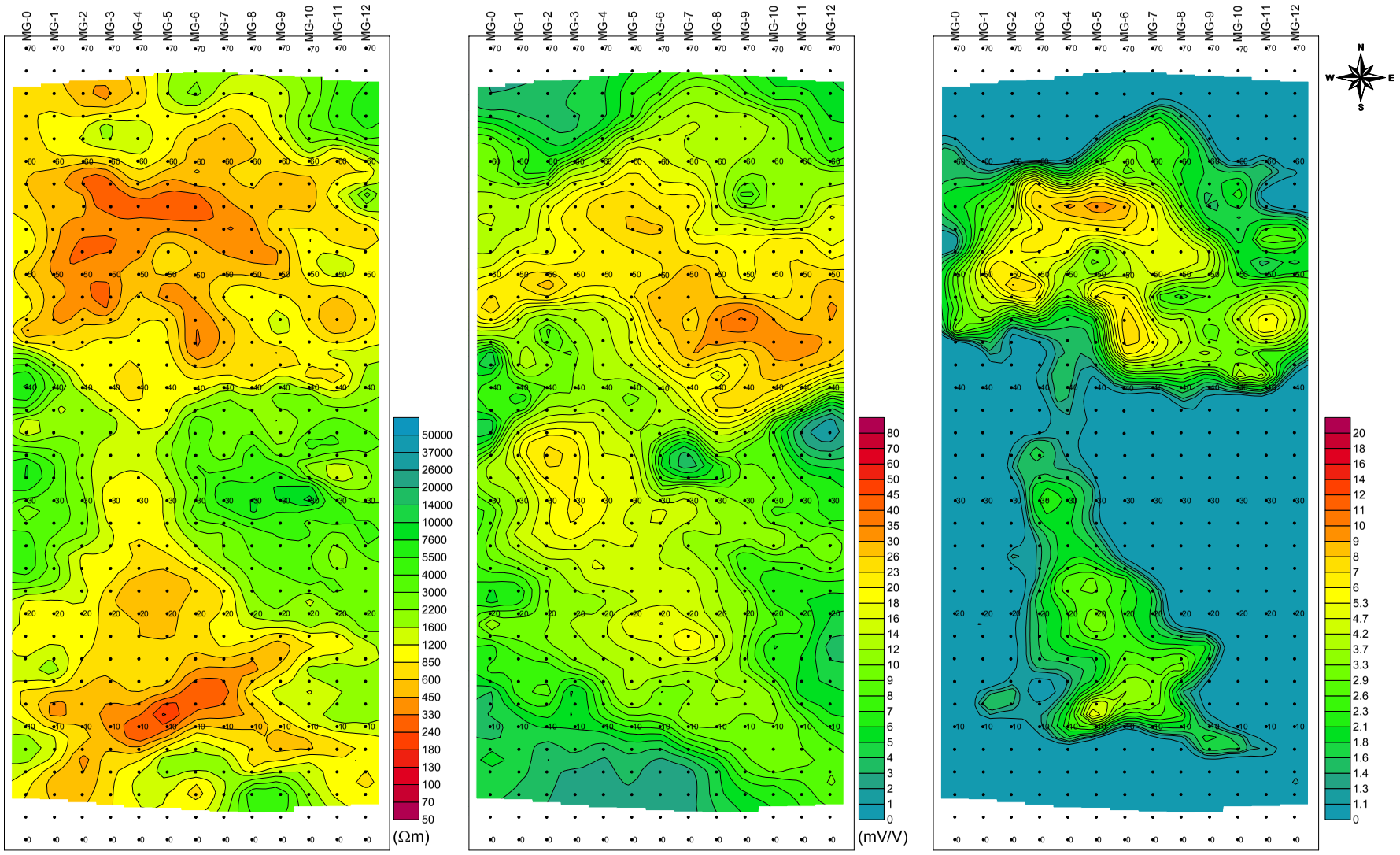

Fig.II-2-45 TDIP plane map for n=3 in Mogoin gol area

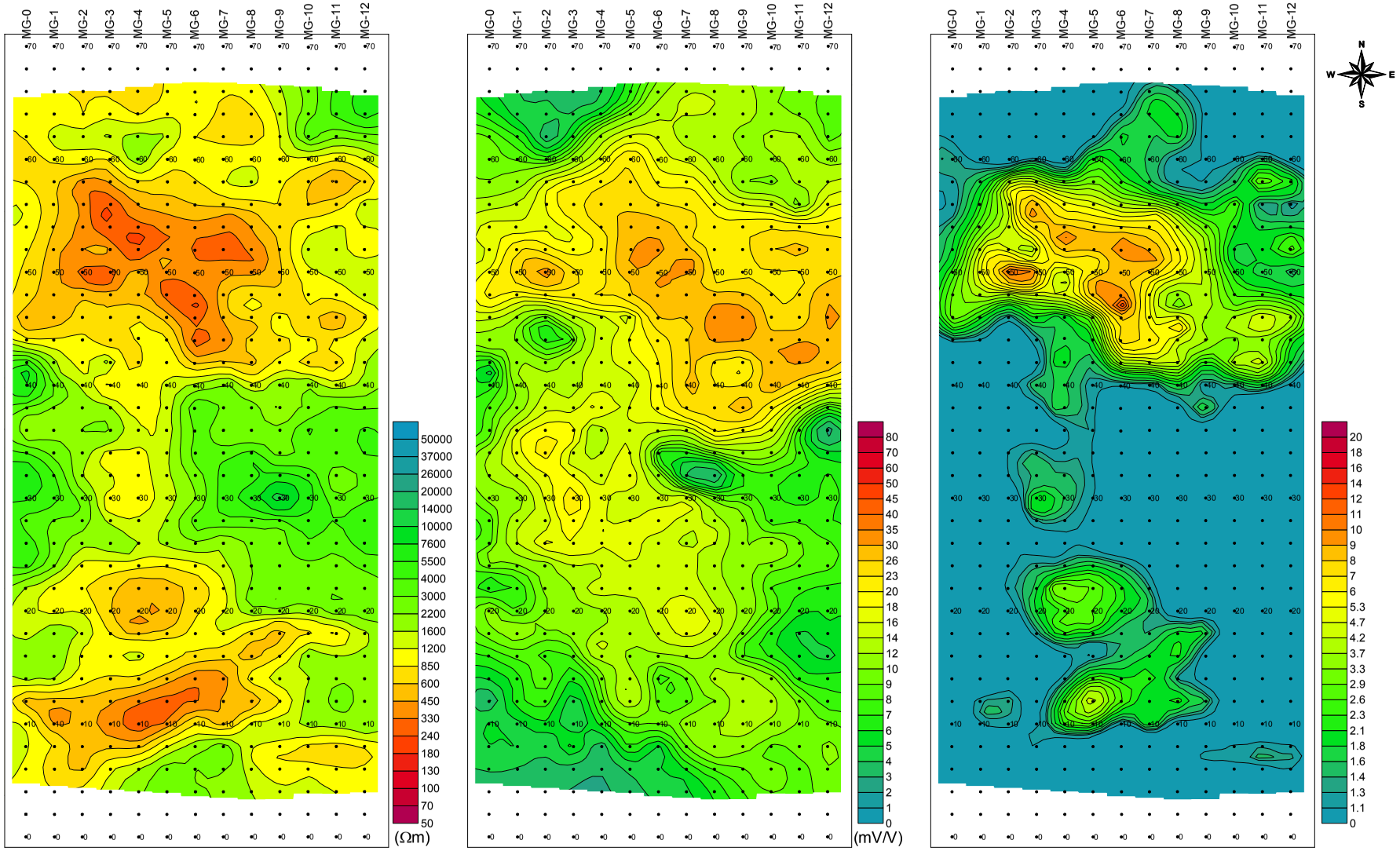

Fig.II-2-46 TDIP plane map for n=4 in Mogoin gol area

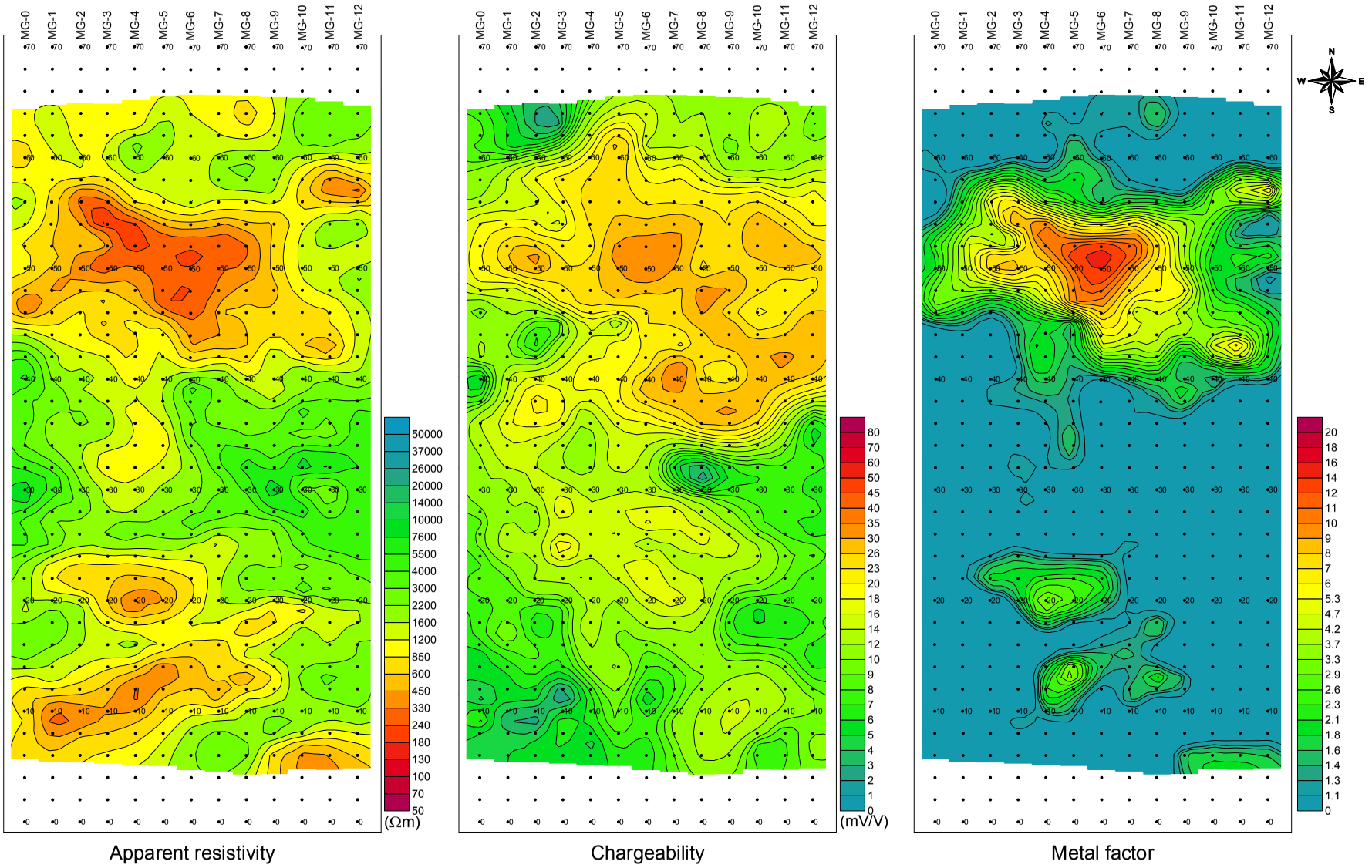

Fig.II-2-47 TDIP plane map for n=5 in Mogoin gol area

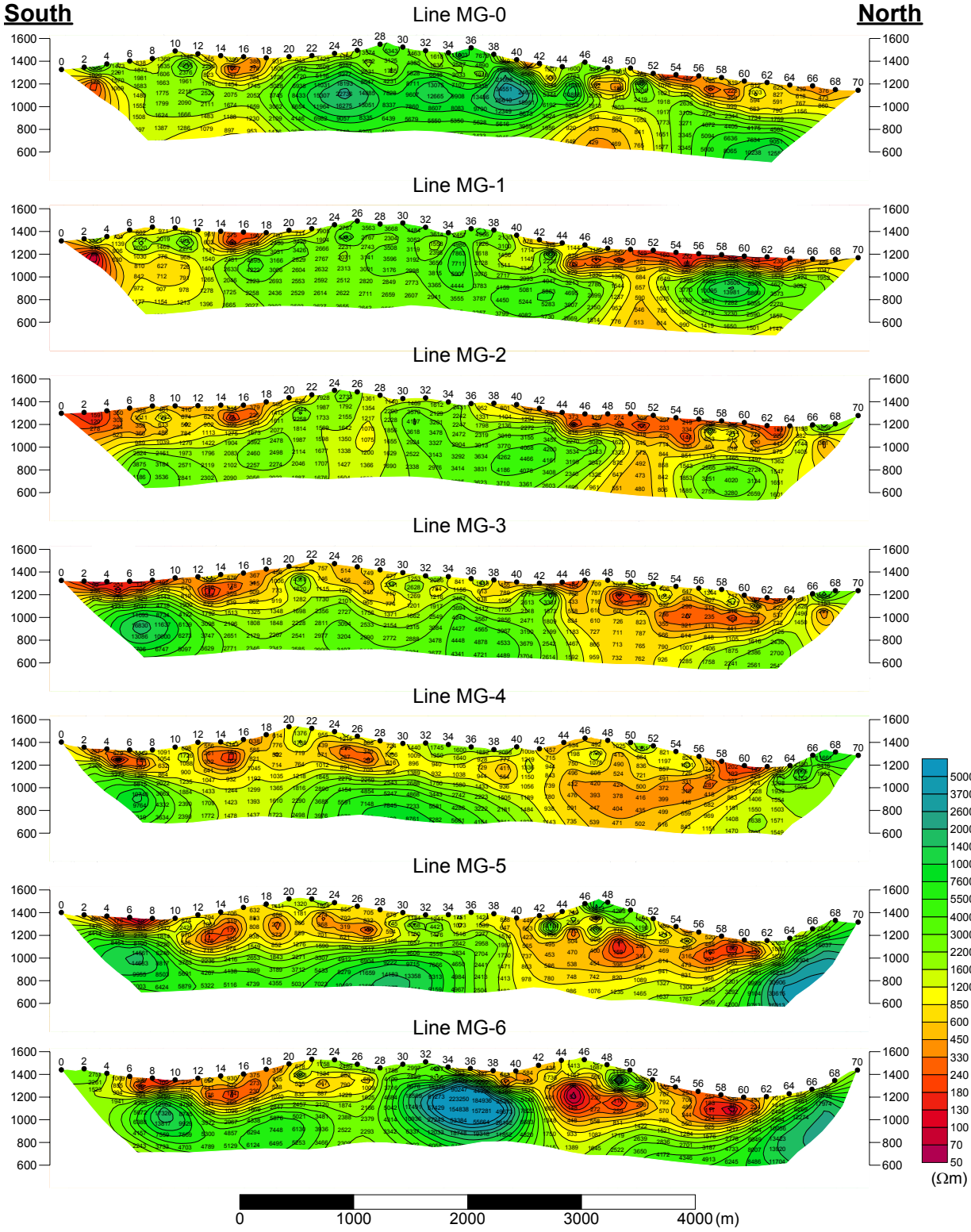

Fig.II-2-48(1)　2D analysis sections for resistivity in Mogoin gol area (MG-0 ~ MG-6)

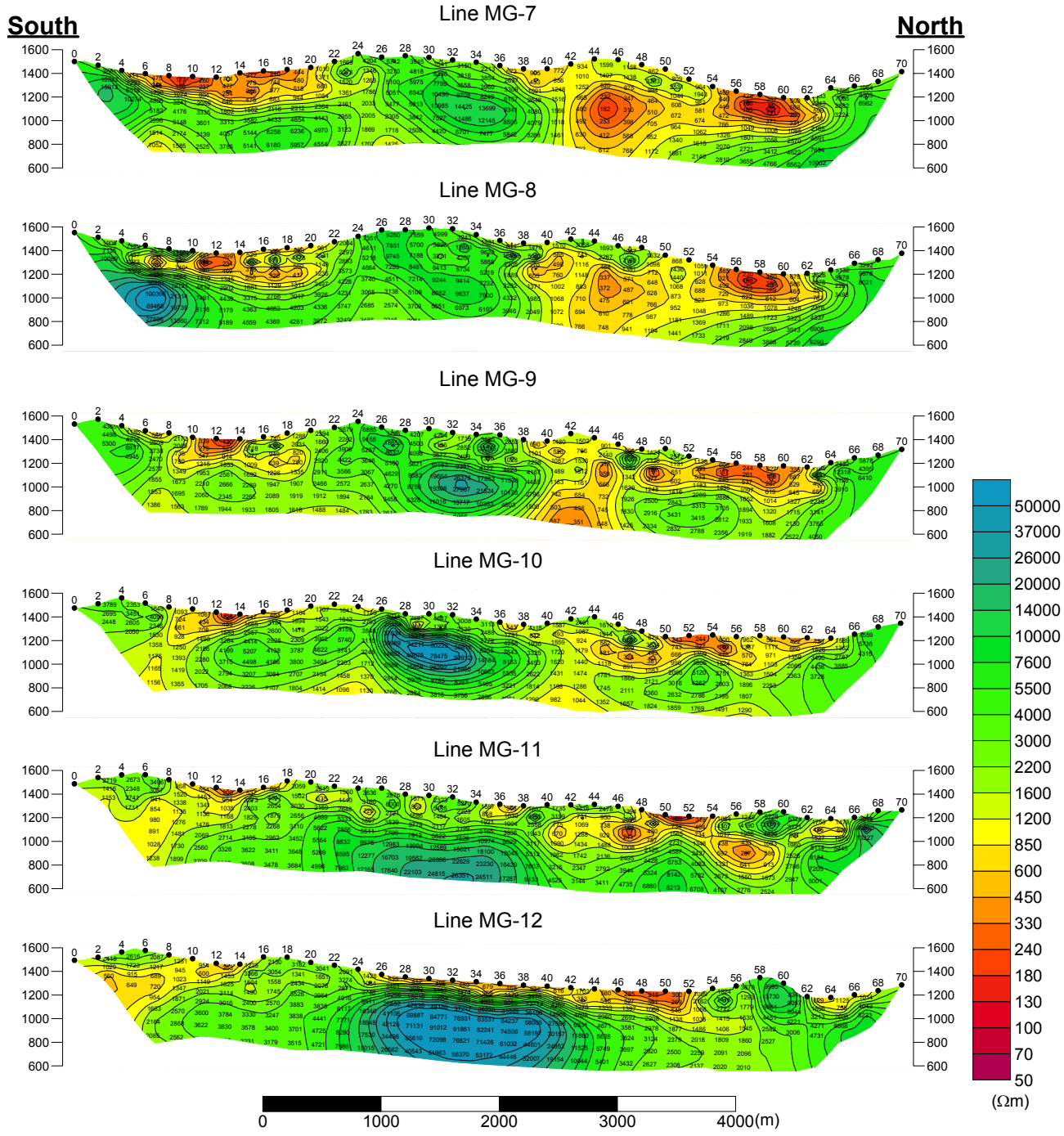

Fig.II-2-48(2)　2D analysis sections for resistivity in Mogoin gol area (MG-7 ~ MG-12)

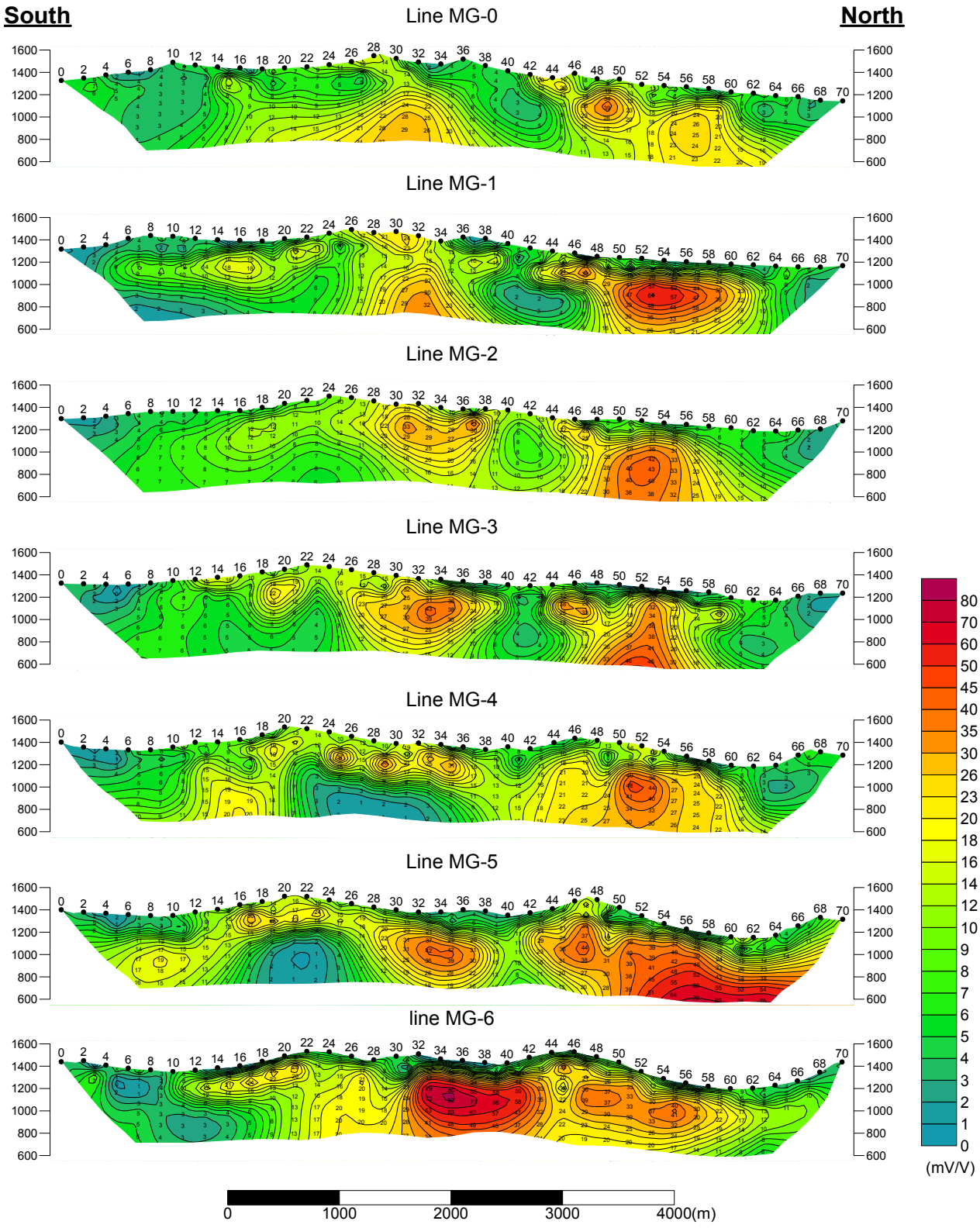

Fig.II-2-49(1)　2D analysis sections for chargeability in Mogoin gol area (MG-0 ~ MG-6)

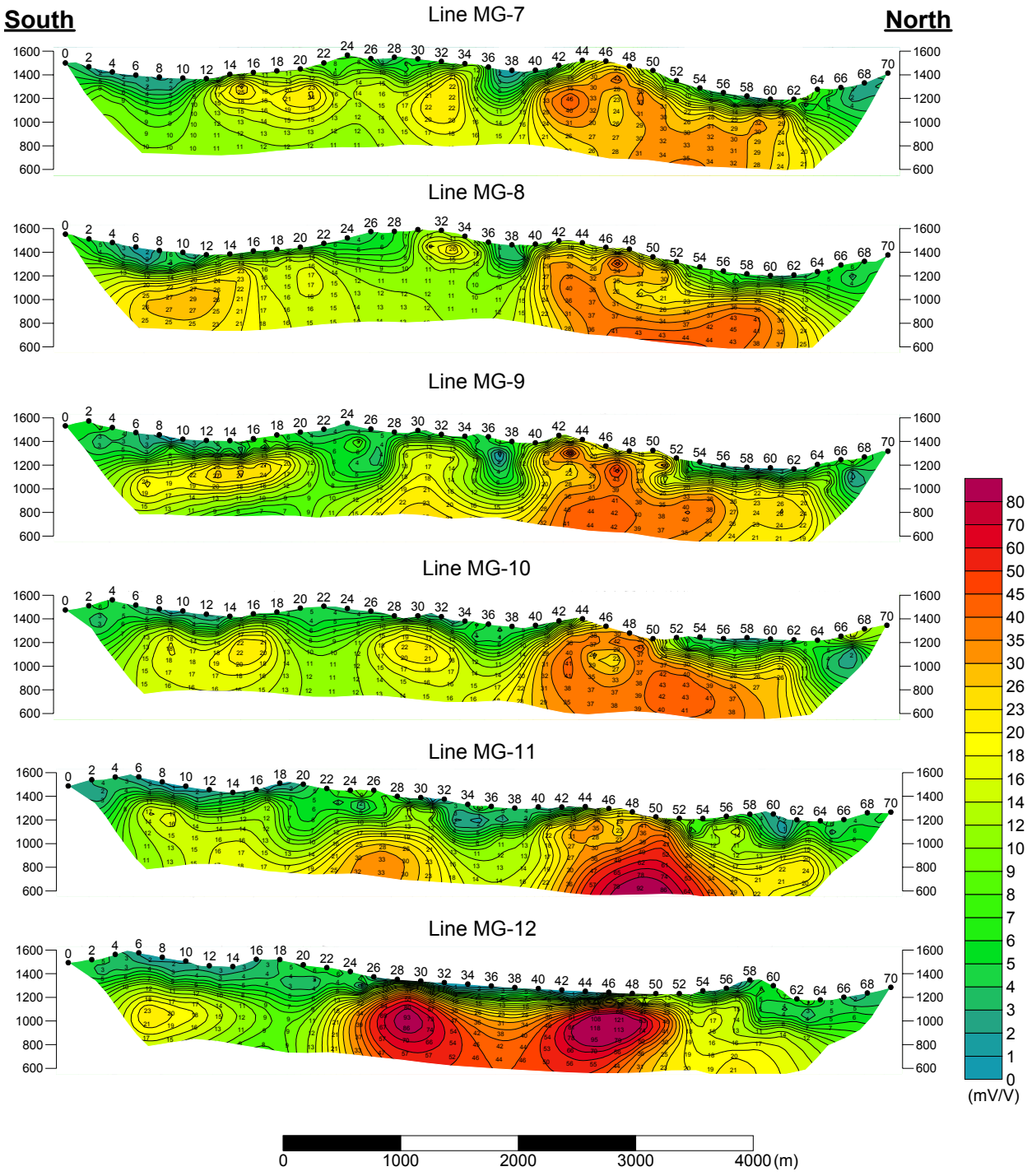

Fig.II-2-49(2)　2D analysis sections for chargeability in Mogoin gol area (MG-7 ~ MG-12)

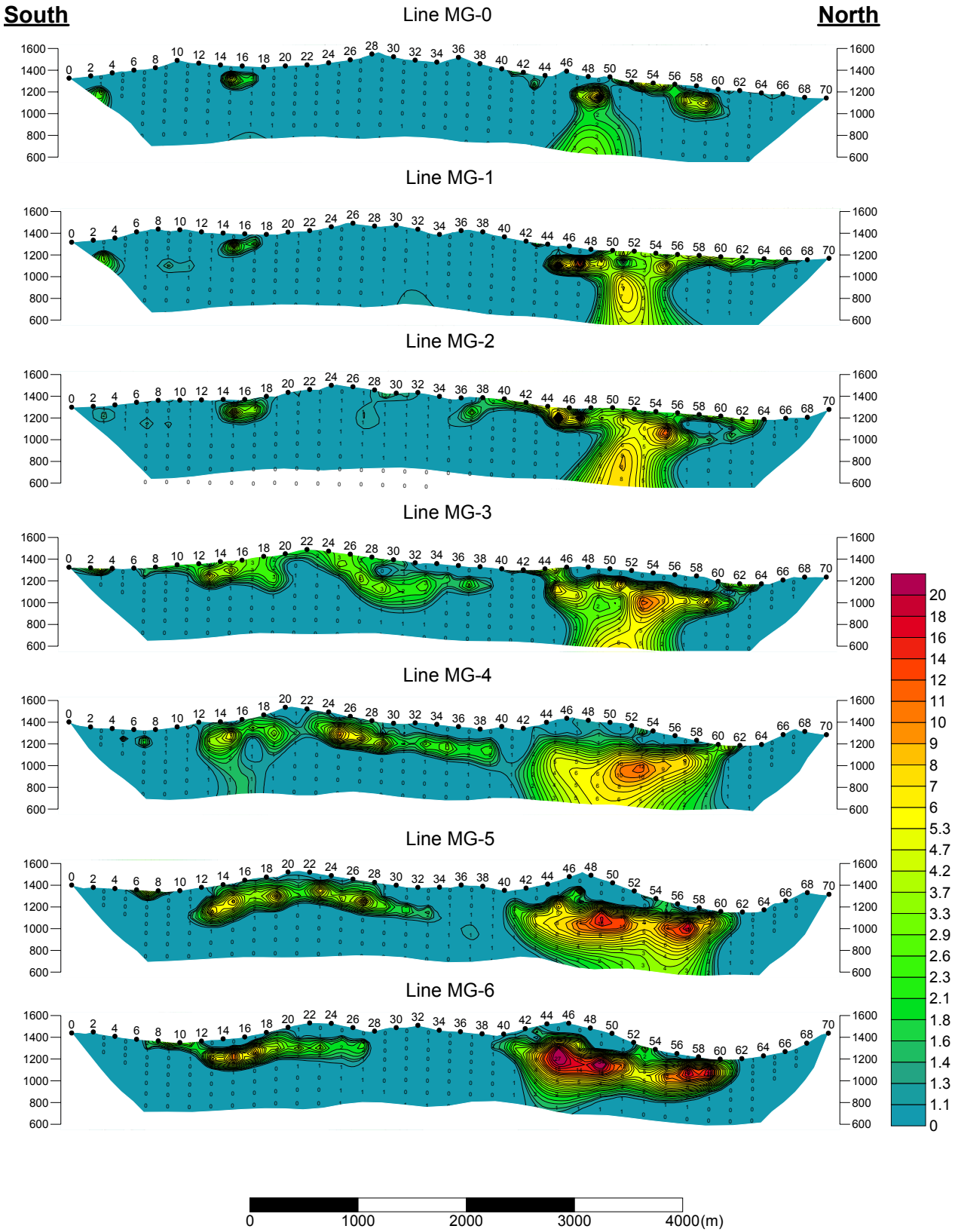

Fig.II-2-50(1) 2D analysis sections for metal factor in Mogoin gol area (MG-0 ~ MG-6)

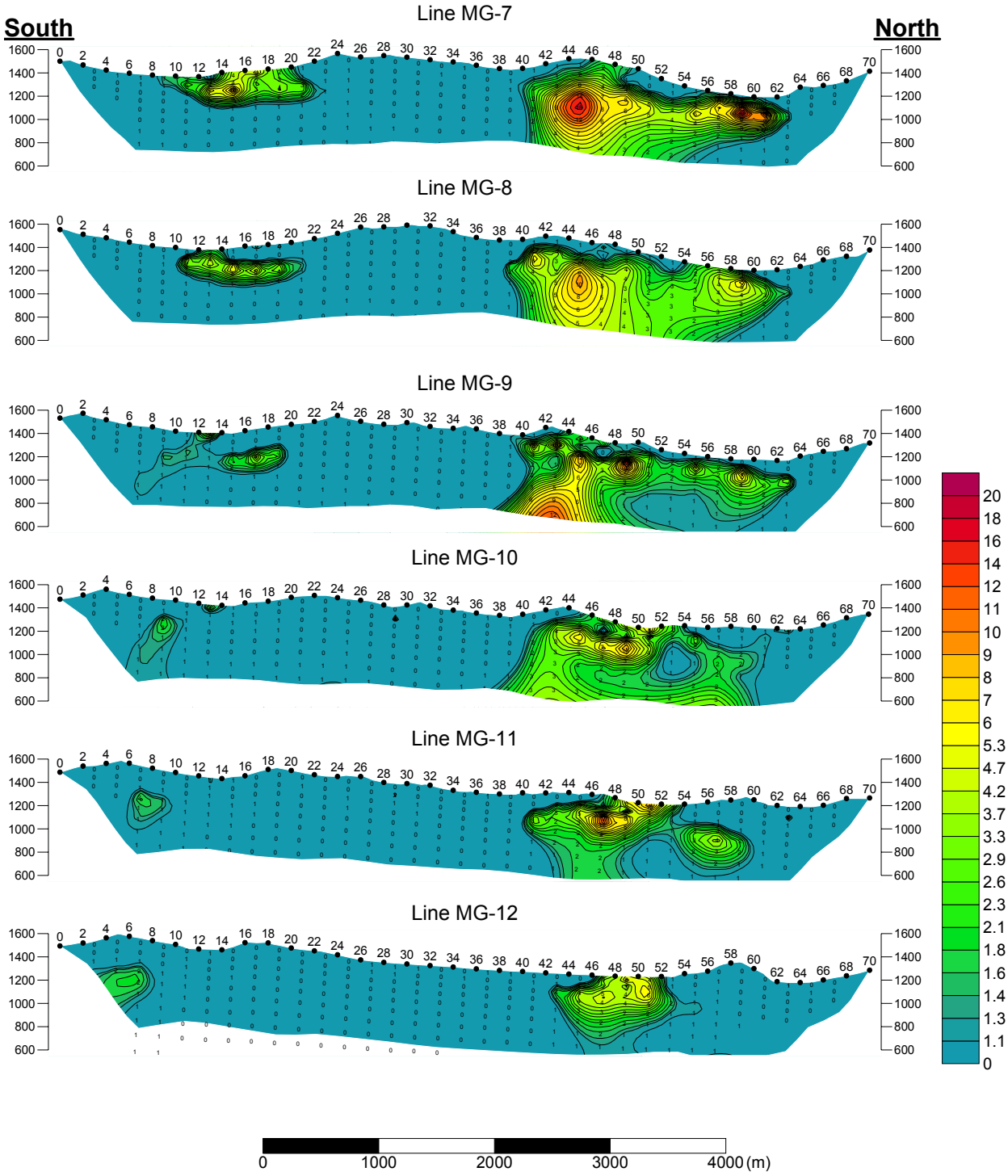

Fig.II-2-50(2)　2D analysis sections for metal factor in Mogoin gol area (MG-7 ~ MG-12)

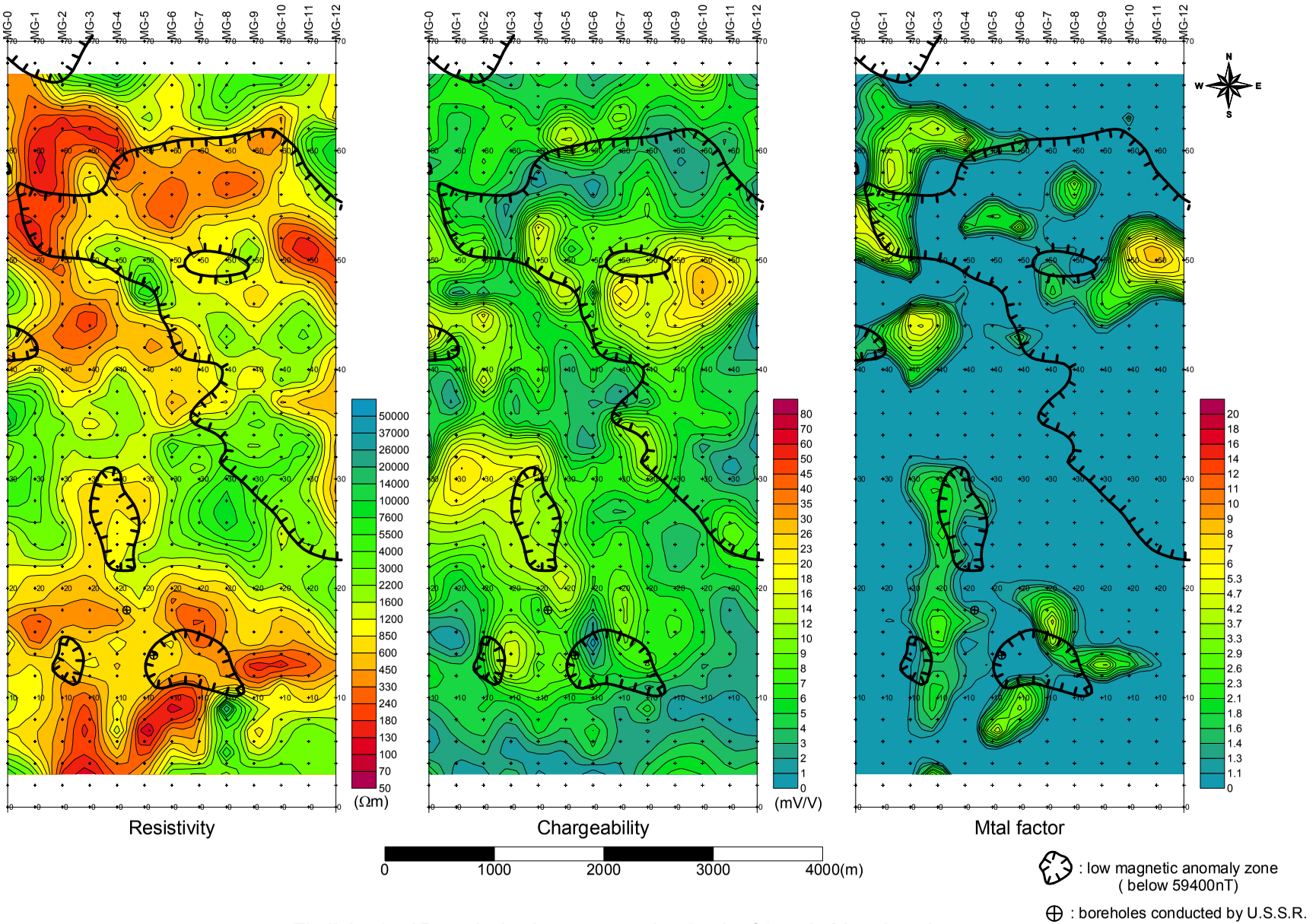

Fig.II-2-51 2D analysis plane map at the depth of 35m in Mogoin gol area

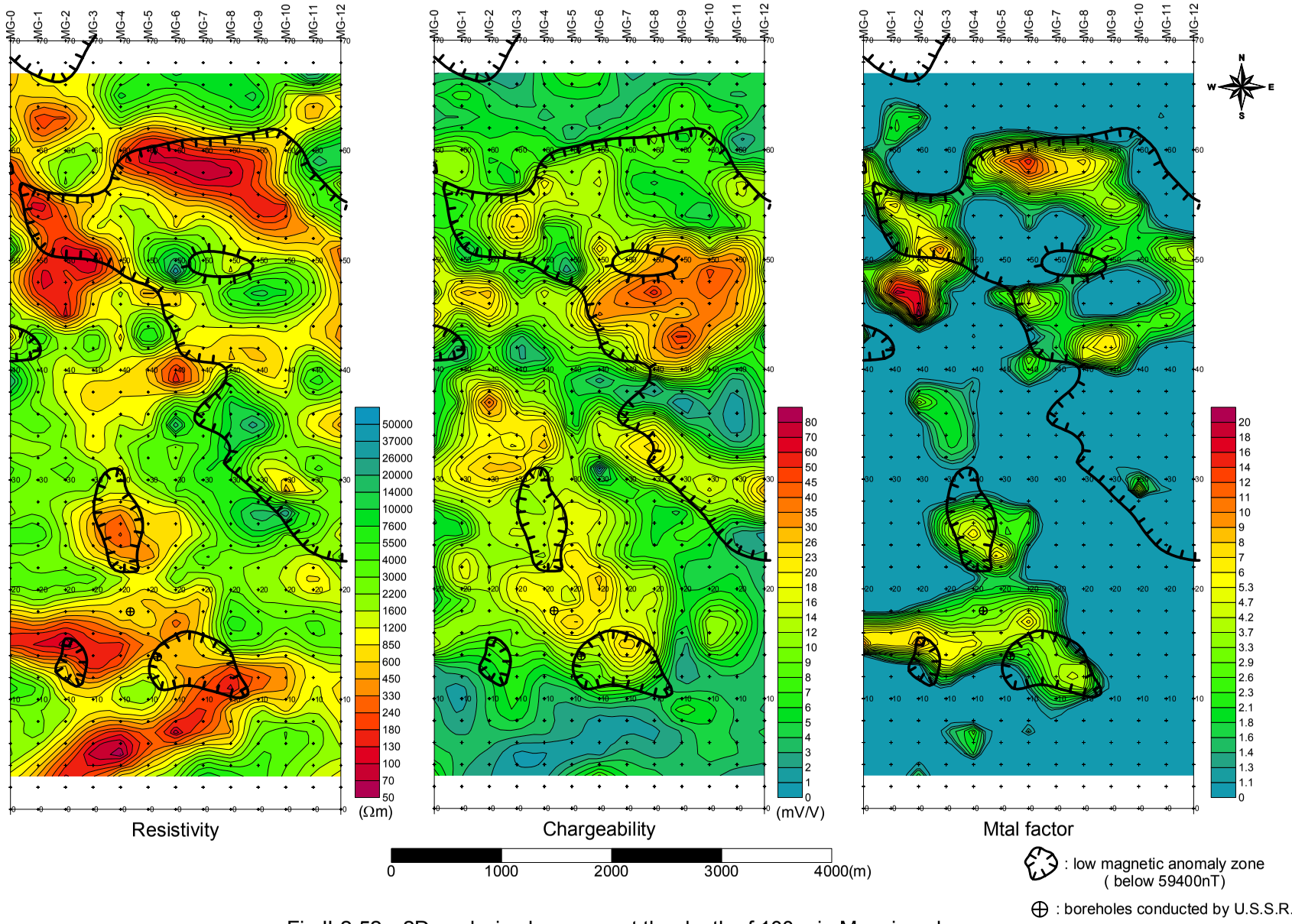

Fig.II-2-52 2D analysis plane map at the depth of 100m in Mogoin gol area

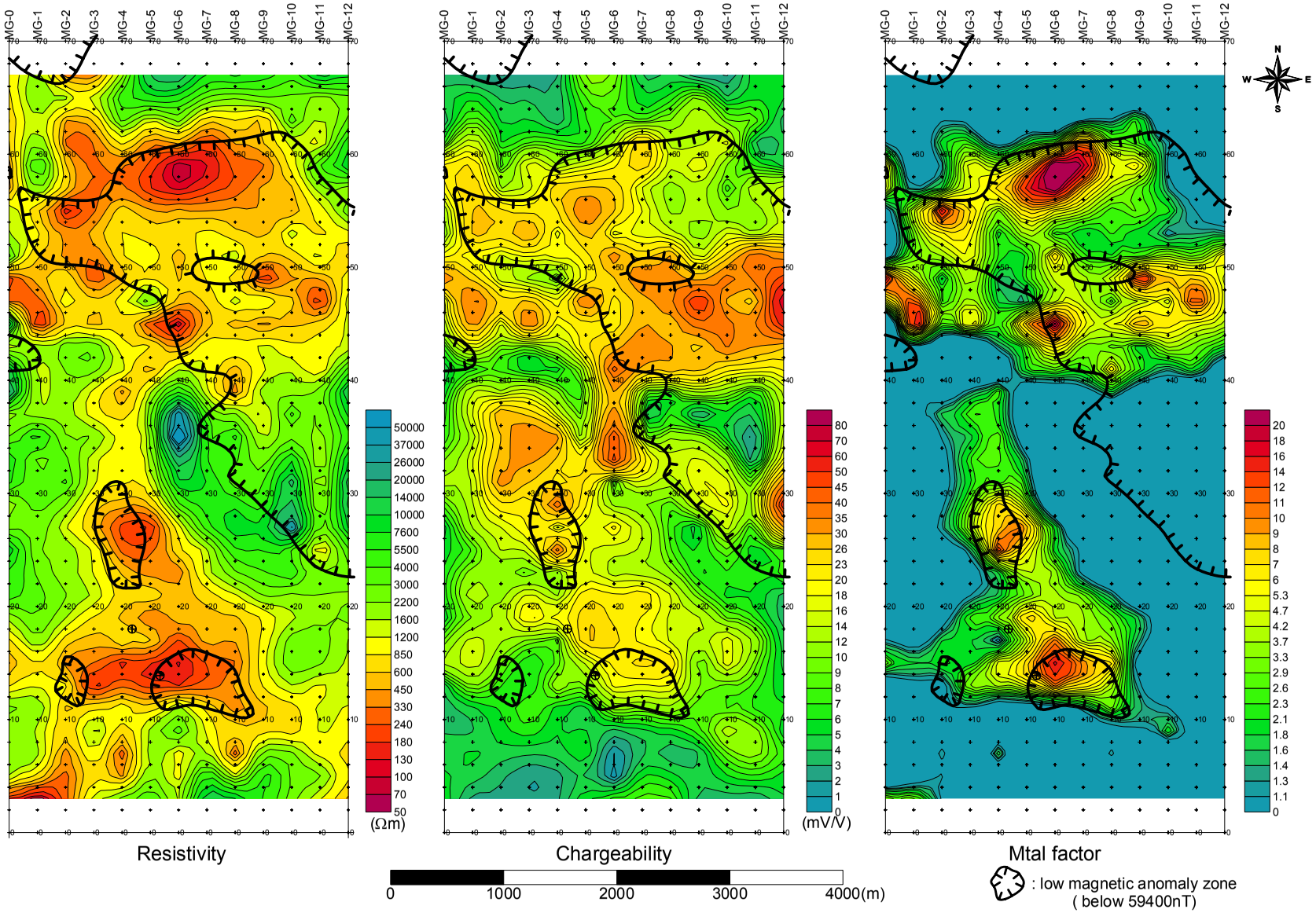

Fig.II-2-53 2D analysis plane map at the depth of 170m in Mogoin gol area

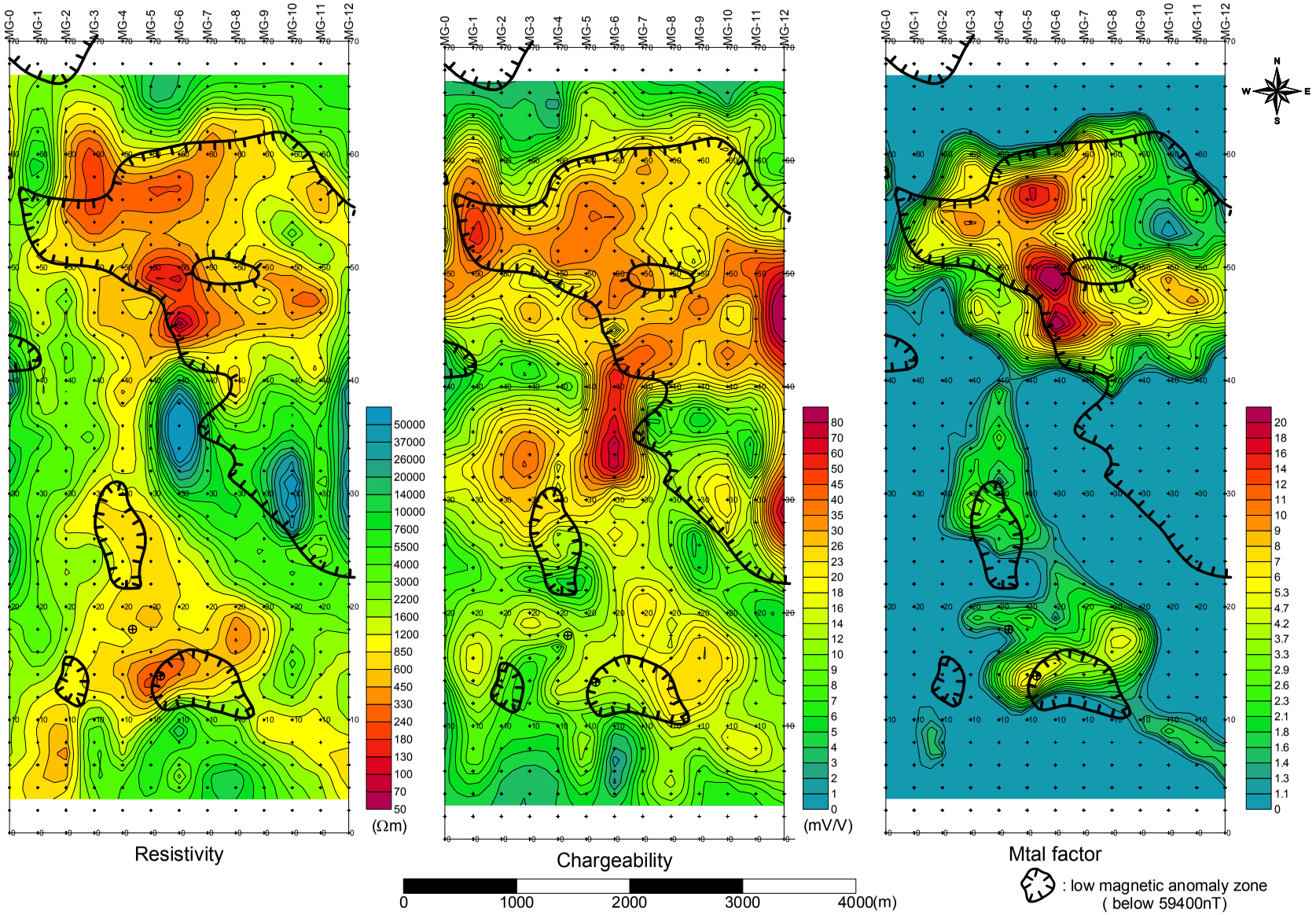

Fig.II-2-54 2D analysis plane map at the depth of 250m in Mogoin gol area

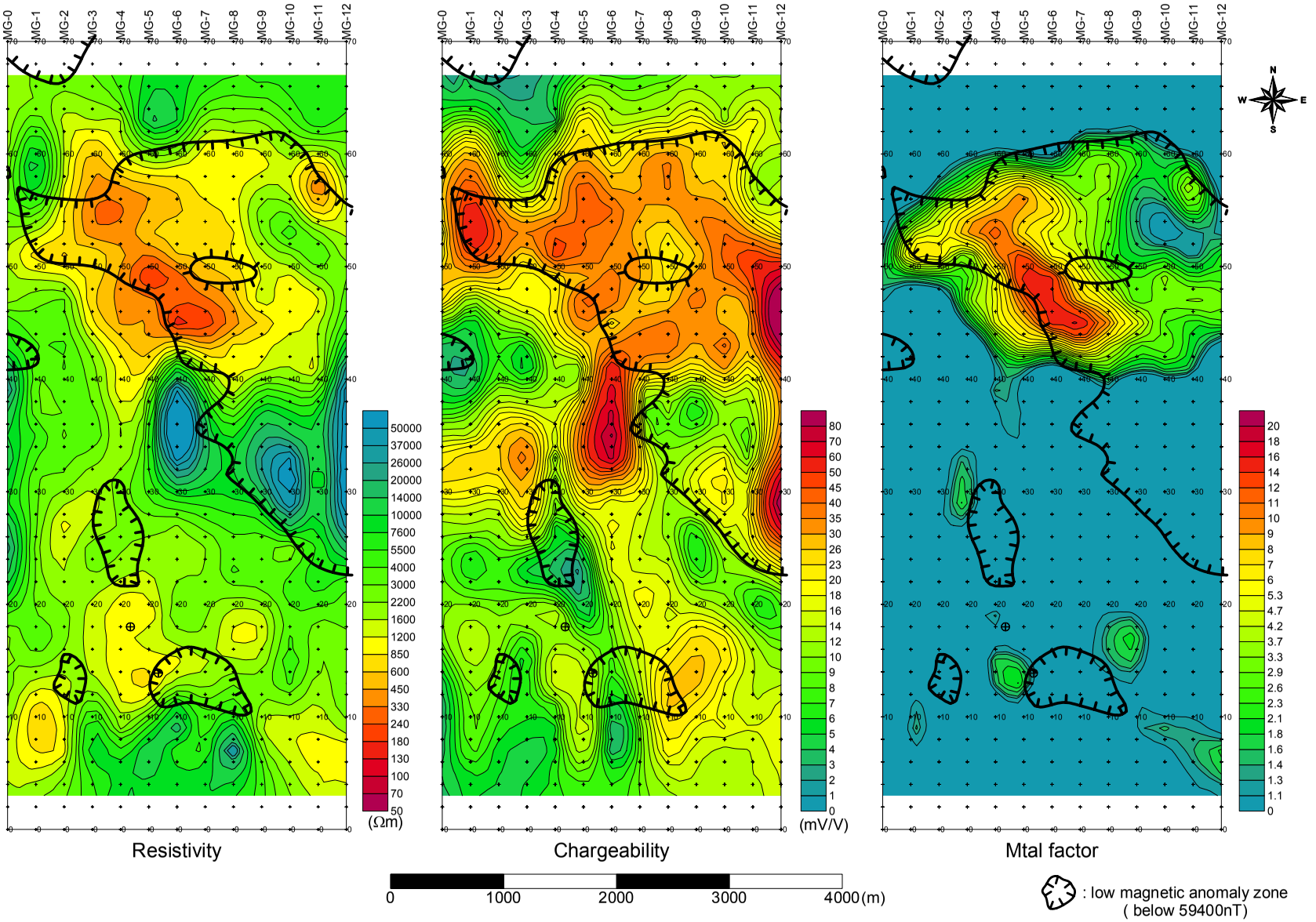

Fig.II-2-55 2D analysis plane map at the depth of 340m in Mogoin gol area

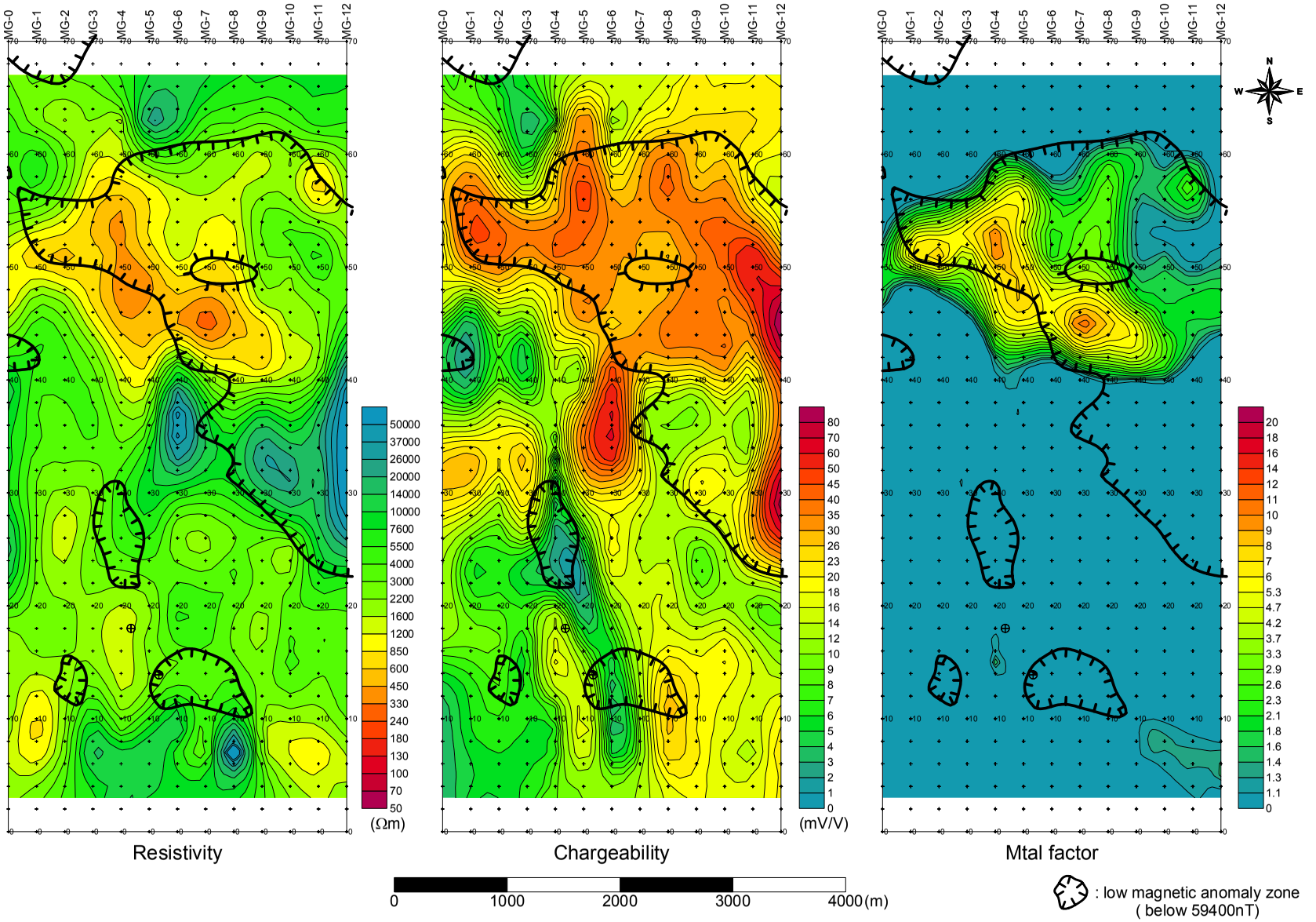

Fig.II-2-56 2D analysis plane map at the depth of 440m in Mogoin gol area

2-5-5 Electrical measurements of rock samples

37 representative rock samples from the survey area were analyzed in order to collect information on electrical properties of rocks.

In general, resistivity and IP measurements in rocks may not reflect in a direct way the intrinsic resistivity or chargeability because of different degree of alteration and water content over the survey area, however clear ideas can be obtained related to the relative variations between rocks units and mineralization.

(1) Measurement method

Measurement of the electrical properties of rock samples, such as resistivity and IP chargeability were carried out on some samples selected from the survey area. The rock samples were formed into a cylindrical shape and thereafter, soaked into water for a reasonable amount of days but not less than 48 hours. Apparent resistivities as well as chargeability values were measured according to the IP time domain procedures in the laboratory. For this purpose, it was used a Lab Downhole Transmitter LDT-10 made by Zonge. During the determinations of the resistivity and chargeability values, the following formulas were utilized:

For Resistivity:

$$\rho = \frac{A}{L} \times \frac{V_p}{I},$$

where ρ is resistivity (Ωm), A the section of the sample (m^2), L the length of the rock sample (m), V_p the voltage (V) and I the current (A)

For Chargeability:

$$M = \frac{1.87}{V_p} \times \int_{t1}^{t2} V_s dT,$$

where M is the chargeability(mV/V), V_p the primary voltage (V), V_s the secondary voltage (mV), dT the sampling interval (sec), $t1$ the off-time voltage 450msec and $t2$ the off-time voltage 1,100msec.

(2) Results

Electrical properties of rocks samples from outcroppings and core drillings were measured in the laboratory. The ore samples from the Erdenet Mine were also measured. Their results are indicated in Table Ⅱ-2-4 (1) and (2).

The resistivity value of ore samples ranges from 7.5 to 4581Ωm and that of the other samples from 1473 to 36kΩm. The chargeability value of ore samples ranges from 4.2 to 145mV/V and that of the other samples from 2.1 to 6.4mV/V.

The ore samples show high chargeability over 100mV/V causing by large amount of sulfide. The resistivity of the ore samples varies widely. It is caused by the difference of content ratio of mineral to host

rock. Lower resistivity value means larger amount of mineral. The sample of No.32 having a vein of pyrite shows anisotropy. The result of the measurement along the vein shows low resistivity and high chargeability affected by mainly pyrite vein, while that across the vein shows high resistivity and low chargeability by mainly host rock.

All the other samples show high resistivity and low chargeability. In general, rock shows high resistivity except for mudstone and shale, and the resistivity varies by the amount of metallic mineral or water. Therefore, high resistivity means that the samples have small porosity and are extremely compact.

Fig.II-2-57 shows correlation between chargeability and resistivity for different types of rock. There is not remarkable correlation between rock type and chargeability or resistivity. The data of andesite and granodiorite show positive correlation between chargeability and resistivity.

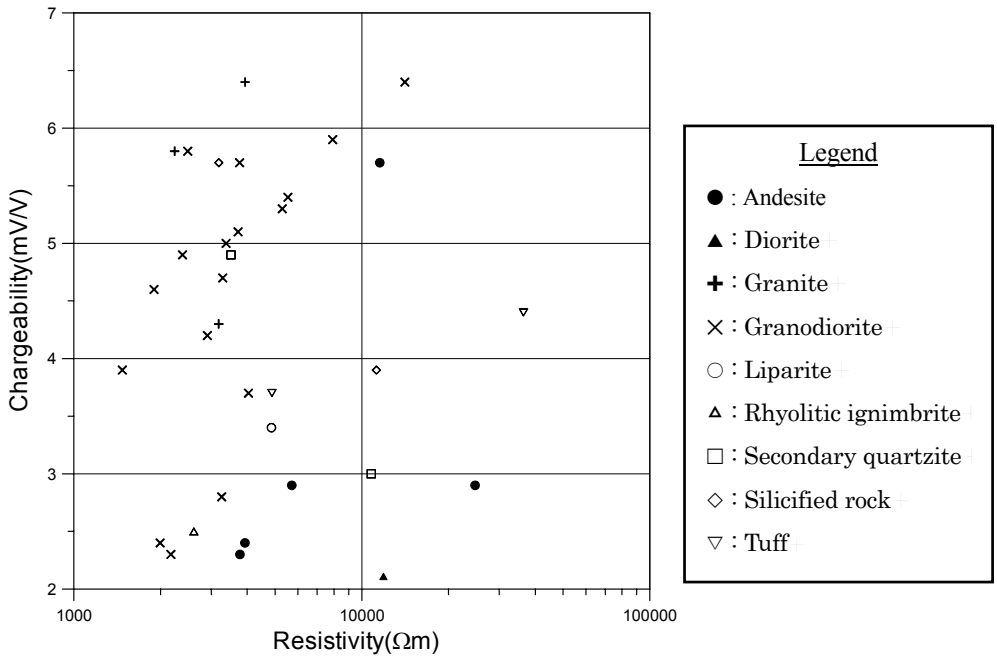

Fig. II-2-57　Correlation between chargeability and resistivity for different types of rock

Table II-2-4 Resistivity and chargeability of outcrop samples

Ser. No.	Sample No.	Area	Coordinates		Rock Name	Geological Unit	Description	Resistivity (Ωm)	Chargeability (mV/V)
			N	E					
1	MA2071	Mogoin gol	5448375	410476	Aphanitic andesite	αβanP2		3771.4	2.3
2	MA2074	Mogoin gol	5449157	410003	Silicified rock	AZ		11227.5	3.9
3	MA2081	Mogoin gol	5447471	410263	Liparite	λJ1		4851.9	3.4
4	MA2082	Mogoin gol	5447376	410221	Andesite	αβanP2		3925.9	2.4
5	MA2083	Mogoin gol	5446885	409720	Secondary quartzite	AZ	white, with malacite+azulite, pyrite holes, lomonite, muscovite.	3512.3	4.9
6	MA2084	Mogoin gol	5446885	409600	Secondary quartzite	AZ		10777.6	3.0
7	MA2088	Mogoin gol	5446153	409721	Silicified argilized rock	AZ	sample from trench, azulite spotted with hematite-limonite-goethite	3187.0	5.7
8	MA2132	Erdenet SE	5429322	445734	Mediume granodiorite	γδ2P2-T1s		1897.9	4.6
9	MA2133	Erdenet SE	5429236	445578	Andesite porphyry	Dαπ		11544.3	5.7
10	MA2138	Erdenet SE	5427557	447309	Mediume granodiorite	γδ2P2-T1s		4039.1	3.7
11	MA2142	Erdenet SE	5426851	444008	Dacitic welded tuff	λtfP1hn1		36411.4	4.4
12	MA2143	Erdenet SE	5426308	445043	Dacitic welded tuff	λtfP1hn1		4875.4	3.7
13	MA2243	Mogoin gol	5447956	408835	Andesite	Dα	with magnetite	5711.6	2.9
14	MB2006	Under/Shand	5402203	440810	Px.ho.bi.Gd.	γδ1P2-T1s	med.grain, massive	5294.4	5.3
15	MB2007	Under/Shand	5402615	441174	Ho.bi.Gd.	γδ1P2-T1s	mod. to strong sili. and kalt. with epi., bi segregate	3288.4	4.7
16	MB2041	Under/Shand	5408603	443260	Ho.bi.Gd.	γδ1P2-T1s	med.grain, euhedral ho.inc., weak sili.and chl.	7921.5	5.9
17	MB2042B	Under/Shand	5409592	442130	Rhyoitic ignimbrite	αtfP1hn1	vitric-crystalline tf., kf.show pink color	2611.0	2.5
18	MB2053	Under/Shand	5406985	441760	Ho.bi.Gd.	γδπ2P2-T1s	pl.porph., strong sili., moderate kalt., heterogeneous	2908.9	4.2
19	MB2069	Under/Shand	5406406	443052	Ho.bi.Gd.	γδ1P2-T1s	med.grain, euhedral ho.inc., bi.segregate	3719.4	5.1
20	MB2088	Under/Shand	5401828	438601	Ho.bi.Gd.	γδ1P2-T1s	coarese grain, massive	3378.7	5.0
21	MB2094	Under/Shand	5400872	441253	Ho.bi.Gd.	γδπ2P2-T1s	pl.porph.,bi.remain	5538.3	5.4
22	MB2096	Under/Shand	5401747	443169	Ho.bi.Gd.	γδπ2P2-T1s	pl.porph., modeate to strong kalt.and epi.alt., bi.remain	2384.1	4.9
23	MB2097	Under/Shand	5401261	441860	Ho.bi.Gd.	γδ2P2-T1s	pl.porph.in place, med.to coar.grain, ho.bi.remain	3765.4	5.7
24	MB2098	Under/Shand	5406114	439905	Ho.bi.Gr.	γδ3P2-T1 s	med.grain, weak to no.sili.,bi.remain	2238.0	5.8
25	MB2099	Under/Shand	5406951	439649	Ho.bi.Gd.	γδ2P2-T1s	med.garain, strong sili.and mod.kalt.	2485.0	5.8
26	MB2100	Under/Shand	5407178	439677	Micro diorite	δ2P2-T1s	glassy	11882.9	2.1
27	MB2101	Under/Shand	5407568	439770	Ho.bi.Gd.	γδ2P2-T1s	pl.porph.n place, strong kalt.and mod.sili.	3261.1	2.8
28	MB2102	Under/Shand	5407260	439406	Strong silicified Gd.	γδ2P2-T1s	aplite-like, pink to gray color	2173.4	2.3
29	MB2103	Under/Shand	5407345	440036	Strong silicified Gr.	γδ2P2-T1s	pl.porph.in place, chl.alt.	3933.6	6.4
30	MB2113	Erdenet Mine			Gr.po.(strong greisenizated)	γπ3P2-T1s	strong silicified and bleached with Py., Cu.(bornite)	7.5	128.6
31	MB2114	Erdenet Mine			Gr.po.(mod. greisenizated)	γπ3P2-T1s	strong silicified and bleached with Py., Cu.	90.4	145.1
32	MB2115	Erdenet Mine			Gr.po.(weak greisenizated)	γπ3P2-T1s	strong silicified and bleached with Py., Cu., Mo.	11.0 / 4580.6	80.9 / 4.2
33	MD2021	Under/Shand	5405319	439616	Bi.Gr.	ξπ2P2-T1 s	kf.porph., mod.silicified, resemble to aplite	3183.1	4.3
34	MD2026	Under/Shand	5408236	442935	Oxidized Gd.	ξπ3P2-T1s	in oxidized zone of Gd.with silicified and bleaching	1994.1	2.4
35	MD2029	Under/Shand	5409132	442938	Bsaltic Ad.	αP1hn1	dyke?, magnetic, dark gray color	24741.7	2.9
36	MD2030	Under/Shand	5410020	442710	Ho.bi.Gd.	γδ1P2-T1s	kf.porph., med.grain, strong to mod.sili., kalt., chl.	1473.2	3.9
37	MD2062	Under/Shand	5400869	441206	Ho.bi.Gd.	γδπ2P2-T1s	pl.porph., mod.kalt.with Cu.	14105.7	6.4

2-6 Further Considerations

The results of the geophysical survey at the Under/Shand area, Mogoin gol area and Erdenet SE area are considered as follows.

3-D analysis was conducted experimentally for the data of each area.

2-6-1 Under/Shand area

In this area, low resistivity zones below 500Ωm are detected along the direction of NW-SE, N-S and NE-SW. These low resistivity zones are considered to reflect fracture or alteration around the boundary of granodiorite or porphyritic granodiorite. The plane maps of 3-D analysis are shown in Figs.II-2-58 to II-2-60.

In the Under/Shand 1 area, a weak IP anomaly zone is detected at the northeast part. High chargeability continues from shallow to deep part, while resistivity shows relatively low value at shallow part(100 to 200m depth), and high value at deeper part(below 240m). Based on the results of analysis and the fact of declination disturbance on the compass, this anomaly is estimated to reflect weak mineralization of magnetite. This anomaly zone is located between 2 high magnetic anomaly zones detected by airborne magnetic survey. The low magnetic anomaly zone is located at the low resistivity zone in the direction of NE-SE. The results of 3-D analysis are almost same as that of 2-D analysis.

In the Under/Shand 2 area, low resistivity anomaly zone is detected along the direction of E-W below the depth of 170m. It is estimated that some alteration affecting to resistivity exists but the alteration is not related to sulphide because the chargeability shows low value. The low resistivity anomaly zone at the deep part is distributed along the south edge of low magnetic anomaly zone. The results of 3-D analysis are almost same as that of 2-D analysis.

In the Under/Shand 3 area, remarkable IP anomaly is detected. This anomaly shows high chargeability(maximum is 58mV/V) and low resistivity, and is considered to reflect the mineralization of sulphide minerals. This IP anomaly zone shows ring-shaped pattern at the depth of 100m to 200m, and continues to deeper part. The anomaly zone extends horizontally 1200m from east to west and 1000m from north to south. It corresponds to the low magnetic anomaly zone detected by airborne magnetic survey. The results of 3-D analysis are almost same as that of 2-D analysis. The sections of 3-D analysis results are shown in Fig.II-2-61.

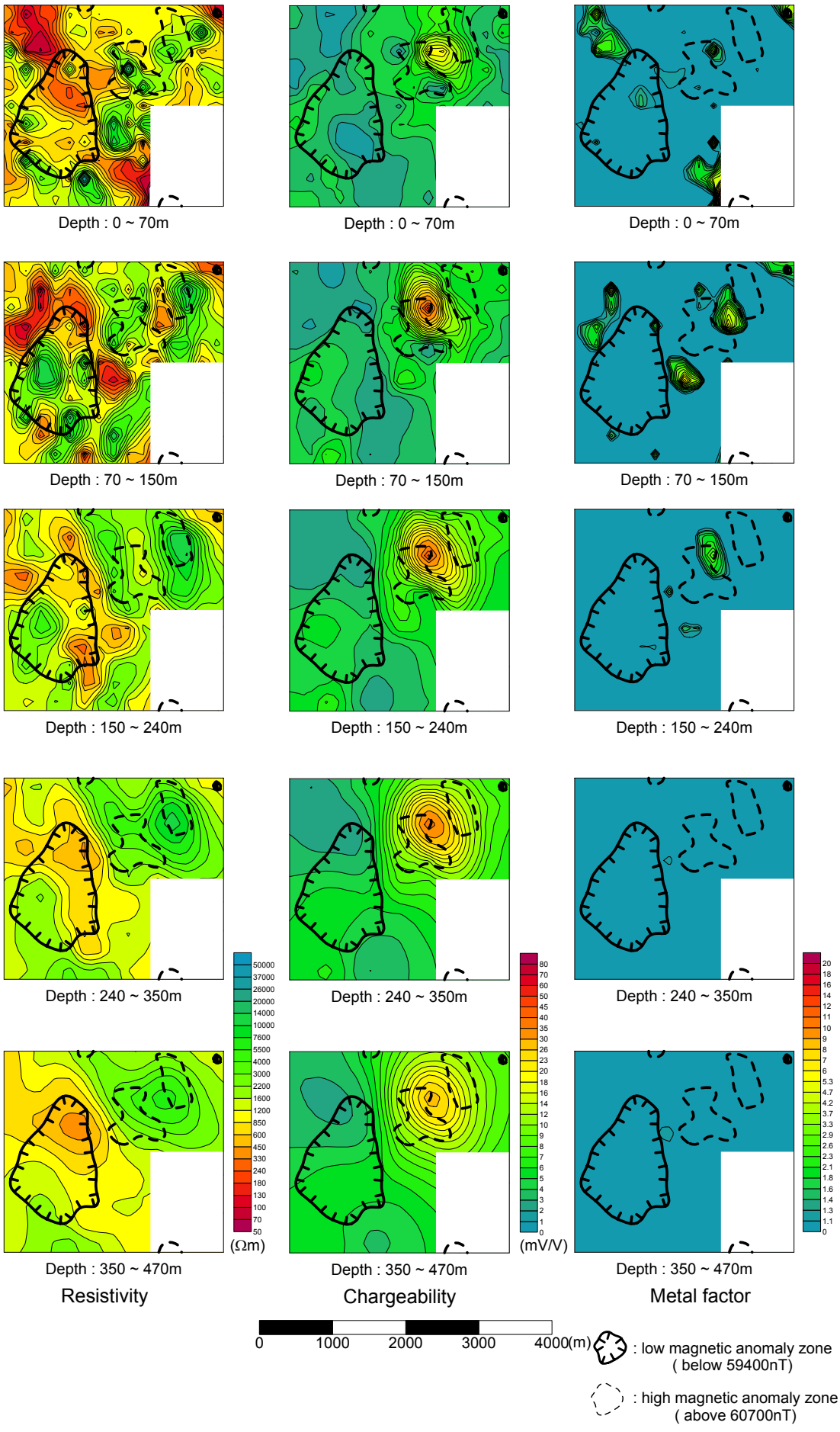

Fig.II-2-58　3D analysis plane map in Under/Shand_1 area

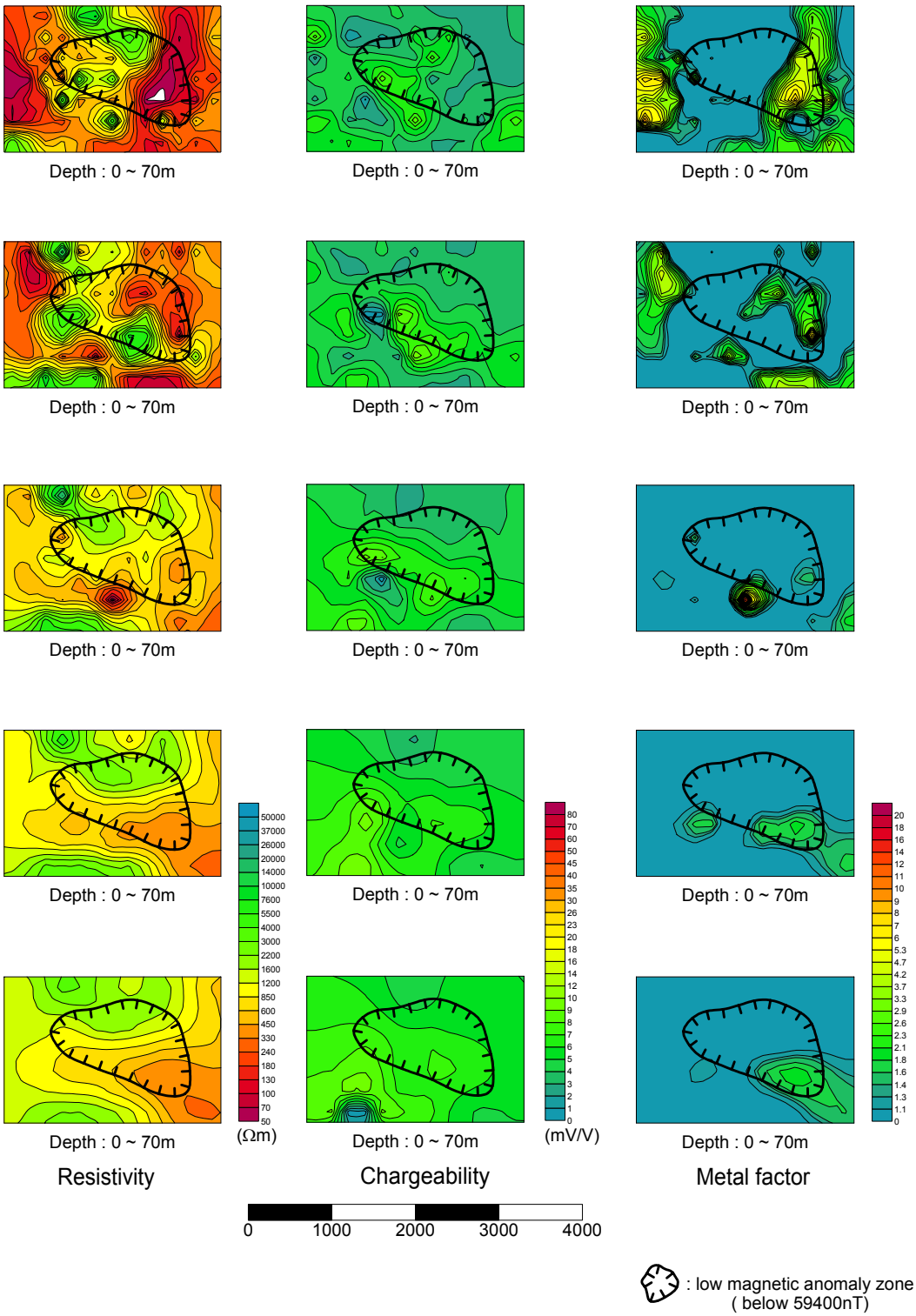

Fig.II-2-59　3D analysis plane map in Under/Shand_2 area

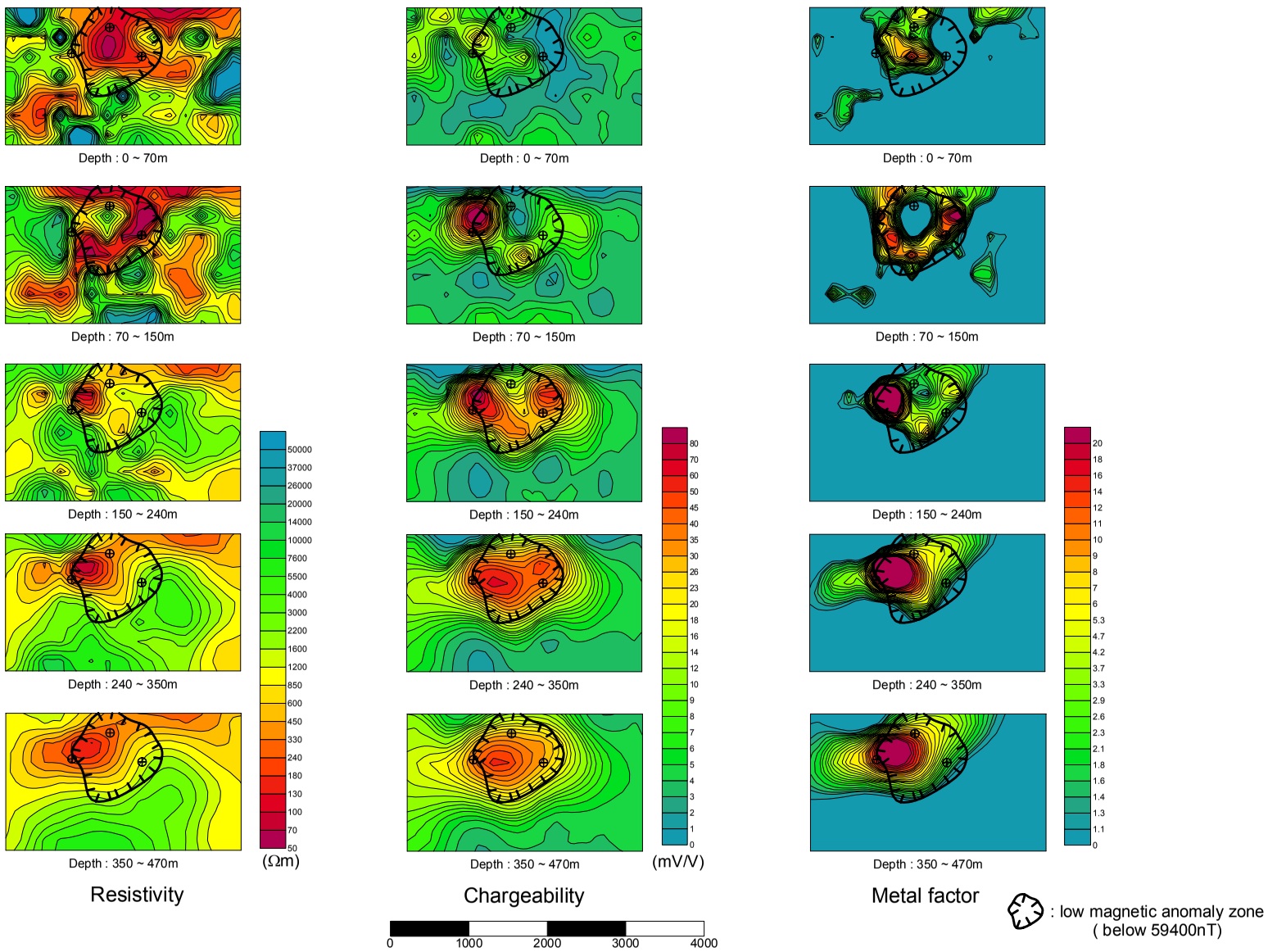

Fig.II-2-60 3D analysis plane map in Under/Shand_3 area

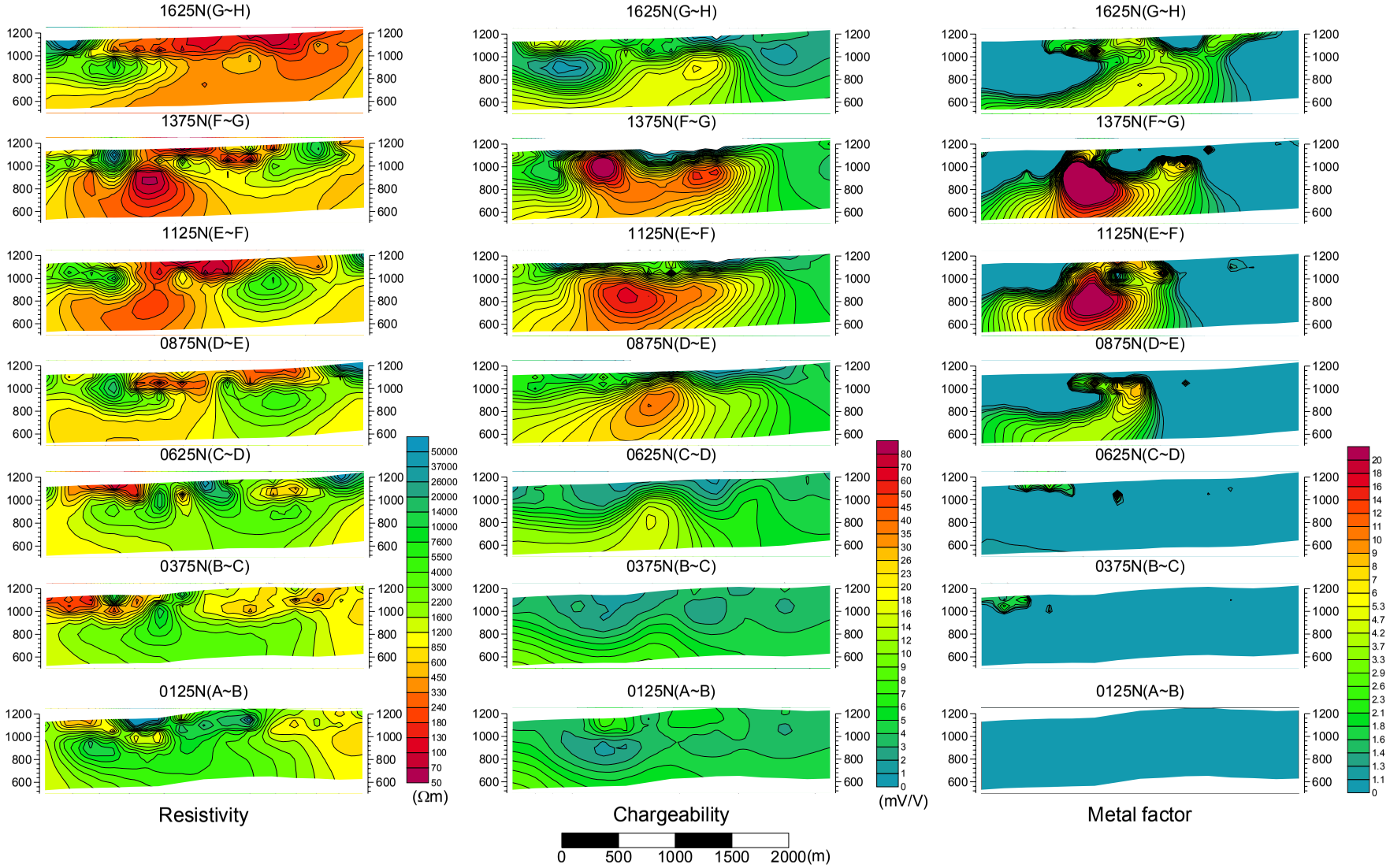

Fig.II-2-61　3D analysis sectionsin Under/Shand_3 area

2-6-2 Mogoin gol area

Remarkable IP anomaly zones are detected under the northern and southern alteration zones. Around the southern alteration zone, low resistivity and high chargeability zone is located above the depth of 200m and no anomaly is recognized at deeper part. Around the northern alteration zone, large scale IP anomaly is detected below the depth of 100m continuously to deeper part. According to the plane map of 340m depth, low resistivity zone under 500Ωm extends in the direction of NW-SE with about 2.0km length and 1.5km width, and high chargeability zone over 20mV/V is distributed continuously from east to west with about 2.0km width to include the low resistivity zone.

The results of 3-D analysis are shown in Figs.II-2-62 to II-2-65. The results is considered to reflect subsurface structure more suitably because those shows no extreme high resistivity or high chargeability value regarded as artifacts such as the results of 2-D analysis at the stations 32 to 42 on the line MG-6 and the stations 24 to 36 on the MG-12. 3-D analysis is possibly effective in such an area that the assumption of two dimensional topography and subsurface structure is unsatisfactory like Mogoin gol area. Except for around the alteration zones, high chargeability is detected at the center part in the west of the survey area (the stations 30 to 40 on the lines MG-1 to MG-3). In this anomaly zone, intruded diorite accompanied by magnetite is recognized. This anomaly is possible to reflect some mineralization, but the intensity of the mineralization is considered to be weak because resistivity value is so high.

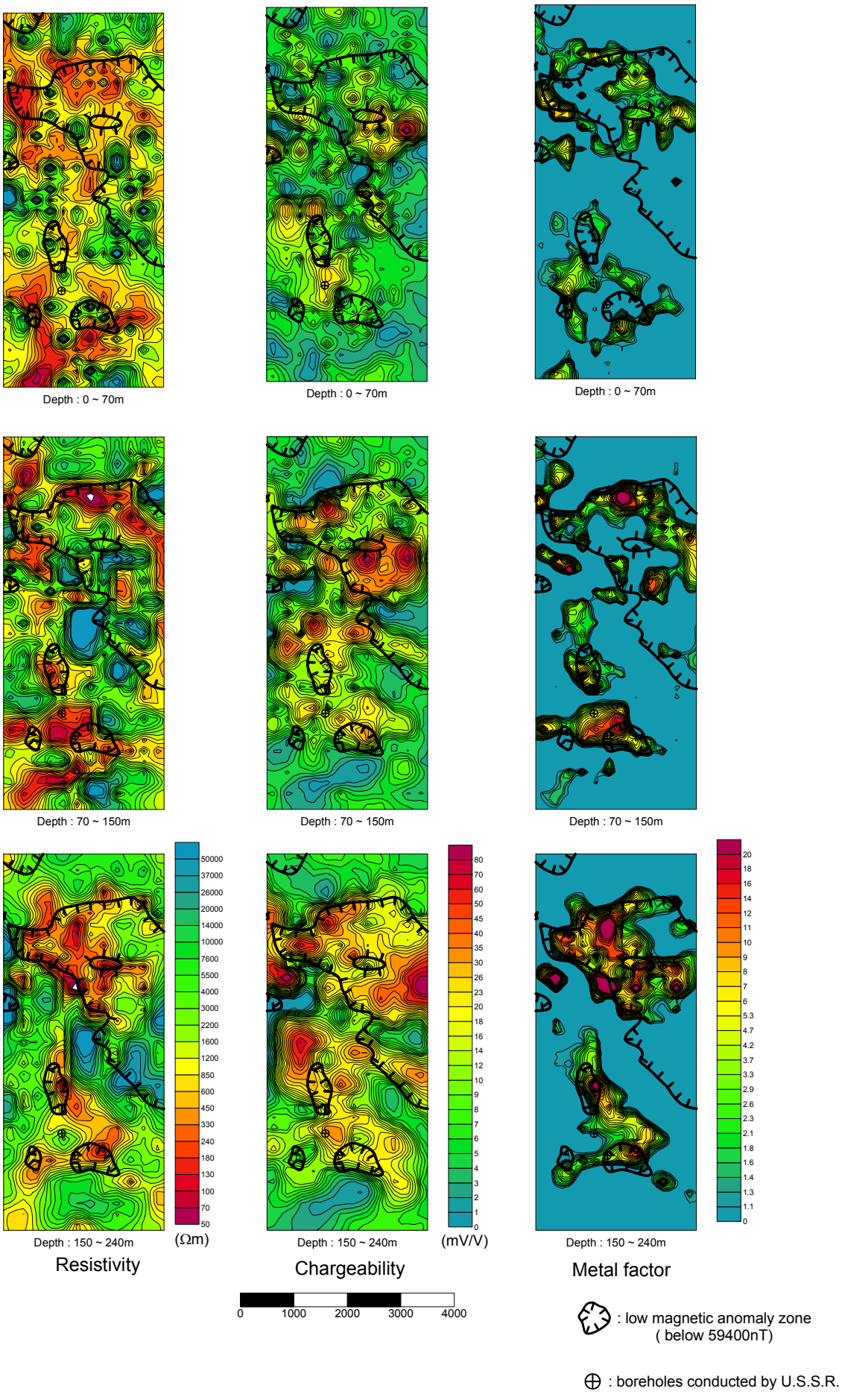

Fig.II-2-62　3D analysis plane map in Mogoin gol area(1)

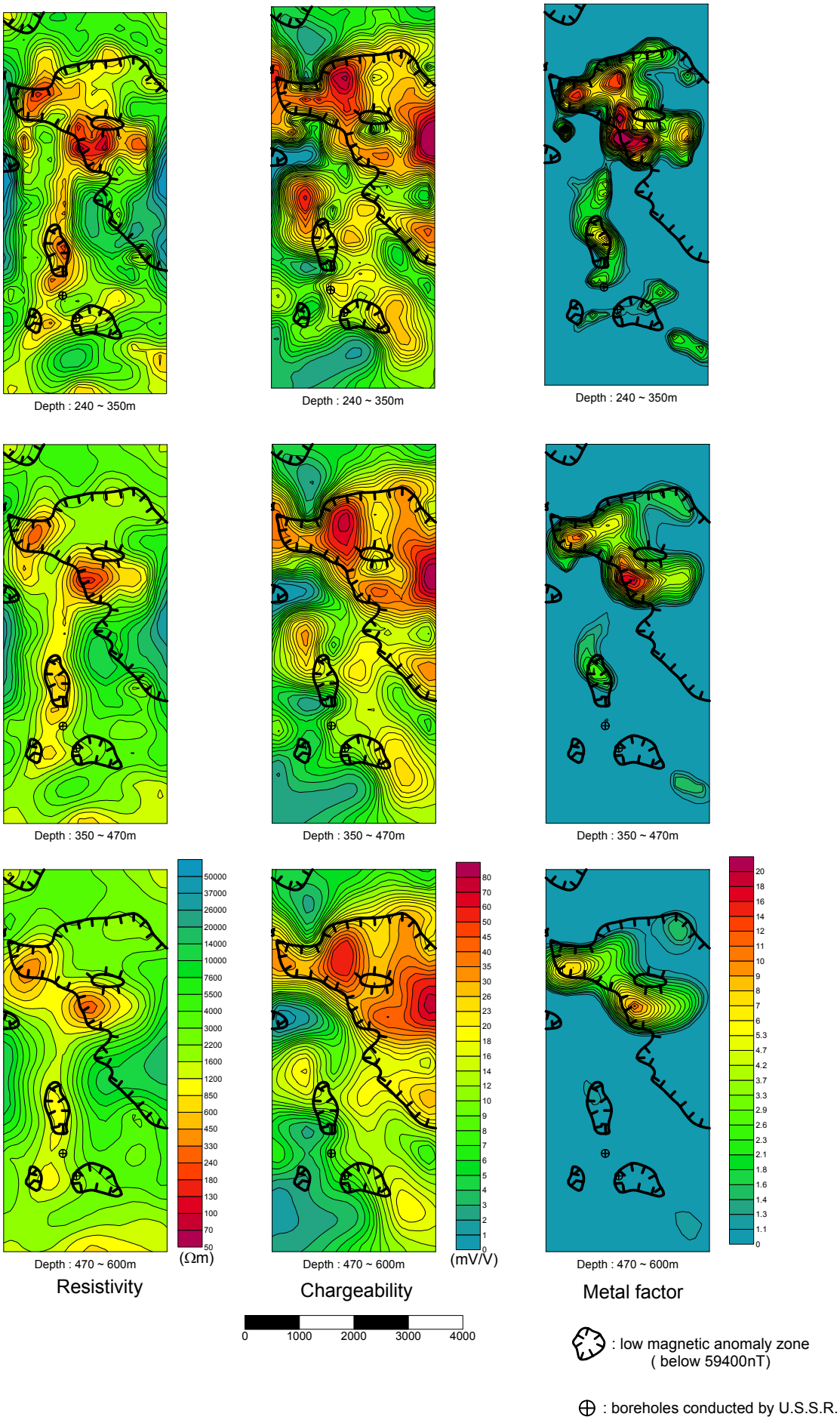

Fig.II-2-63　3D analysis plane map in Mogoin gol area(2)

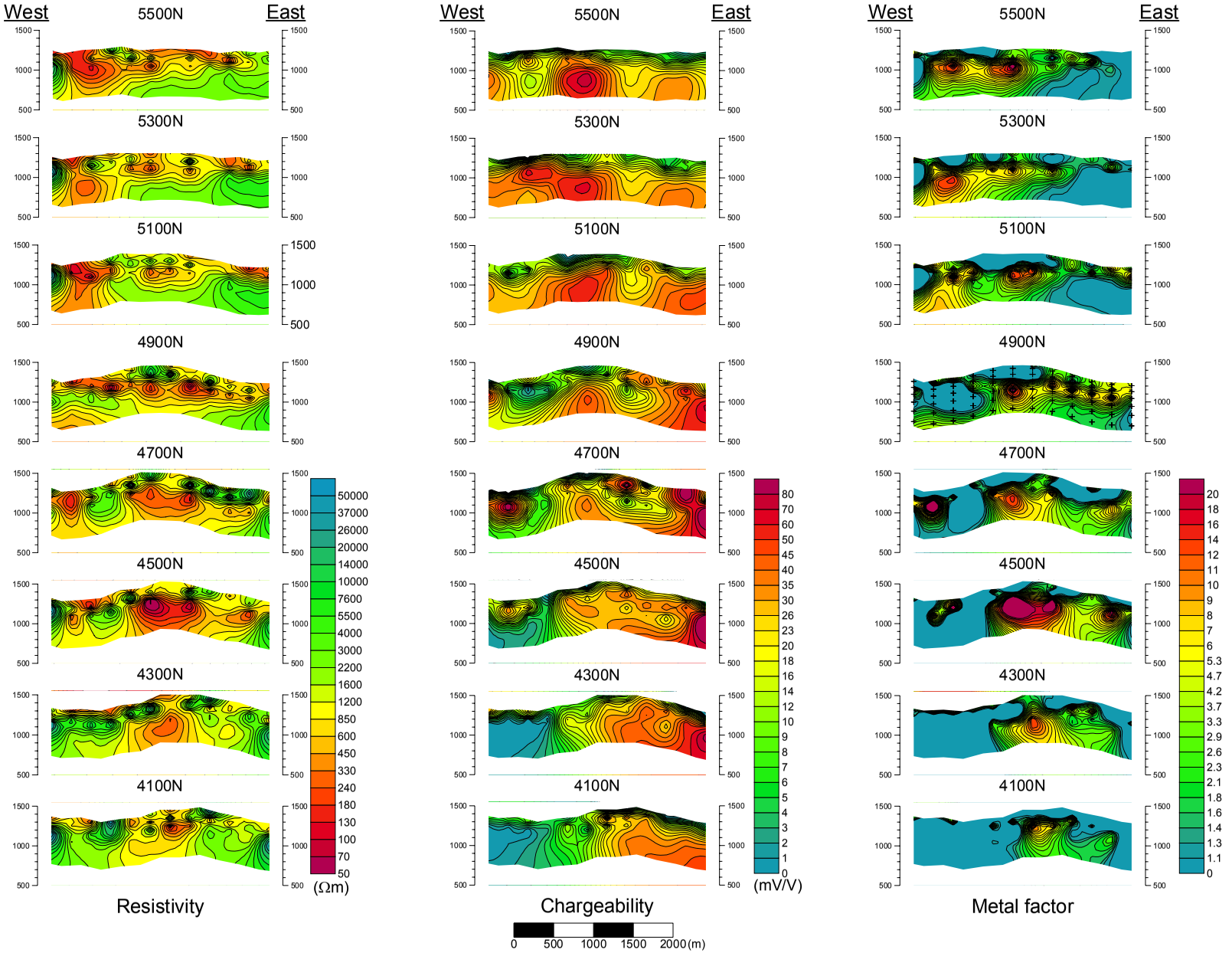

Fig.II-2-64　3D analysis sections at the north part of Mogoin gol area(4100N – 5500N)

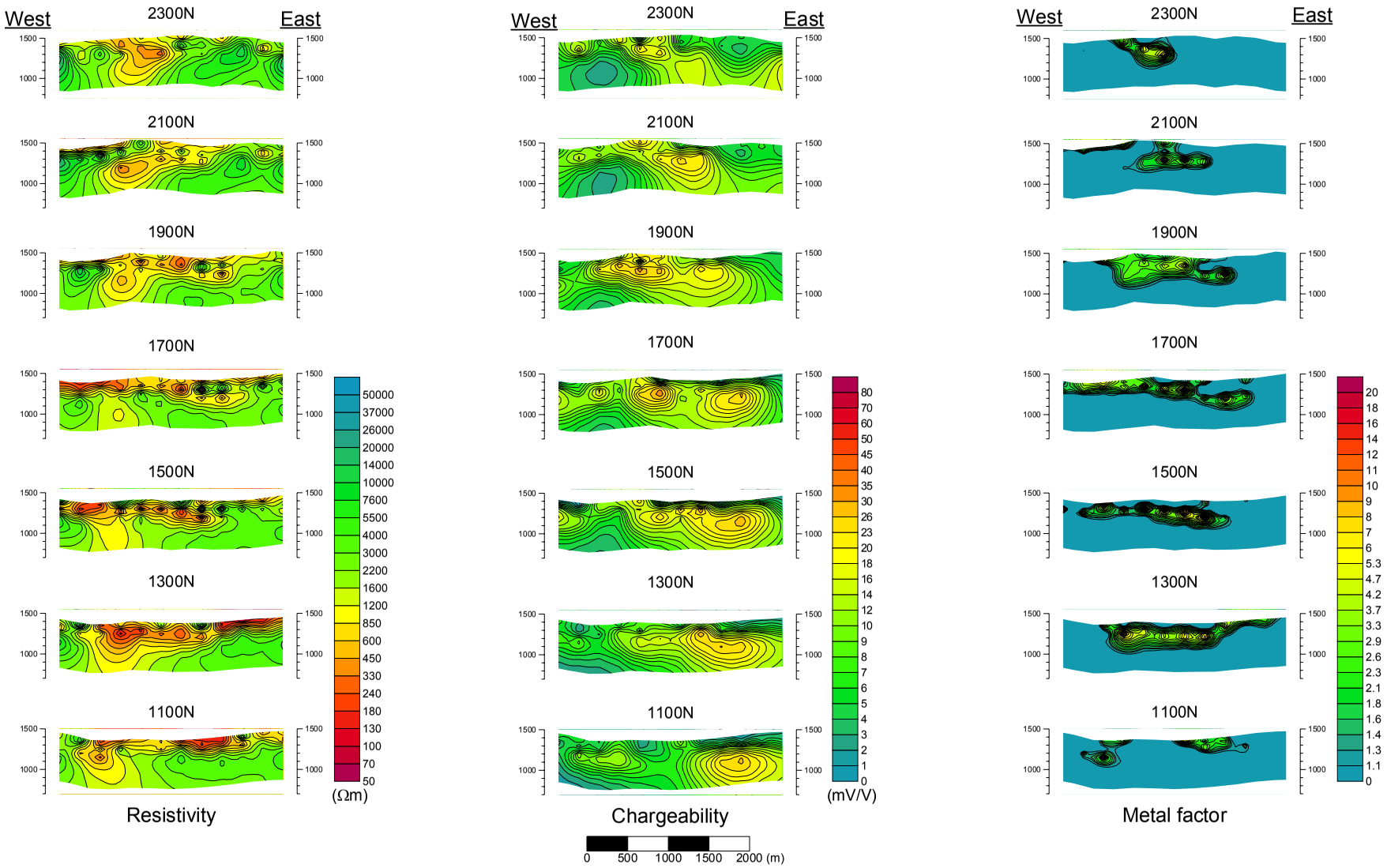

Fig.II-2-65 3D analysis sections at the south part of Mogoin gol area(1100N – 2300N)

2-6-3 Erdenet SE area

Low resistivity is distributed widely at the center part of this area, and it corresponds to the area of underlain by Quaternary sediments. Remarkable high resistivity is detected at the south of the area, and it is considered to reflect dacite and rhyolitic tuff. No chargeability anomaly is detected. Though there is no good correlation between low magnetic anomaly zone and resistivity or chargeability, chargeability is relatively high at the margin of the low magnetic anomaly zone. If the low magnetic anomaly is caused by intrusive rock, the chargeability anomaly is possible to reflect some weak mineralization. Low resistivity anomaly is detected at the southeast of the area, and it extends from shallow to deep part below the depth of 150m. This anomaly is located at the northwestern edge of high magnetic anomaly zone, and it is estimated that conductive intruded rock exists.

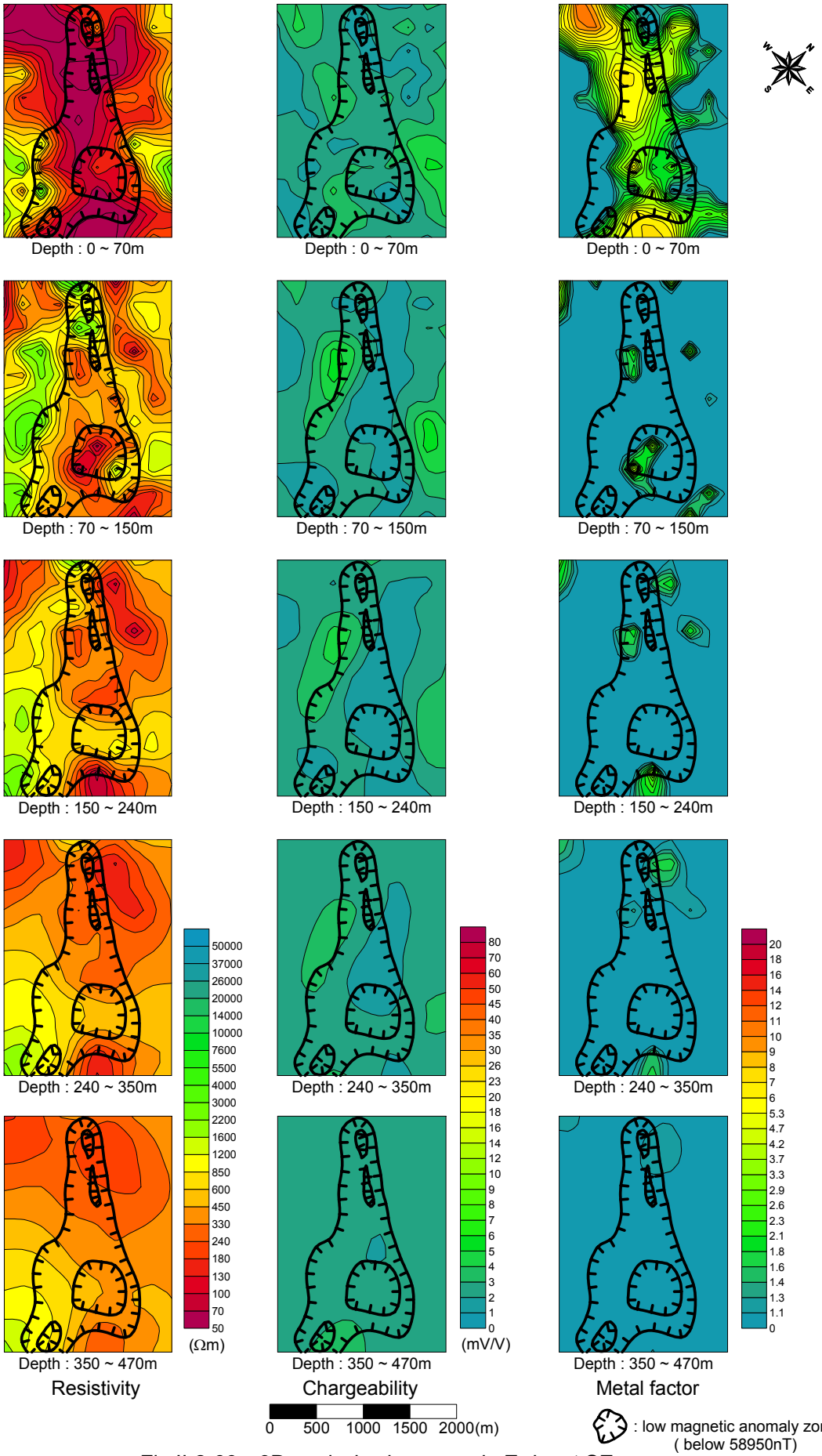

Fig.II-2-66 3D analysis plane map in Erdenet SE area

CHAPTER 3 CONSIDERATIONS

Based on results obtained by geological mapping and geophysical (IP) prospecting carried out during second phase of the Cooperative Mineral Exploration in the Erdenet SE, Under/Shand and Mongoin gol areas, the following considerations were summarized:

3-1 Erdenet SE area

An interpretation map including geological mapping and geophysical (IP) prospecting results is shown in the Fig.II-3-1.

Geology of the survey area presents lower Permian volcanic rocks, late Permian granites, stocks, dykes and Quaternary deposits. The late Permian granites called Selenge complex is mainly composed of granitic rocks and adakitic granodiorite showing an K-Ar dating of 196Ma. The main tectonic trend is represented by dykes developed along NE-SW and fault developed along N-S and NW-SE directions. Potential mineralization or alteration zones were not detected by geological mapping.

Phase I airborne magnetic and radiometric surveys detected an NW-SE elongated low magnetic anomaly, measuring 3km NW-SE and 2km NE-SW and is largely covered by Quaternary sediments. At north of the low magnetic anomaly, adakitic diorite of northern portion showed no mineralization.

IP results of survey area showed lower resistivity in comparison with similar terrain. Low resistivity related to Quaternary sediments was also detected at the central part of the survey area while high resistivity related to dacite to rhyolitic tuffs was detected at southern part of the survey area. Areas of low magnetism in airborne survey have no direct relationship with ground resistivity and chargeability results, but it was found spots of high chargeability surrounding areas of airborne low magnetism. There are possibilities that intrusive rocks show low magnetism and weak mineralizations show high chargeability. Low resistivity at depth of 150m in southeastern part of the survey area is probably associated to intrusive body at the northern section of high magnetic anomaly.

Due to the low possibility of finding mineralization in the survey area, further exploration program is not recommended.

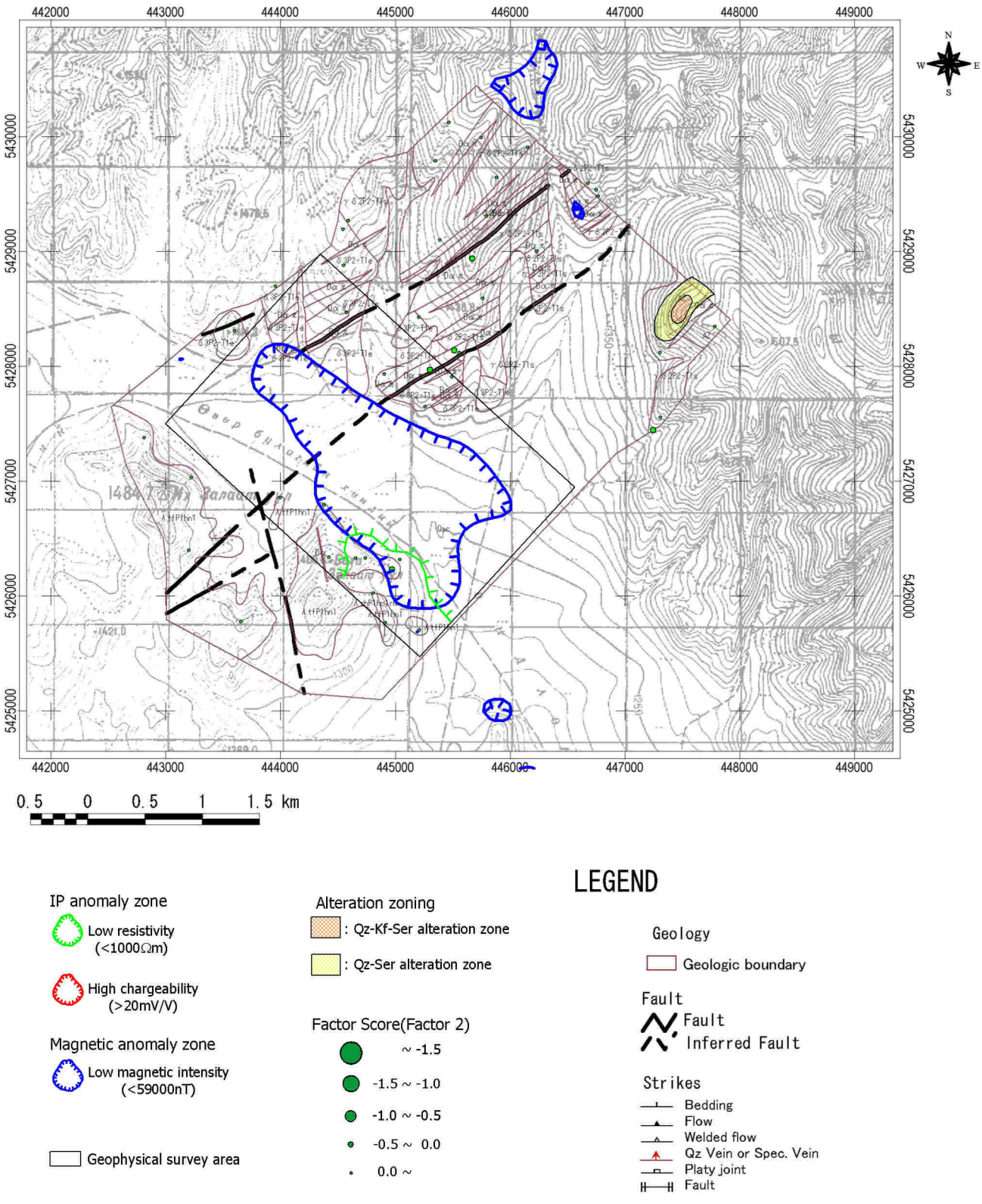

Fig.II-3-1 Compiled map in the Erdenet SE area

3-2 Under/Shand area

An interpretation map including geological mapping and geophysical (IP) prospecting results is shown in the Fig.II-3-2.

The area presents Permian to Tertiary volcanic rocks, late Permian granites, stocks, dykes and Quaternary deposits. The main faults have NW-SE trend at southern part and NE-SW and N-S trends at northern part of the survey area. Strong silicification and bleaching zone is present in the Under/Shand_1 area.

Alteration minerals including mainly sericite were observed at the central part of the strong silicification and bleaching zone and sericite-chlorite alteration assemblage was found outwards, which forms a weak alteration zoning. Low magnetic anomaly detected by airborne magnetic survey has dimensions of 1km N-S direction and 0.7km along E-W direction. Ground IP prospecting performed in the area found anomaly of below 500Ω・m elongating NW-SE direction. This IP anomaly is getting smaller below approximately 250m depth and changes the direction into NS. High IP anomalies above 1,000Ω・m coincide with distributions of granodiorite and porphyritic granodiorite which are open to depth. The area having chargeability up to 27mV/V at the station 18 to 20 on the line J has an extension of 300m east-west and 500m north-south, which is estimated to reflect weak mineralizations.

The Under/Shand_2 area covered by Quaternary shows airborne low magnetic anomaly with the dimensions of 2km N-S direction and 1km E-W direction. Ground IP prospecting results showed good correlation between surface resistivity below 500Ω・m and granodiorite outcrops. Resistivity between 200 and 500Ω・m is supposed to correlate with fracturing zone and alteration zone. Chargeability was detected up to approximately 10mV/V which showing lower generally and no IP anomaly.

Mineralization of the Under/Shand_3 area is represented by Cu-Mo porphyry Shand mineralization. Surface resistivity below 500Ω・m detected by ground IP prospecting was related to terrace deposits. Granodiorite was interpreted to lie beneath terrace deposits and it probably shows many fracturing and alteration zones at depth. Interpreted horizontal plans of chargeability anomaly show a ring structure with dimension of 1,000m x 1,200m at depth of deeper than 100m. The chargeability enlarges at depth and it shows the maximum IP anomaly at the depth of 250m.

A significant IP anomaly was detected at the Shand showing in the Under/Shand_3 and a halo of sericite-chlorite alteration was observed the surrounding area. This showing is considered as a prospective site because of favorite geology and geophysical features for porphyry Cu-Mo deposits but the existing information tells that 17 drillholes of above 400m lengths each were already penetrated within the area and preliminary ore resources has already been calculated. Continuing exploration is considered not necessary for the Shand showing.

On the other hand, IP prospecting with semi-detailed geological mapping is recommended at

pyrite mineralization zones in northwest part of Under/Shand_3 area and at central east of the Under/Shand area for confirming and delineating mineralizations.

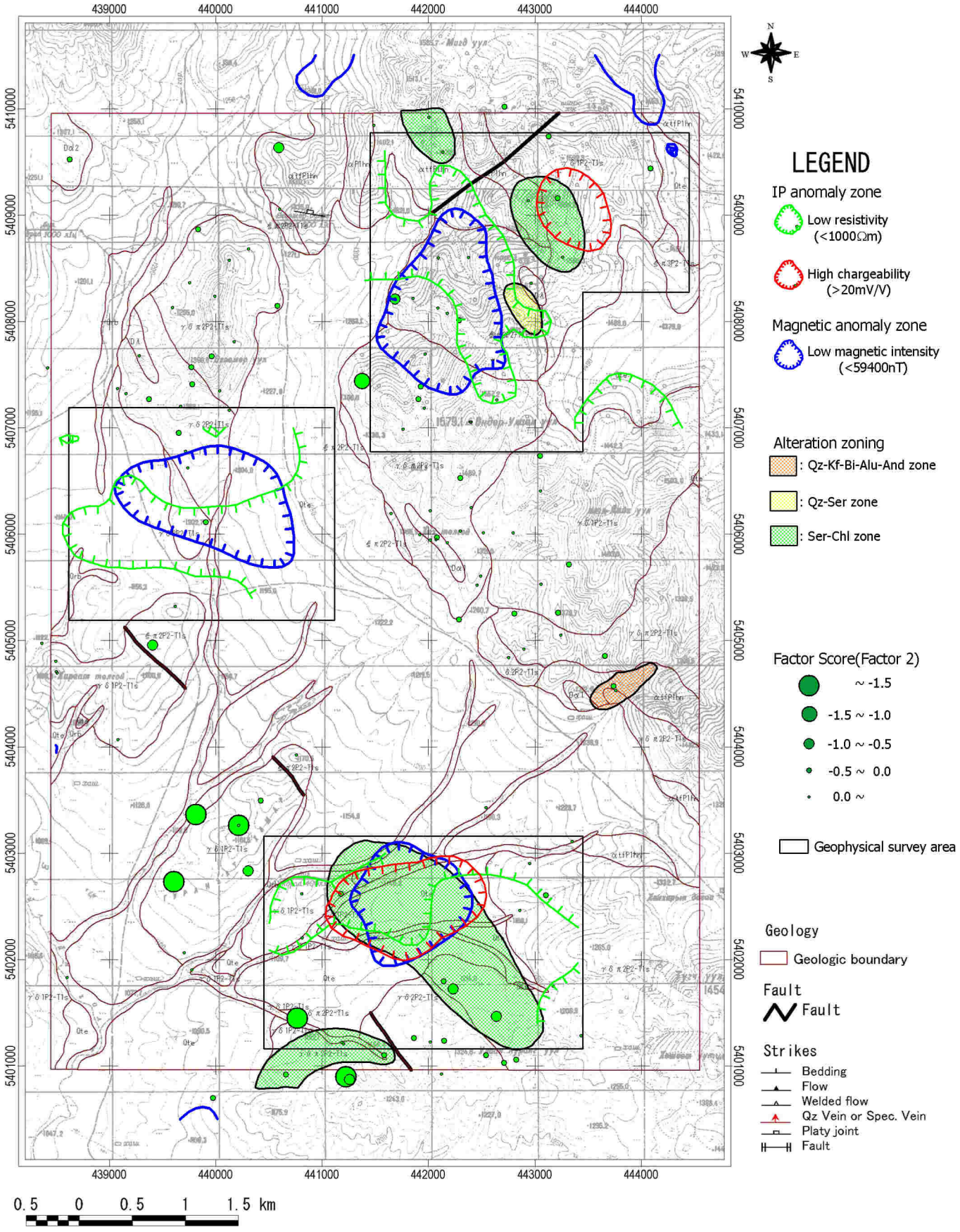

Fig.II-3-2 Compiled map in the Under/Shand area

3-3 Mogoin gol area

An interpretation map including geological mapping and geophysical (IP) prospecting results is shown in the Fig.II-3-3.

The area presents upper Permian alkali type volcanic rock and upper Tertiary to lower Jurassic volcanic rocks, Permian to Tertiary granites, Jurassic stocks and dykes and Quaternary sediments. At north of the area around Mount Shar Chuluut and its southern part, a white silicified alteration zone is extended. Directions of main faults are prominent NNW-SSE, NW-SE and E-W at northern part, NW-SE and E-W at central part and NE-SW and E-W at southern part of the area. Mineralizations are composed of north white silicification alteration, south white silicification alteration with secondary silicificied rocks and magnetite zones related to intrusions of liparites and diorite dykes.

At north white silicification zone, quartz and quartz-sericite alteration zone is distributed in the central part and sericite-chlorite alteration, chlorite alteration zone are present outward, which indicates alteration zoning in association with forming a porphyry Cu-Mo deposit. This alteration zoning is similar to that of the upper portion developed in high sulfidation epithermal acidic alteration zone of porphyry Cu-Mo deposits. The ore grades return up to 0.026%Cu, 0.001%Mo, 0.021%Pb and 0.004%Zn. There are some high value samples among rock chemical samples. Judging from these results, it is thought that a porphyry Cu-Mo deposit will probably exist at relatively deeper depth if it does. At south white silicification zone, quartz and quartz-sericite is distributed in the central part and it changes suddenly to unaltered rock outward, which shows no alteration zoning. The ore grades return 0.009%Cu, 0.006%Pb and 0.002%Zn. Rock magnetization measurement detected relatively low magnetic anomaly in the north white silicification alteration zone. Rock magnetization data here is possible to the results of rock demagnetization effect caused by forming of a porphyry Cu-Mo deposit. IP of north white silicification zone showed high resistivity/low chargeability from surface to the depth of 100m but a large IP anomaly having low resistivity/high chargeability zone from the depth of 100m open to depth.

Geophysical and geological information indicated that the north white silicification zone has high potential to host a porphyry type Cu-Mo deposit, so a drilling campaign is recommended in the area. As IP anomaly continues to the east of the zone, IP geophysical prospecting and geological mapping are further recommended. Simultaneously, a geochemical prospecting here is necessary for understand geochemical features.

At south white silicification zone, quartz and quartz-sericite alteration zone is distributed in the central part but unaltered rocks are present outside the zone, which shows no alteration zoning. The ore grades return up to 0.009%Cu, 0.006%Pb and 0.002%Zn. Maximum value of rock samples carry 39ppmCu, 5ppmMo, 60ppmPb and 12ppmZn. Though is highly considered that a porphyry Cu-Mo deposit will exist at deeper depth with not perfect alteration zoning. Low rock magnetization, which is thought to be the result of demagnetization caused by forming a porphyry Cu-Mo deposit,

was detected. IP in south white silicification zone indicated low resistivity/high chargeability zone is limited from surface to the depth of 200m and no anomaly was detected below this depth.

Accordingly, a drilling program is recommended within south white silicification zone.

At west center of the area (measuring points 30 to 40 on the lines MG-1 to 3), high chargeability spot is observed from shallower to depth. Around here diorite intrudes with high magnetite contents. High chargeability spot is probably related to mineralization, but at this site, the low resistivity indicates weak mineralization.

It is recommended a drilling program within IP anomalies detected outside of the white silicification zones aiming to understand the feature of IP anomalies zones.

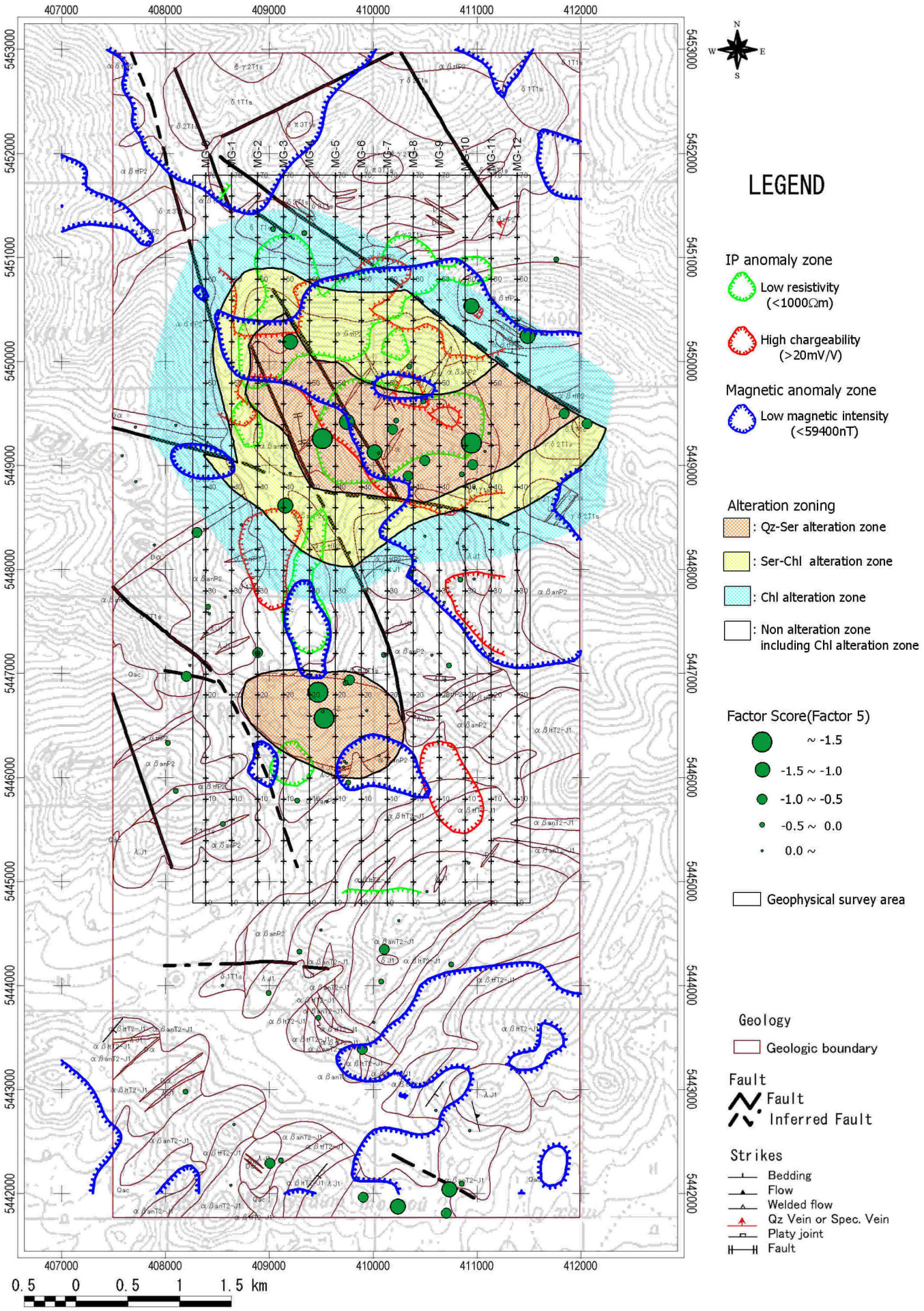

Fig.II-3-3 Compiled map in the Mogoin gol area

CHAPTER 4 DRILLING SURVEY

4-1 Background and Objectives for Drilling Survey

In Phase I survey, data compilation, geological survey and airborne geophysical survey have conducted in the western Erdenet area where has 5,500 km^2. In Phase II, geological survey and TDIP geophysical survey have conducted in the Erdenet SE area, Under/Shand area and Mogoin gol area where were the potential areas in the project area.

According to the survey results in the phase I and II, drilling survey has conducted in the high chargeability zone detected by TDIP electric survey in the Mogoin gol area in order to clarify the geology and mineralization and study relationship among the TDIP geophysical anomaly, geology and mineralization.

4-2 Location of Survey Area and Amount of Works

The drilling survey area is located in the Mogoin gol area where located at 30 km northwestern part from Erdenet Mine City. The drilling survey locations are indicated in Fig. II-4-1 and the drilling sites are shown Fig. II-4-2 and Fig. II-4-3. The confirmation of the drilling site locations was conducted by using two GPS apparatus, which were GPS 315 of MAGELLAN. The locations of two drilling holes were shown the below:

MJME-M1: Latitude is 49 degrees, 12 minutes and 5 seconds. Longitude is 103 degrees, 44 minutes and 48 seconds. (5450594 North, 408695 East)

MJME-M2: Latitude is 49 degrees, 11 minutes and 40 seconds. Longitude is 103 degrees, 47 minutes and 1 second. (5450594 North, 408695 East)

Amounts of works for the drilling survey are shown Table I-1-1 and Table I-1-2.

4-3 Survey Methods

The drilling survey was conducted in the Mogoin gol area as shown Fig. II-4-1.

4-3-1 Field Survey

(1) Drilling Hole Location, Depth, Direction and Inclination

The drilling sites, depth, direction and inclination were shown Fig. II-4-2, Fig. II-4-3 and Table I-1-1.

(2) Method

The drilling method is a wireline method of diamond drilling that is appropriate for geological setting and objection of drilling.

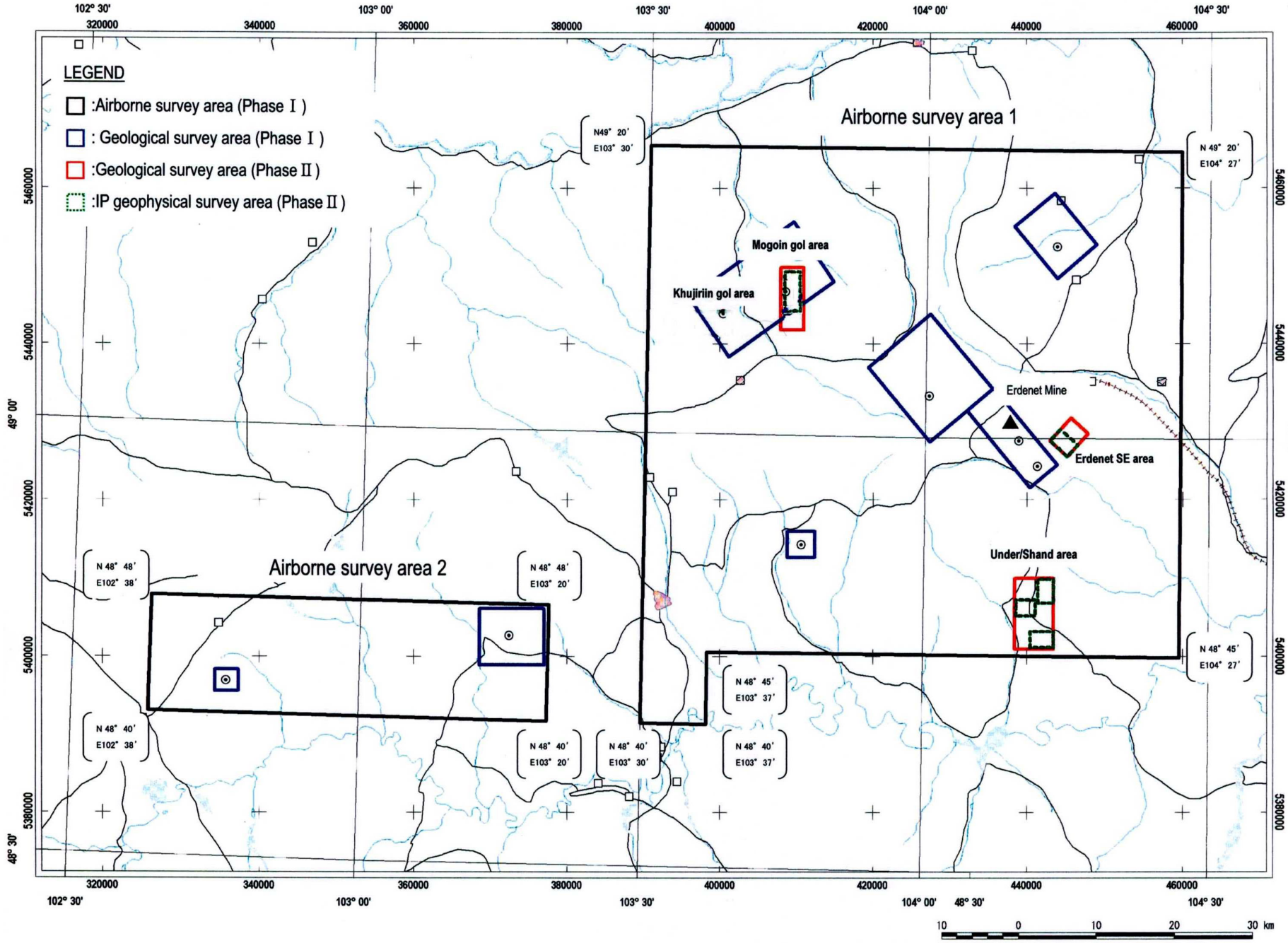

Fig.II-4-1 Location map of the drilling survey area in the Western Erdenet area

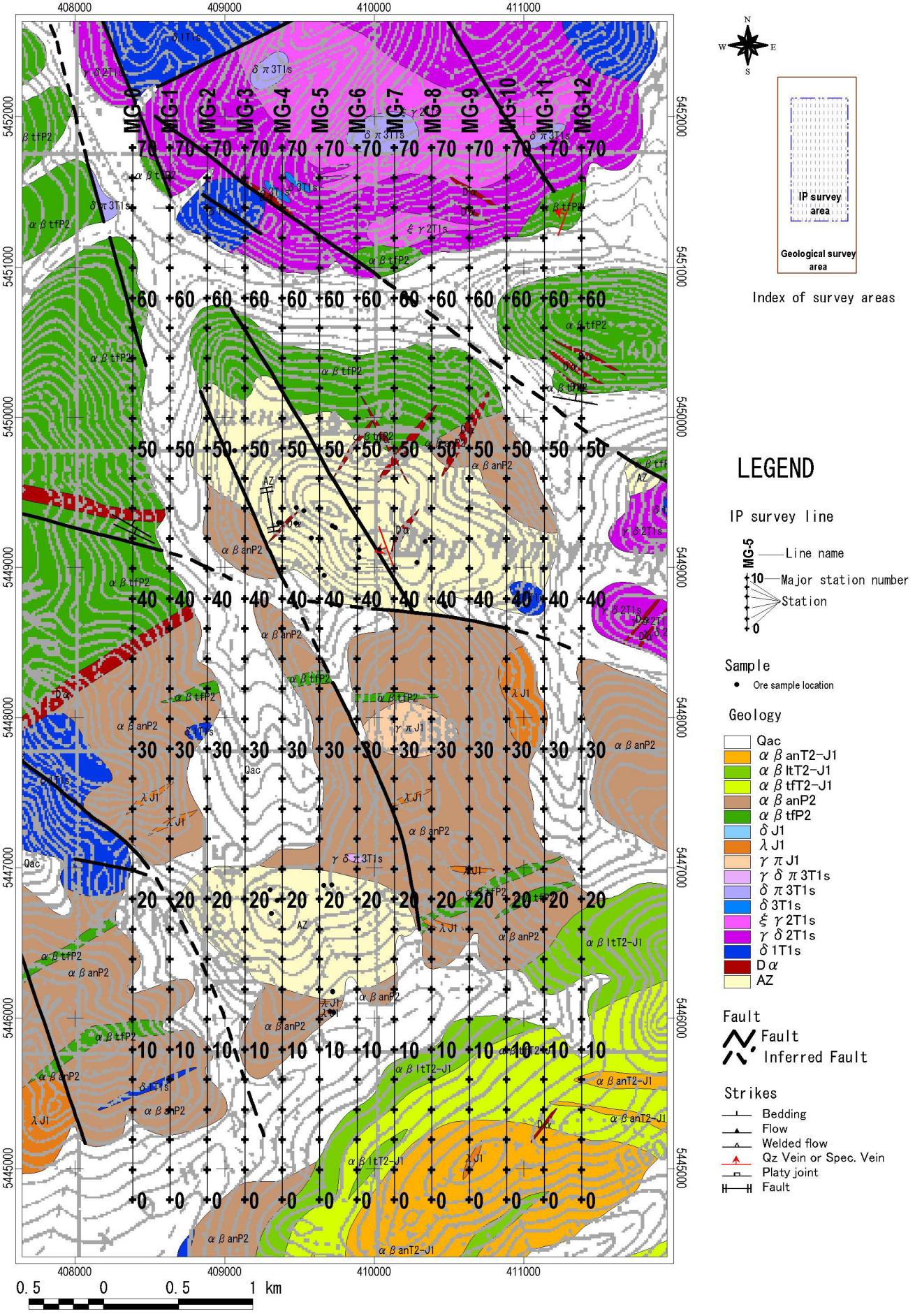

Fig.II-4-2 Drilling sites of MJME-M1 and MJME-M2 in the geological map of the Mogoin gol area

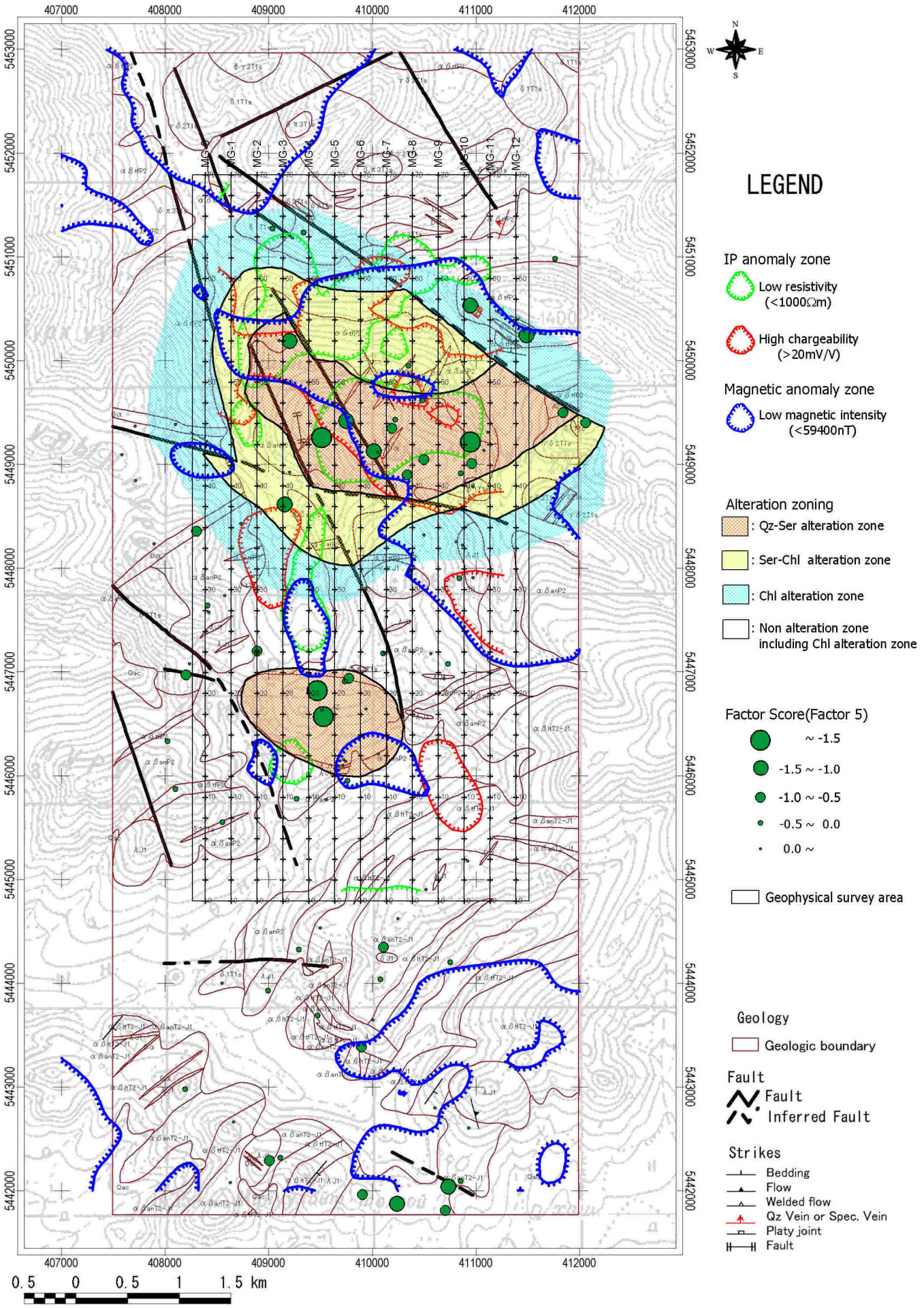

Fig.II-4-3 Drilling sites of MJME-M1 and MJME-M2 in the compiled map of the Mogoin gol area

(3) Drilling Equipments and Casing Pipes

Drilling rigs were MKS-5 type drilling machine made in Russia. Maxim depth of drilling was 800m by BQ size. Drilling equipments were shown Appendix 15. Casing pipes were prepared 60% of planned drilling length.

(4) Drilling Core Diameter

Diameter of drilling core is more than BQ size.

(5) Core Sampling and Core Recovery

a) Core recovery was more than 70 % after arriving at basements. All coring at the mineralized parts, hole bottom part and geologic contact parts was tried.

b) Slime samples and fragmental samples of core were collected, if core were not collected.

(6) Treatment of Drilling Cores

a) Arrows showing bottom direction were marked on the core boxes. The core boxes were kept in the stock of the Geological Information Center of MRAM.

b) Collection depths of cores and slimes were exactly written inside and outside of the core boxes.

(7) Core Logging

a) Rock phases and alterations were described with attention on geologic boundaries.

b) In case of encounter with mineralization, mineralization type (network, vein, dissemination, massive etc.), kinds of ore mineral and accessory minerals, paragenesis etc. were detail described and made sketches.

c) Geologic important parts of drilling cores were taken pictures, made thin sections and polished thin sections.

(8) Laboratorial Test and Chemical Analysis

a) Samples for laboratorial test and chemical analysis were collected from the most suitable parts of drilling cores.

b) Contents and amount of works were shown Table I-1-2.

(9) Mud Water, Mud Waster, etc.

Location and method for dealing with mud-water, mud waste, water waste, oil and etc. will be decided by considering surrounding condition and environments.

(10) Restoration Work

After completion of drilling work, the drilling site will be restored.

(11) Repairing Road

During and after drilling work, the road will be repaired to avoid the problems with the residents.

4-3-2 Period of Drilling Works

Drilling period and drilling progress of hole No. MJME-M1 and MJME-M2 were shown appendix 15.

Drilling period: MJME-M1: 17th of January 2003 to 19th of February 2003 (for 34 days)
MJME-M2: 27th of January 2003 to 16th of February 2003 (for 46 days)

MJME-M2 hole was encountered pyrite mineralized zones, strong silicified rocks and wide sheared fault zones. Accordingly, efficiency of drilling was very low.

4-4 Survey Results

4-4-1 Laboratory Tests Results

Samples for laboratory tests were taken from two drilling holes in the Mogoin gol area in order to geological interpretation. The tests included thin section analysis, polished thin section analysis, X-ray analysis, fluid inclusion analysis and chemical analysis of ore samples. Results of these tests are presented in Appendix 16.

(1) Results of Thin Section Analysis

The samples for clarifying typical rock, 13 rock samples were collected from two drilling cores. Rock thin sections were made and observed under microscope. The results of rock observation for thin sections are shown Appendix 16 (1).

The results of rock observation are shown that the rocks are Permian volcanic rocks and granites, Triassic diorite porphyry and granodiorite, Triassic to Jurassic andesite dyke and alteration rock from the mineralized zone.

(2) Description of Polished Thin Section for Ore Samples

Twenty ore samples were collected from the mineralized zone of two drilling cores, and polished thin section were made and observed under microscope. The results of observation for ore polished thin sections are shown Appendix 16 (2).

The following ore minerals are observed pyrite, goethite, hematite, limonite, chalcopyrite and azurite. Alteration minerals of quartz, muscovite, sericite, chlorite, epidote, and carbonate are observed.

(3) X-ray Diffraction Analysis

Fifty-eight samples of general rock and altered rocks were collected from two drilling cores. The results of X-ray diffraction analysis for rock and ore samples are shown Appendix 16 (3).

The detected alteration minerals are quartz, plagioclase (albite), potassic feldspar, hornblende, sericite, chlorite, kaolinite, epidote, clinoptilolite, stellerite, laumontite, stilbite, analcite, pyrophyllite, gypsum, pyrite, goethite, and hematite.

The alteration mineral assemblages are classified below.

MJME-M1: 1) Sericite
2) Chlorite-sericite
3) Chlorite
4) Chlorite-Epidote
5) Other minerals – stellerite, clinoptilolite

MJME-M2: 1) Quartz-sericite- (kaolin)
2) Chlorite-sericite
3) Chlorite
4) Other minerals – clinoptilolite, laumontite, stilbite, analcite, pyrophyllite, gypsum

(4) Ore Assay Analysis

Six hundred and twenty ore samples for the ore chemical analysis were collected from two drilling cores in the areas, were analyzed and the results of ore chemical analysis data are shown Appendix 16 (4).

Analytical data of ore analysis for MJME-M1 hole show the following: Gold values are less than Au 0.01 g/t to Au 0.01 g/t in maximum. Copper values are less than Cu 0.001 % to Cu 0.100 % in maximum. Lead values are Pb 0.002 % to Pb 0.021 % in maximum. Zinc values are Zn 0.002 % to Zn 0.021 % in maximum. Sulfur values are S 0.03 % to S 1.39 % in maximum. Silica values are SiO_2 38.5 % to SiO_2 63.3 %. Iron values are Fe 1.96 % to Fe 8.20 %.

Analytical data of ore analysis for MJME-M2 hole show the following: Gold values are less than Au 0.01 g/t to Au 0.28 g/t in maximum. Silver values are less than Ag 5 g/t to Ag 137 g/t in maximum. Arsenic values are less than As 0.001 %/t to As 0.002 %/t in maximum. Copper values are less than Cu 0.001 % to Cu 0.802 % in maximum. Molybdenum values are less than Mo 0.001 % to Mo 0.001 % in maximum. Lead values are Pb 0.002 % to Pb 0.011 % in maximum. Zinc values are Zn 0.002 % to Zn 0.115 % in maximum. Sulfur values are S 0.02 % to S 9.75 % in maximum. Silica values are SiO_2 44.1% to SiO_2 97.1 %. Iron values are Fe 0.24 % to Fe 11.0 %.

Maximum value of copper is Cu 0.802 % in interval of 196.65m to 196.80m of MJME-M2.

Other values at the interval are Au 0.28 g/t, Ag 61 g/t, Pb 0.002 %, Zn 0.009 %, S 3.29 %, SiO_2 86.8 % and Fe 3.93 %.

The values of more than Cu 0.100 % are Cu 0.100 % at a 2.00 m interval of 383.00m to 385.00m of MJME-M1, Cu 0.160 % at a 2.06 m interval of 330.00m to 332.60m of MJME-M2.

(5) Fluid Inclusion Test

Analytical samples for fluid inclusion test were collected 3 samples from MJME-M1 hole and 3samples from MJME-M2 hole, total 6 samples. The results of homogenization temperature and salinity and the histogram of homogenization temperature are shown Appendix 16 (5).

As the results of microscopic observation, the most inclusions are less than 10 micrometer in diameter and very fine. The homogenization temperature and salinity were measured by using 5 to 15 inclusions in a sample.

According to the results of fluid inclusion test, the measured homogenization temperatures show wide temperature range from 17 degrees C to 291 degrees C in all samples. The temperatures are concentrated around 150 degrees C. The salinity values of fluid inclusion show generally less than 10 % and low values. The salinity values of samples with liquid CO2 in the fluid inclusion are NaCl 28.9 % in maximum and high value.

The average homogenization temperature of MJME-M1 drilling cores is 147 degrees C to 165 degrees C and the average salinity value is NaCl 3.9 % to NaCl 17.3 %. The average homogenization temperature of MJME-M2 drilling cores is 173 degrees C to 188 degrees C and the average salinity value is NaCl 1.8 %.

(6) Measurement of Resistivity and Chargeability

Analytical samples for measurement of resistivity and chargeability collected 10 samples from MJME-M1 hole and MJME-M2 hole. The measurement results of resistivity and chargeability are shown Appendix 16 (6).

In MJME-M1 hole, the resistivity values are 3,000 ohm m to10,640 ohm m and the chargeability values are 4.38 mV/V to 8.83 mV/V. In MJME-M2 hole, the resistivity values are 531ohm m to 7,783 ohm m and the chargeability values are 2.83 mV/V to 16.80 mV/V.

4-4-2 Drilling Survey

(1) MJME-M1 Hole

This hole is located at geophysical survey point of MG1-58 where is located in the western part of the Shar chuluut Mountain of the Mogoin gol area. The drilling site is on the Quaternary deposits consisting of stream sediments and debris deposits. The geology around drilling site is Permian to Triassic volcanic rocks and granitic rocks, andesitic dykes and Quaternary deposits.

Geology: Drilling cores of MJME-M1 are mainly composed of Quaternary deposits from 0.00m to 56.20m and basements from 56.20m to 501.80m. The basements are Permian to Triassic volcanic rocks, Triassic granitic rocks, diorite porphyry, micro-granodiorite and andesitic dykes. The below is shown drilling core logging. The drilling column is shown Appendix 17. The geologic cross section of MJME-M1 is shown Fig. II-4-4.

0.00m – 1.20m:	Surface soil including sand, soil and gravel
1.20m – 2.00m:	Sand, silt and granule
2.00m – 3.80m:	Cobble gravel to pebble gravel: including silicified rock and green andesitic rock
3.80m – 4.50m:	Granule including silt with gravel
4.50m – 6.70m:	Cobble gravel to pebble gravel
6.70m – 9.95m:	Sandy silt with pebble gravel
9.95m – 10.50m:	Gravel of white silicified rock with pyrite holes
10.50m – 12.70m:	Light grey sandy silt with pebble gravel
12.70m – 18.00m:	Bolder gravel to cobble gravel including sand layer with sub-angular to sub- rounded fragments
18.00m – 18.35m:	Brown sand
18,35m – 19.90m:	Gravel of light yellowish grey silicified rock with many pyrite holes
19.90m – 20.00m:	Brown to reddish brown silt with pebble gravel
20.00m – 31.70m:	Reddish brown silt with granule including white silicified rocks
31.70m – 37.70m:	Yellow, weathered sandy silt
37.70m – 40.10m:	Brown silt including white clay
40.10m – 40.60m:	Brown pebble gravel to granule brown silt
40.60m – 41.00m:	Brown sandy silt
41.00m – 41.20m:	Bolder gravel to cobble gravel and pebble gravel including brown silt
41.20m – 41.60m:	Brown silt
41.60m – 43.00m:	Brown to reddish brown silt with granule
43.00m – 45.80m:	Silt to sand in upper parts and pebble gravel in lower part
45.80m – 46.20m:	Pebble gravel with matrix of silt
46.20m – 56.20m:	Bolder gravel to cobble gravel and pebble gravel, non core in lower part
56.20m – 58.20m:	Light greenish grey, andesitic tuff, brecciaed. Alteration is weal silicification, weak argillization, weak chloritization, and weak epidotization including epidote veinlets. Mineralization is weak pyrite dissemination.
58.20m – 76.70m:	Light grey, moderate to strong silicified rock. Alteration is strong silicification, moderate to weak sericitization, weak chloritization and weak epidotization including epidote veinlets (75.00m to 76.70m). Argillization along the fractures. Mineralization is weak pyritization.
76.70m – 82.10m:	Light grey, moderate silicified rock. Alteration is moderate silicification, weak sericitization, weak chloritization and weak epidotization including epidote veinlets. Argillization along the fractures. Mineralization is weak pyrite dissemination.
82.10m – 86.30m:	Light grey, strong silicified rock with brecciation. Alteration is strong silicification, moderate to weak sericitization, weak chloritization, and weak epidotization including epidote veinlets. Moderate argillization along the fractures. Mineralization

is weak pyrite dissemination.

86.30m – 107.20m: Light grey, moderate silicified rock. Alteration is moderate silicification, weak sericitization, weak chloritization, and weak epidotization including epidote veinlets. Weak argillization along the fractures. Mineralization is pyrite dissemination.

107.20m – 111.30m: Grey to greenish grey, andesite dyke (angle: 30 to 70 degrees). Alteration is weak sericitization, moderate chloritization.

111.30m – 112.45m: Grey andesitic tuff. Alteration is strong silicification, moderate sericitization, weak chloritization, and weak epidotization including epidote veinlets. Mineralization is moderate pyrite dissemination.

112.45m – 117.45m: Light brownish grey, hornblende porphyritic micro-granodiorite. Alteration is weak chloritization, weak epidotization.

117.45m – 117.80m: Grey to greenish grey, andesite dyke. Alteration is weak sericitization, moderate chloritization.

117.80m – 126.20m: Light brownish grey, hornblende porphyritic micro-granodiorite. Alteration is weak chloritization, weak epidotization. 119.10m to 120.70m, weak silicification, weak chloritization, weak epidotization. Mineralization is including pyrite veinlets.

126.20m – 126.50m: Grey to greenish grey, andesite dyke. Alteration is weak sericitization, moderate chloritization.

126.50m – 138.90m: Light brownish grey, hornblende porphyritic micro-granodiorite. Alteration is weak chloritization, weak epidotization. Calcite veinlets. Mineralization is including pyrite veinlets and chalcopyrite spots.

138.90m – 148.10m: Grey to greenish grey, andesitic tuff. . Alteration is moderate silicification, strong argillization, weak sericitization, moderate chloritization, and weak epidotization with epidote veinlets. Mineralization is weak pyrite dissemination and veinlets along the epidote veins.

148.10m – 155.50m: Grey to greenish grey, andesitic tuff. . Alteration is weak argillization, weak chloritization. Mineralization is weak pyrite dissemination.

155.50m – 157.40m: Brownish grey andesite dyke. Alteration is moderate silicification, strong argillization, weak sericitization, moderate chloritization, and weak epidotization with epidote veinlets. Mineralization is weak pyrite dissemination and veinlets along the epidote veins.

157.40m – 167.00m: Grey to greenish grey, andesitic tuff. Alteration is moderate silicification, strong argillization, weak sericitization, moderate chloritization, and weak epidotization with epidote veinlets, quartz-epidote-chlorite-calcite veinlets. Mineralization is weak pyrite dissemination and pyrite veinlets along the epidote veins.

167.00m – 190.90m: Pinkish grey, hornblende micro-granodiorite. Alteration is moderate chloritization, weak epidotization with epidote veinlets, clay-calcite veinlets and quartz veinlets.

190.90m – 194.30m: Pinkish grey, hornblende micro-granodiorite intruded in and grey andesite dyke. Calcite- epidote-clay veinlets.

194.30m – 214.85m: Grey to greenish grey, diorite porphyry. Alteration is weak chloritization, weak epidotization. Calcite-epidote veinlets, calcite veinlets. Mineralization is weak pyrite dissemination and veinlets along the epidote veins.

214.85m – 232.50m: Pinkish grey, hornblende micro-granodiorite. Alteration is weak chloritization, weak epidotization with clay-calcite veinlets. Mineralization is weak pyrite dissemination and veinlets along the epidote veins. Chalcopyrite spots located at 218.70m, 223.50m and 224.10m

232.50m – 237.40m: Greenish grey silicified tuff. Alteration is moderate silicification, weak chloritization, weak epidotization, clay-calcite veinlets and calcite-epidote veinlets along the fractures. Mineralization is weak pyrite dissemination.

237.40m – 267.40m: Grey to greenish grey diorite porphyry. Alteration is moderate chloritization, weak epidotization with epidote veinlets, quartz veinlets, calcite veins and pinkish clay. Mineralization is weak pyrite dissemination along epidote veinlets. Chalcopyrite spots located in 260.50m to 260.70m

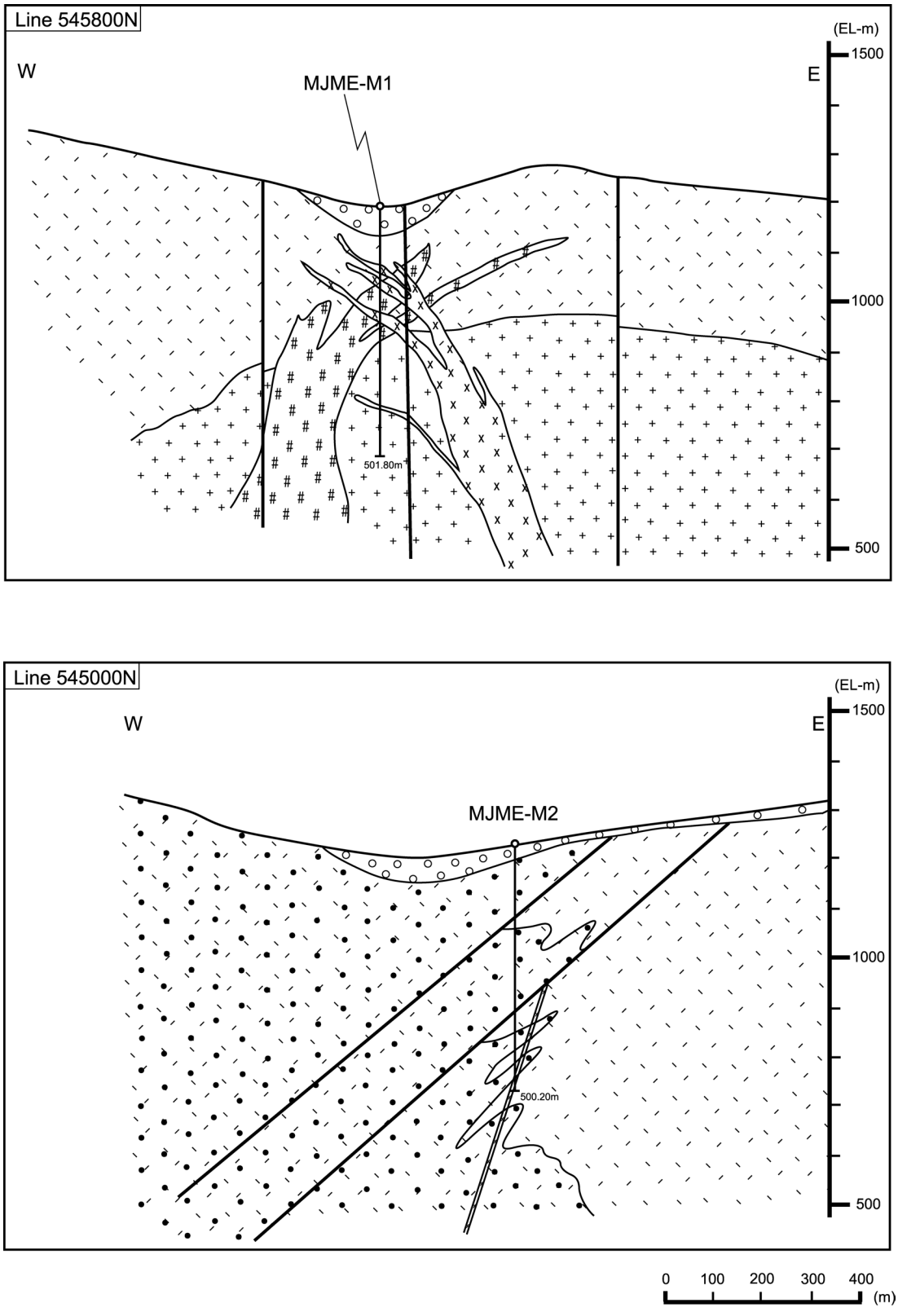

Fig.II-4-4 Cross sections of MJME-M1 and MJME-M2 on the line 545800N and the line 545000N

267.40m – 304.10m: Granodiorite of Selenge Complex. Alteration is moderate chloritization, weak epidote veins along the fractures, quartz veinlets, calcite veins and pinkish clay veins. Andesite dyke with angle of 30 degrees. Mineralization is weak pyrite dissemination along epidote veinlets. Chalcopyrite spots located in 272.80m and 295.30m.

304.10m – 304.15m: Pinkish aplite dyke with potassium feldspar

304.15m – 314.60m: Granodiorite of Selenge Complex. Alteration is moderate chloritization, weak epidote veins along the fractures, quartz veinlets, calcite veins and pinkish clay veins. Andesite dyke with angle of 30 degrees. Mineralization is weak pyrite dissemination along epidote veinlets. Chalcopyrite spots located in 310.70m and 311.60m.

314.05m – 314.60m: Pinkish aplite dyke with potassium feldspar

314.60m – 348.90m: Granodiorite of Selenge Complex. Alteration is moderate chloritization, weak epidote with pyrite dissemination, quartz veinlets, calcite veins, pinkish clay veins and calcite-chlorite- quartz veins. Quartz vein including pyrite and few chalcopyrite. Calcite-epidote vein including pyrite-chalcopyrite veins. Mineralization is weak pyrite dissemination along epidote veinlets. Chalcopyrite spots located in 334.60 to 334.70m and 340.00m to 348.00m.

348.90m – 350.90m: Dark grey basaltic dyke with weak chloritization.

350.90m – 358.00m: Granodiorite of Selenge Complex. Alteration is moderate chloritization, weak epidote, and quartz veinlets with pyrite along the fractures, epidote veins with pyrite dissemination.

358.00m – 376.00m: Granodiorite of Selenge Complex. Alteration is moderate chloritization, weak epidote, partly silicification, and calcite veins along the fractures, calcite-quartz veins. Quartz vein including pyrite. Calcite-epidote vein including pyrite veins. Mineralization is weak pyrite dissemination in the minerals of hornblende and biotite. Chalcopyrite spots located in 361.30m, 361.50m and 369.30m.

376.00m – 405.60m: Granodiorite of Selenge Complex. Alteration is moderate chloritization, weak epidotization, partly silicification, and calcite veins along the fractures, calcite-quartz veins. Quartz vein including pyrite. Calcite-epidote vein including pyrite veins. Mineralization is weak pyrite dissemination in the minerals of hornblende and biotite. Chalcopyrite spots located in 385.00m.

405.60m – 407.20m: Light brownish grey micro-granodiorite with hornblende.

407.20m – 414.95m: Granodiorite of Selenge Complex. Alteration is weak to moderate chloritization, weak epidotization, quartz veinlets along the fractures. Quartz-epidote vein is including a few of pyrite and epidote veins. Mineralization is weak pyrite veins including chalcopyrite. Pyrite locating in minerals of hornblende and biotite.

414.95m – 415.30m: Andesite dyke.

415.30m – 425.00m: Granodiorite of Selenge Complex. Alteration is weak to moderate chloritization, weak epidotization, quartz veinlets along the fractures. Quartz-epidote vein is including a few of pyrite and epidote veins. Mineralization is pyrite sulphide veins including chalcopyrite. Pyrite existing in minerals of hornblende and biotite. Chalcopyrite spots located in 417.00m and 419.00m.

425.00m – 426.20m: Andesite dyke.

426.20m – 431.20m: Granodiorite of Selenge Complex. Alteration is weak to moderate chloritization, weak epidotization.

431.20m – 431.40m: Andesite dyke.

431.40m – 431.90m: Granodiorite of Selenge Complex. Alteration is weak to moderate chloritization, weak epidotization. Weak pyrite dissemination.

431.90m – 432.50m: Andesite dyke.

432.50m – 432.85m: Granodiorite of Selenge Complex. Alteration is weak to moderate chloritization, weak epidotization and epidote-calcite veins. Mineralization is weak pyrite dissemination.

432.85m – 433.05m: Andesite dyke.

433.05m – 436.00m: Granodiorite of Selenge Complex. Alteration is weak to moderate chloritization, weak epidotization, epidote veins and epidote-calcite veins. Mineralization is weak

pyrite dissemination.

436.00m – 436.15m: Andesite dyke.

436.15m – 445.40m: Granodiorite of Selenge Complex. Alteration is weak to moderate chloritization, weak epidotization and epidote-calcite veins. Mineralization is weak pyrite dissemination.

445.40m – 448.90m: Andesite dyke.

448.90m – 449.20m: Granodiorite of Selenge Complex. Alteration is weak to moderate chloritization, weak epidotization

449.20m – 450.40m: Andesite dyke.

450.40m – 454.15m: Granodiorite of Selenge Complex. Alteration is weak to moderate chloritization, weak epidotization, quartz vein along the fractures, quartz-epidote-calcite veins, epidote veins and calcite veins. Mineralization is weak pyrite dissemination.

454.15m – 454.40m: Andesite dyke.

454.40m – 457.60m: Granodiorite of Selenge Complex. Alteration is weak to moderate chloritization, weak epidotization, weak clay veins, quartz vein along the fractures, quartz-epidote-calcite veins, epidote veins and calcite veins. Mineralization is weak pyrite dissemination.

457.60m – 457.90m: Andesite dyke.

457.90m – 465.30m: Granodiorite of Selenge Complex. Alteration is weak to moderate chloritization, weak epidotization, quartz vein along the fractures, quartz-epidote-calcite veins with pyrite, epidote veins and calcite veins. Mineralization is weak pyrite dissemination in the minerals of hornblende and biotite.

465.30m – 465.40m: Andesite dyke.

465.40m – 501.80m: Granodiorite of Selenge Complex. Alteration is moderate chloritization, weak epidotization, quartz vein along the fractures, quartz-epidote-calcite veins with pyrite, epidote veins and calcite veins. Mineralization is weak pyrite dissemination in the minerals of hornblende and biotite.

501.50m: Bottom of MJME-M1 hole

Alteration: According to the results of X-ray diffraction analysis, main mineral of silicified rock from 56 m to 167 m indicated the presence of quartz, plagioclase, chlorite, sericite and pyrite. Mineral assemblages of alteration are quartz-sericite-chlorite type or quartz-sericite type. Other mineral is stellerite, a kind of zeolite minerals. The detected main mineral of micro-granodiorite from 112m to 232m indicated the presence of quartz, plagioclase, hornblende, chlorite and pyrite. Mineral assemblages of alteration indicate propylite alteration mineral assemblage. Other mineral is clinoptilolite, a kind of zeolite minerals. The detected main mineral of diorite porphyry from 194m to 267m indicated the presence of quartz, plagioclase, hornblende, chlorite, sericite and pyrite. Mineral assemblages of alteration indicate propylite alteration type and quartz-sericite-chlorite type. The detected main mineral of Selenge Complex granodiorite from 165m to 501.80m indicated the presence of quartz, plagioclase, hornblende, chlorite and pyrite. Mineral assemblages of alteration indicate propylite alteration type and quartz-sericite type. Potassium feldspar is detected in drilling cores from 440m to 501m. Other minerals are epidote, clinoptilolite and stellerite.

Mineralization: The results of the microscopic observation for ore indicated that ore minerals of chalcopyrite are occurred in polished thin sections of 261.55m, 334.60m, 347.80m, 369.30m, 418.40m and 499.40m. Ore mineral of galena are occurred in the polished thin sections of 334.60m and 347.80m. Ore mineral of sphalerite are occurred in the polished thin section of 418.40m. In the polished thin section of 418.40m, Ore minerals of chalcopyrite, galena and sphalerite are coexisting. Alteration

minerals related to mineralization are presented quartz-sericite-chlorite type and quartz-chlorite-epidote type with calcite alteration and zeolite alteration.

The ore assay results indicated that copper values in silicified rock are less than Cu 0.001 % to Cu 0.004 %, lead values Pb 0.005 % to Pb 0.018 % and Zinc values less than Zn 0.002 % to Zn 0.017 %. The copper values in micro-granodiorite and diorite porphyry are Cu 0.002 % to Cu 0.011 %, lead values Pb 0.006 % to Pb 0.010 % and Zinc values less than Zn 0.009 % to Zn 0.014 %. The copper values in Selenge Complex granodiorite are less than Cu 0.001 % to Cu 0.100 %, lead values Pb 0.006 % to Pb 0.010 % and Zinc values less than Zn 0.009 % to Zn 0.014 %. In the drilling core with more than Cu 0.100 %, the alteration with epidote, quartz and calcite is strong and a little of chalcopyrite minerals were observed. The copper values are relatively high in the intrusive rocks.

(2) MJME-M2 Hole

This hole is located at geophysical survey point of MG12-50 where is located in the eastern part of the Shar chuluut Mountain of the Mogoin gol area. The drilling site is on the Quaternary deposits consisting of stream sediments and debris deposits. The geology around drilling site is mainly Permian to Triassic volcanic, andesitic dykes and Quaternary deposits.

Geology: Drilling cores of MJME-M1 are mainly composed of Quaternary deposits from 0.00m to 34.20m and basements from 34.20m to 500.20m. The basements are Permian to Triassic volcanic rocks and andesitic dykes. The below is shown drilling core logging. The drilling columns are shown Appendix 17. The geologic cross section of MJME-M2 is shown Fig. II-4-4.

0.00m – 2.40m:	Surface soil including gravel
2.40m – 4.65m:	Grey silt including cobble gravel and pebble gravel
4.65m – 4.85m:	Cobble gravel
4.85m – 8.00m:	Silt and sand with granule
8.00m – 8.20m:	Pebble gravel
8.20m – 8.75m:	Granule to pebble gravel
8,75m – 12.60m:	Grey sandy silt
12.60m – 13.40m:	Sandy silt with granule
13.40m – 14.50m:	Pebble gravel with sub-angular to sub-rounded gravel
14.50m – 16.40m:	Purplish grey Cobble gravel to pebble gravel with sub-angular to sub-rounded gravel
16.40m – 17.30m:	Pebble gravel
17.30m – 17.80m:	Khaki brown silty pebble gravel
17.80m – 18.60m:	Khaki brown to purplish grey granule
18,60m – 18.70m:	Grey silt
18.70m – 24.00m:	Pebble gravel with silt
24.00m – 24.40m:	Pebble gravel to granule
24.40m – 25.80m:	Pebble gravel
25.80m – 26.20m:	Brown silt
26.20m – 29.00m:	Yellow, brown and reddish brown, weathered silts with granule
29.00m – 29.60m:	White clay with granule and pebble gravel (Fault clay?)
29.60m – 30.20m:	Light brown silt-sand with granule
30.20m – 30.90m:	Light grey argillized and sericite-altered rock
30.90m – 34.20m:	White Cobble to pebble gravel with angular to sub-angular fragments
34.20m – 39.20m:	Light grey silicified rock. Alteration is moderate silicification, moderate sericitization, weak chloritization and weak clay veinlets. Fractures are developed.

39.20m – 44.20m: Light grey silicified rock. Alteration is moderate silicification, moderate sericitization, and spotted chloritization. Mineralization is moderate pyrite dissemination and pyrite veinlets. Fractures are developed.

44.20m – 79.90m: Light grey to grey, pyrite disseminated rock with brecciation (quartz- sericite rock). Auto-brecciated rock to brecciated silicified rock from 44m to80m. Very strongly brecciated part from 56m to 70m. Alterations are moderate silicification, moderate sericitization, chloritization spotted. White clay veinlets along fractures. Epidote veinlets from 53m to 60m. The matrix among in the brecciated fragments is filled by pyrite. Quartz veinlets from 55m to 69m.

79.90m – 96.40m: Light grey to grey, pyrite disseminated rock with brecciation (quartz- sericite rock). Very strong silicified cock from 80m to101m. Alterations are very strong silicification, strong sericitization, and weak chloritization. White calcite and kaolinite veinlets along fractures. Mineralizations are very strong pyrite dissemination, pyrite network veins and druse (3 cm in diameter) in core.

96.40m – 106.80m: Grey pyrite disseminated, silicified rock (quartz-sericite (-chlorite) rock). Brecciated silicified rock from 105m to 107m. Strong chloritized rock along the fractures. Alterations are strong silicification, strong sericitization and weak chlorite veinlets along the fractures. Mineralizations are strong to moderate pyrite dissemination and pyrite network veins. Spotted chalcopyrite in the chloritized zone in the fractures from 104.20m to 105.00m. Quartz veins (2 to 3 mm in width) from 106.75 to 106.80m include a few of chalcopyrite.

106.80m – 110.30m: Grey pyrite disseminated, silicified rock. The matrix is white clays. Fluorite veins filed in the fractured zone and clacks Alterations are strong silicification, strong sericitization and weak chloritization. Mineralizations are moderate pyrite dissemination in the silicified rock and pyrite network veins.

110.30m – 112.00m: Greenish grey andesite to porphyritic andesite (angle: 10 degrees).

112.00m – 116.10m: White to light grey argillized and silicified rock. The matrix is argillized. Specularite veins and chlorite veins are filed in the fractured zone and clacks. Alterations are strong silicification, strong sericitization and weak chloritization. Mineralizations are moderate pyrite dissemination in the silicified rock and azurite spots in the 112m. Milky silicified rocks with strong pyrite dissemination are appeared in the lower part.

116.10m – 121.90m: Milky white to light grey rock originated by granitic rock. Mineralization is weak pyrite dissemination. Original rock may be granitic rock because of development of fracture, texture etc. of silicified rock. The part from 117m to 122m is very hard and silicified rock. Specularite is observed in the fractures around 116.95m. Very fine chalcopyrite is observed from116.80m to 121.40m.

121.90m – 126.50m: Light grey strong silicified rock. Alterations are strong silicification, strong sericitization, weak chloritization and clay veins along the fractures and clacks. Mineralization is weak to moderate pyrite dissemination.

126.60m – 134.00m: Light grey strong silicified rock. Alterations are strong silicification, moderate sericitization and weak chloritization along the fractures. Mineralization is weak pyrite dissemination, pyrite veinlets and quartz-chlorite-specularite veins with pyrite.

134.00m – 141.10m: White to light grey, very hard and strong silicified rock with brecciation. Druse (2mm to 20mm) developed. Alterations are strong silicification and moderate sericitization, weak chloritization and argillization along the fractures. Mineralization is weak pyrite dissemination, pyrite-chalcopyrite veinlets and chlorite-specularite veins.

141.10m – 150.80m: Light grey, argillized and silicified rock with brecciation. Alterations are strong silicification, moderate sericitization and weak chloritization. Quartz veinlets and pyrophylite-clay-fluorite veins filled in the fractures and clacks. Mineralization is weak pyrite dissemination.

150.80m – 160.40m: Drilling cores could not be recovered. The part was clay that was filled in the open faults and open clacks. By the geologic boundary, the very strong silicified of hanging whale was divided into volcanic tuff of Permian to Triassic age. The fault zone is probably continued to the NW-SE fault in the geologic map. The fault may be big.

160.40m – 161.20m: Greenish grey andesitic tuff. Alterations are moderate to strong chloritization, weak silicification in part and weak argillization. Mineralization is weak pyrite veinlets, quartz -hematite veins and chlorite veins with a few of pyrite.

161.20m – 164.10m: Drilling cores could not be recovered. The part was clay and sand that was filled in the open faults and open clacks.

164.10m – 168.60m: Greenish grey andesitic tuff. Alterations are moderate to strong chloritization, weak silicification in part and weak argillization. Mineralization is weak pyrite veinlets, quartz -hematite veins and chlorite veins with a few of pyrite.

168.60m – 173.00m: Dark grey andesite. Alterations are moderate chloritization and weak epidote in parts. Mineralization is weak pyrite dissemination and pyrite veinlets.

173.00m – 183.80m: Greenish grey andesitic tuff. Alterations are weak silicification, moderate to strong chloritization and pinkish clay veinlets. Mineralization is weak pyrite dissemination and chlorite-pyrite veinlets along the fractures.

183.80m – 189.85m: Grey andesite to dolerite dyke. Alterations are moderate chloritization and weak epidotization, and pinkish clay veinlets.

189.85m – 193.60m: Grey andesitic tuff to silicified tuff. Alterations are strong silicification, moderate chloritization and weak argillization, and fluorite veinlets, quartz-hematite veinlets and specularite veinlets. Mineralization is moderate pyrite dissemination and pyrite veinlets along the fractures.

193.60m – 193.90m: Greenish grey andesite dyke. Alterations are moderate to weak chloritization and weak silicification, clay veinlets and fluorite veins. Mineralization is weak pyrite dissemination.

193.90m – 195.70m: White silicified rock. Alterations are strong silicification, clay veinlets. Mineralization is weak pyrite dissemination, pyrite veinlets and pyrite-chalcopyrite veins (3mm to 7mm in width).

19570m – 195.90m: Dark greenish grey andesite dyke. Alterations are moderate to weak chloritization and weak silicification and clay veinlets. Mineralization is weak pyrite dissemination.

195.90m – 197.23m: White silicified rock. Alterations are strong silicification and clay veinlets. Mineralization is weak pyrite dissemination, pyrite veinlets and pyrite-chalcopyrite veins (3mm to 7mm in width).

197.23m – 198.30m: Greenish grey andesite dyke. Alterations are moderate to weak chloritization, weak silicification and clay veinlets. Mineralization is very weak pyrite dissemination.

198.30m – 199.00m: White, very hard silicified rock. Alterations are strong silicification, strong sericitization and clay veinlets along the fractures. Mineralization is weak pyrite dissemination and pyrite veinlets.

199.00m – 206.75m: Greenish grey andesite dyke. Alterations are weak chloritization and weak silicification. Mineralization is very weak pyrite dissemination.

206.75m – 208.70m: White, very hard silicified rock. Alterations are very strong silicification, strong sericitization and clay veinlets along the fractures. Mineralization is weak pyrite dissemination and pyrite veinlets.

208.70m – 208.85m: Greenish grey andesite dyke. Alterations are moderate to weak chloritization. Mineralization is very weak pyrite dissemination and pyrite veinlets.

208.85m – 217.10m: Light brownish grey, silicified rock. Alterations are strong silicification, sericite-clay veinlets, pyrophylite veinlets and fluorite veinlets along the fractures. Mineralization is weak pyrite dissemination in host rock, and quartz veinlets and sulphide veinlets (1mm to 3mm).

217.10m – 218.95m: White and red spotted, hard silicified rock with red hematite minerals. Alterations are very strong silicification, clay veinlets. Mineralization is weak pyrite dissemination and pyrite veinlets.

218.95m – 223.60m: Dark brownish grey, andesitic tuff breccia. Alterations are hematite formation, weak chloritization and weak epidotization, and clay veinlets, quartz veinlets and pyrophylite- fluorite veinlets.

223.60m – 241.85m: White, very hard silicified rock. Alterations are very strong silicification, agate alteration and clay veinlets along the fractures. Mineralization is weak pyrite.

241.85m – 246.05m: Dark brownish grey, silicified tuff. Alterations are moderate silicification, weak chloritization, quartz veinlets and hematite veinlets. Mineralization is weak pyrite dissemination, pyrite veinlets and quartz-hematite-chlorite vein with chalcopyrite.

246.05m – 247.20m: White argillized and silicified rock with fluorite veinlets. Mineralization is pyrite dissemination.

247.20m – 254.85m: Grey to brownish grey silicified rock. Alterations are strong silicification, weak chloritization, weak epidotization, fluorite veinlets, clay veinlets and hematite veinlets. Mineralization is strong pyrite dissemination and pyrite veinlets.

254.85m – 256.90m: Greenish grey andesite dyke.

256.90m – 258.40m: Dark brownish grey, silicified rock. Alterations are moderate silicification, weak chloritization, weak epidotization, hematite formation, clay veinlets, fluorite veinlets and hematite veinlets. Mineralization is weak pyrite dissemination and pyrite veinlets.

258.40m – 264.00m: Greenish grey andesite dyke with clay veinlets. Alterations are weak chloritization and weak epidotization.

264.00m – 265.20m: Dark brownish grey, silicified rock with brecciation. Alterations are moderate silicification, weak chloritization, weak epidotization, hematite formation, clay veinlets, fluorite veinlets and quartz veinlets. Mineralization is weak pyrite dissemination and pyrite veinlets.

265.20m – 268.80m: Greenish grey andesite dyke with clay veinlets. Alterations are weak chloritization and weak epidotization, and quartz-hematite vein with pyrite.

268.80m – 273.80m: Greenish grey, silicified tuff. Alterations are weak silicification, weak chloritization and weak epidotization. Mineralization is weak pyrite dissemination and pyrite veinlets.

273.80m – 282.30m: Greenish grey andesite dyke with quartz veinlets. Alterations are weak chloritization and weak epidotization.

282.30m – 290.00m: Greenish grey, silicified tuff. Alterations are weak silicification and weak chloritization, and clay veinlets, quartz-epidote veins and potassium feldspar veinlets along the fractures. Mineralization is weak pyrite dissemination and pyrite veinlets.

290.00m – 296.50m: Greenish grey andesite dyke with quartz veinlets. Alterations are weak chloritization and weak epidotization.

296.50m – 307.20m: Light grey, silicified and sericitizated tuff breccia with brecciation. Alterations are moderate silicification and moderate chloritization, and kaolin-clay veinlets, quartz-epidote veins, quartz veinlets, fluorite veinlets and potassium feldspar veinlets along the fractures. Mineralization is strong pyrite dissemination and moderate pyrite veinlets.

307.20m – 307.75m: Greenish grey andesite dyke with quartz-hematite veinlets. Alterations are weak chloritization and weak epidotization.

307.75m – 309.90m: Greenish grey, silicified tuff. Alterations are weak silicification, moderate chloritization and weak epidotization, and pinkish clay veinlets and quartz veins. Mineralization is weak pyrite dissemination.

309.90m – 310.80m: Greenish grey andesite dyke with fractures by faulting.

310.80m – 312.20m: Dark greenish grey silicified tuff with brecciation. Alterations are moderate silicification, weak sericitization, moderate chloritization, weak epidotization and moderate argillization. Mineralization is moderate pyrite dissemination.

312,20m – 313.85m: Greenish grey andesite dyke with clay veinlets. Alterations are strong chloritization. Mineralization is weak pyrite dissemination.

313.85m – 315.90m: Grey to dark grey silicified tuff with brecciation. Alterations are moderate silicification, weak sericitization, weak epidotization and moderate argillization, and pyrophylite veinlets. Mineralization is moderate pyrite dissemination.

315.90m – 319.10m: Greenish grey andesite dyke with quartz veinlets. Alterations are weak chloritization and weak epidotization, and quartz-chlorite veinlets.

319.10m – 328.85m: Grey silicified tuff with brecciation. Alterations are moderate silicification, weak sericitization, weak epidotization and moderate to strong argillization, and quartz veinlets. Mineralization is moderate pyrite dissemination, chlorite-pyrite veinlets and pyrite veins.

328.85m – 332.60m: Light grey argillized rock with brecciation. Drilling cores are flakes and core recovery is low. Alterations are argillization and strong silicification, and pyrophylite veinlets. Mineralization is strong pyrite dissemination, quartz-pyrite

veinlets and pyrite veins.

332.60m – 337.20m: Light grey clay and slimes. The part is fault zone and clacked zone. Mineralization is strong pyrite dissemination.

337.20m – 343.20m: Light grey silicified tuff with brecciation. Drilling cores are flakes and core recovery is low. Alterations are moderate silicification, moderate argillization, moderate sericitization, and quartz veinlets, clay veinlets and fluorite veinlets. Mineralization is strong pyrite dissemination, quartz-pyrite network veinlets and pyrite veins.

343.20m – 350.00m: Light grey tuff with brecciation. Alterations are moderate silicification, moderate sericitization, and gypsum veins, clay veinlets, quartz veinlets and fluorite veinlets. Mineralization is strong pyrite dissemination, quartz-pyrite network veinlets and pyrite veins.

350.00m – 352.00m: Dark greenish grey welded tuff. Alterations are weak silicification, moderate chloritization and weak epidotization. Mineralization is weak pyrite dissemination.

352.00m – 354.20m: Dark greenish grey tuff. Alterations are weak silicification.

354.20m – 362.35m: Dark greenish grey tuff. Alterations are weak silicification, moderate chloritization and moderate epidotization.

362.35m – 362.70m: Dark greenish grey andesite dyke. Alterations are moderate chloritization and moderate epidotization.

362.70m – 362.90m: Dark grey tuff. Alterations are weak silicification, moderate chloritization and moderate epidotization.

362.90m – 366.35m: Dark greenish grey andesite dyke. Alterations are moderate chloritization and moderate epidotization.

366.35m – 366.50m: Dark grey tuff. Alterations are weak silicification, moderate chloritization and moderate epidotization.

366.50m – 369.40m: Dark greenish grey andesite dyke. Alterations are moderate chloritization and moderate epidotization.

369.40m – 379.20m: Dark grey tuff. Alterations are weak silicification, moderate chloritization and moderate to weak epidotization. Mineralization is weak pyrite dissemination.

379.20m – 380.30m: Brownish grey tuff. Alterations are weak silicification, moderate chloritization and moderate to weak epidotization. Mineralization is weak pyrite dissemination.

380.30m – 388.50m: Light grey, silicified tuff. Alterations are moderate silicification and moderate sericitization. Mineralization is weak to moderate pyrite dissemination and pyrite veinlets.

388.50m – 393.35m: Dark grey andesitic welded tuff. Alterations are moderate silicification and moderate sericitization. Mineralization is moderate pyrite dissemination.

393.35m – 403.95m: Light grey tuff with brecciation and sheared structure. Alterations are moderate silicification and moderate sericitization. Mineralization is weak to moderate pyrite dissemination and pyrite veinlets.

403.95m – 405.85m: Greenish grey andesite dyke. Alterations are moderate chloritization and moderate epidotization.

405.85m – 407.00m: Light grey, sericitizated and silicified tuff with brecciation and sheared structure. Alterations are strong silicification and moderate sericitization. Mineralization is weak pyrite dissemination and pyrite veinlets.

407.00m – 407.85m: Grey andesitic welded tuff with brecciation and sheared structure. Alterations are strong silicification and moderate sericitization. Mineralization is weak pyrite dissemination and pyrite veinlets.

407.85m – 413.25m: Grey sheared and silicified tuff with brecciation and sheared structure. Alterations are strong silicification and moderate sericitization. Mineralization is weak to moderate pyrite dissemination and pyrite veinlets.

413.25m – 413.85m: Greenish grey andesite dyke. Alterations are moderate chloritization and moderate epidotization.

413.85m – 420.55m: Grey sheared and silicified tuff with brecciation and sheared structure. Alterations are strong silicification and moderate sericitization. Mineralization is strong pyrite dissemination, pyrite veinlets and stockwork pyrite.

420.55m – 424.70m: Greenish grey tuff with brecciation and sheared structure. Alterations are strong silicification and moderate sericitization. Mineralization is strong pyrite dissemination and pyrite veinlets.

424.70m – 425.35m: Greenish grey andesite dyke. Alterations are moderate chloritization and moderate epidotization.
425.35m – 425.50m: Greenish grey tuff. Alterations are strong silicification and moderate sericitization. Mineralization is weak pyrite dissemination and pyrite veinlets.
425.50m – 425.80m: Greenish grey andesite dyke. Alterations are moderate chloritization and moderate epidotization.
425.80m – 432.40m: Greenish grey tuff. Alterations are weak silicification, moderate sericitization, moderate chloritization and moderate epidotization. Mineralization is weak pyrite dissemination and pyrite veinlets.
432.40m – 445.20m: Grey, silicified and sericitizated tuff. Alterations are moderate silicification, moderate sericitization, moderate chloritization and moderate epidotization. Mineralization is weak pyrite dissemination and pyrite veinlets.
445.20m – 456.30m: Greenish grey tuff. Alterations are moderate silicification, moderate sericitization, moderate chloritization and moderate epidotization. Mineralization is weak pyrite dissemination and pyrite veinlets.
456.30m – 457.85m: Grey, silicified and sericitizated tuff. Alterations are moderate silicification, moderate sericitization and moderate chloritization. Mineralization is weak pyrite dissemination and pyrite veinlets.
457.85m – 461.15m: Dark grey to greenish grey tuff. Alterations are weak silicification, weak sericitization and weak chloritization. Mineralization is weak pyrite dissemination and pyrite veinlets.
461.15m – 461.30m: Grey, silicified and sericitizated tuff. Alterations are moderate silicification and moderate sericitization. Mineralization is moderate pyrite dissemination and pyrite veinlets.
461.30m – 462.00m: Dark grey to greenish grey tuff. Alterations are weak silicification, weak sericitization and weak chloritization. Mineralization is weak pyrite dissemination and pyrite veinlets.
462.00m – 462.25m: Grey, silicified and sericitizated tuff. Alterations are moderate silicification and moderate sericitization. Mineralization is moderate pyrite dissemination and pyrite veinlets, pyrite-chalcopyrite veins (2mm to 4mm in width).
462.25m – 470.05m: Dark grey to greenish grey tuff. Alterations are weak silicification, weak sericitization and weak chloritization. Mineralization is weak pyrite dissemination and pyrite veinlets.
470.05m – 474.05m: Greenish grey andesite dyke. Alterations are moderate chloritization and moderate epidotization.
474.05m – 474.85m: Greenish grey tuff. Alterations are weak silicification, weak sericitization, weak chloritization and weak epidotization. Mineralization is weak pyrite dissemination and pyrite veinlets.
474.85m – 474.95m: Greenish grey andesite dyke. Alterations are moderate chloritization and moderate epidotization.
474.95m – 475.40m: Greenish grey tuff. Alterations are weak silicification, weak sericitization, weak chloritization and moderate epidotization. Mineralization is weak pyrite dissemination and pyrite veinlets.
475.40m – 477.00m: Greenish grey andesite dyke. Alterations are moderate chloritization and moderate epidotization.
477.00m – 477.30m: Greenish grey tuff. Alterations are weak silicification, moderate sericitization, weak chloritization and moderate epidotization. Mineralization is weak pyrite dissemination and pyrite veinlets.
477.30m – 479.35m: Greenish grey andesite dyke. Alterations are moderate chloritization and moderate epidotization.
479.35m – 481.20m: Greenish grey tuff. Alterations are weak silicification, moderate sericitization, weak chloritization and moderate epidotization. Mineralization is weak pyrite dissemination and pyrite veinlets.
481.20m – 487.85m: Greenish grey andesite dyke. Alterations are moderate chloritization and moderate epidotization.
487.85m – 488.50m: Brownish grey sheared and silicified tuff. Alterations are moderate silicification, moderate sericitization and weak chloritization. Mineralization is weak pyrite

dissemination and pyrite veinlets.

488.50m – 493.05m: Brownish grey micro-granodiorite dyke. Alterations are weak sericitization, weak chloritization and moderate epidotization.

493.05m – 493.30m: Brownish grey micro-granodiorite dyke. Alterations are weak sericitization, weak chloritization and moderate epidotization.

493.30m – 498.40m: Brownish grey micro-granodiorite dyke. Alterations are weak sericitization, weak chloritization and moderate epidotization.

498.40m – 499.95m: Greenish grey tuff. Alterations are weak silicification, weak sericitization and weak chloritization. Mineralization is moderate pyrite dissemination and pyrite veinlets.

499.95m – 500.20m: Greenish grey tuff. Alterations are moderate silicification, moderate sericitization and weak chloritization. Mineralization is moderate pyrite dissemination and pyrite veinlets, and quartz vein with chalcopyrite spots at 499.55m.

500.20m: Bottom of MJME-M2 hole.

Alteration: According to the results of X-ray diffraction analysis, main mineral of silicified rock from 34 m to 100m indicated the presence of quartz, plagioclase, chlorite, sericite and pyrite. Mineral assemblages of alteration are quartz-sericite-chlorite-pyrite type. Other mineral is potassium feldspar. The detected main mineral of silicified rock from 100m to 120m indicated the presence of quartz and pyrite. Other mineral is chlorite-sericite, chlorite and pyrophylite. The detected main mineral of silicified rock from 120m to 161m indicated the presence of quartz, plagioclase and potassium feldspar. Other mineral is chlorite, chlorite- sericite and clinoptilolite. The detected main mineral of silicified rock from 180 m to 260 m indicated the presence of quartz, chlorite and sericite. Mineral assemblages of alteration are quartz-sericite-chlorite-pyrite type and quartz-sericite type. The detected main mineral of andesite duke at 280 m indicated the presence of plagioclase, hornblende and sericite. Mineral assemblages of alteration are propylite alteration minerals. Other mineral is pyrite. The detected main mineral of silicified tuff from 300m to 320m indicated the presence of quartz, chlorite and sericite. Mineral assemblage of alteration is quartz-sericite-chlorite-pyrite type. Other mineral is analcite. The detected main mineral of silicified tuff from 340m to 380m indicated the presence of quartz, chlorite, sericite and gypsum. Mineral assemblage of alteration is quartz-sericite-chlorite-pyrite type. The detected main mineral of silicified tuff from 400m to 440m indicated the presence of quartz, plagioclase and hornblende. Other minerals are laumontite, stilbite and gypsum. The detected main mineral of silicified tuff from 460m to 500m indicated the presence of quartz, plagioclase, hornblende and chlorite. Mineral assemblage of alteration shows propylite alteration. Other minerals are laumontite and gypsum. The detected main mineral of micro-granodiorite at 491m indicated the presence of plagioclase, hornblende and chlorite. Mineral assemblage of alteration shows propylite alteration. Other mineral is gypsum.

Mineralization: The results of the microscopic observation for ore indicated that ore minerals of chalcopyrite are occurred in polished thin sections of 104m to 119m, 244m and 462m to 500m. Ore mineral of azurite occurred in the polished thin sections of 104m, 217m and 392m. Ore mineral of sphalerite are occurred in the polished thin section of 104m to 106m and 406m to 411m. In the polished thin section of 104m to 106m, ore minerals of chalcopyrite and sphalerite are coexisting. Alteration minerals related to mineralization are mainly presented quartz-sericite-chlorite-zeolite-pyrite type until

160m and quartz- muscovite-sericite-zeolite-pyrite type from 160m to 320m and quartz-sericite—zeolite-pyrite type.

The ore assay results indicated that copper values in silicified rock from 34.20m to 160m are less than Cu 0.001 % to Cu 0.015 %, lead values less than Pb 0.001 % to Pb 0.010 % and Zinc values Zn 0.002 % to Zn 0.115 %. Maximum values of other elements are Au 0.04 g/t and Mo 0.002 %. The copper values in silicified rock from 160.40m to 337.20m are less than Cu 0.001 % to Cu 0.015 %, lead values less than Pb 0.001 % to Pb 0.010 % and Zinc values less than Zn 0.001 % to Zn 0.015 %. Maximum values of other elements are Au 0.28 g/t, Ag 0.137 g/t and Mo 0.002 %. The copper values in silicified rock from 337.20m to 500.20m are less than Cu 0.001 % to Cu 0.065 %, lead values Pb 0.003 % to Pb 0.018 % and Zinc values Zn 0.001 % to Zn 0.076 %. Maximum values of other elements are Au 0.02 g/t and Mo 0.002 %.

(5) Discussion

According to the results of drilling survey that was conducted in the western part and the eastern part of the Shal Chuluut Mountain in the Mogoin gol area, the geologic cross section connected between MJME-M1 and MJME-M2 drilling holes is shown Fig. II-4-5.

The drilling cores of MJME-M1 indicated that the geology presented volcanic tuff of Permian to Triassic age, granodiorite of Selenge Complex of Triassic age, diorite porphyry and micro-granodiorite of Triassic to Jurassic age and andesite dyke. The alterations related to mineralization are propylite alteration with pyritization, sericite-chlorite type alteration. The alteration shows the intermediate to acidic alteration as the hydrothermal alteration overprinting on the diagenesis. The mineralization seems to be of the rim of the polymetallic mineralization consisting of chalcopyrite-sphalerite-galena or the porphyry copper type mineralization.

The drilling cores of MJME-M2 indicated that the geology presented the silicified and argillized volcanic tuff of Permian to Triassic age, micro-granodiorite of Triassic to Jurassic age and andesite dyke. The fault zones are detected around 160m and 335m of drilling hole in depth and are reverse faults.

Upper part from 160m indicated mainly the sericite-chlorite type alteration including potassic feldspar and pyrophylite. The hydrothermal mineralization is thought to be genetical approximate temperature of 300 degrees C. The brecciation and many pyrite ore minerals are characterized the mineralization in the MJME-M2 drilling core. The hydrothermal mineralization shows the intermediate to acidic alteration. The mineralization is the active pyritization including sulphide vein with pyrite, chalcopyrite and sphalerite, which is polymetallic type or porphyry copper type.

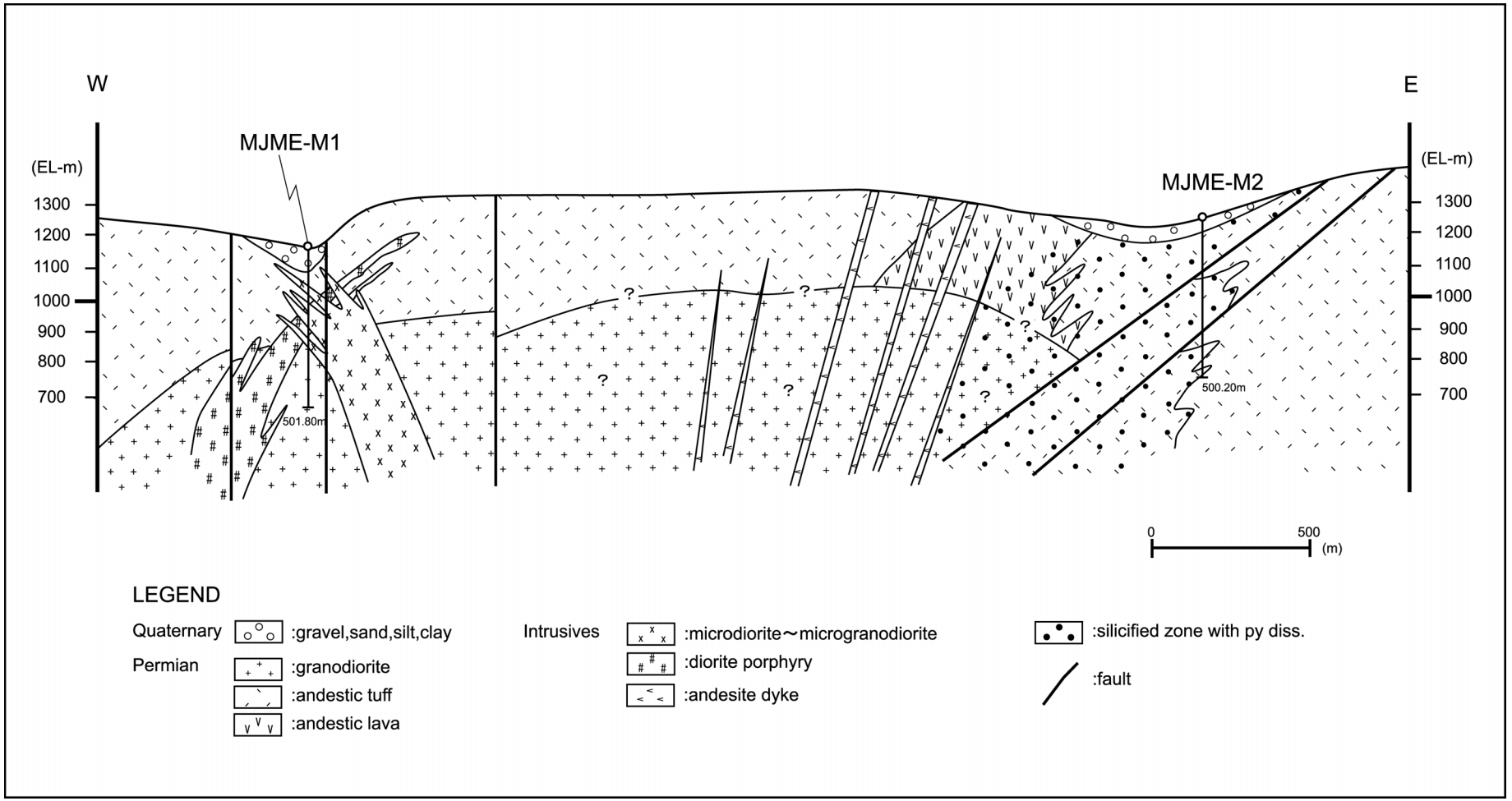

Fig.II-4-5　Cross section connected MJME-M1 drilling hole and MJME-M2 drilling hole

In the silicified tuff from 160m to 335m, the quartz-sericite-chlorite type alteration to the quartz-sericite type alteration is confirmed and accompanies of analcite. The hydrothermal alteration seems to be a type of the intermediate to acidic alteration. Activity of mineralization is high pyritization accompany with chalcopyrite and sphalerite.

In the silicified tuff from 335m to 500m, quartz-sericite alteration type alteration and propylite alteration with zeolite minerals of laumontite and stilbite are detected and many gypsum veins are confirmed. The alteration is thought to be the alteration that hydrothermal alteration is overprinted on the diagenesis alteration. Ore minerals are pyrite, chalcopyrite and sphalerite in the sulphide veins and azurite in the argillized zones.

Alteration and mineralization of the silicified tuff between two fault zones of 160m and 335m shows a middle nature of the upper part and the lower part.

According to the results of the fluid inclusion test, the homogenization temperatures are 147 degrees C to 165 degree C in the MJME-M1 drilling core and 173 degrees C to 188 degree C in the MJME-M2 drilling core, which are relatively low. The salinity values are NaCl 3.9 % to NaCl 17.3 % in the MJME-M1 and NaCl 1.8 % in the MJME-M2. Maximum homogenization temperature in all data is 291 degrees C. On the other hand, salinity values are less than NaCl 10 % in most data, but show the highest vale of NaCl 28.9 % in a sample from MJME-M1 that inclusions include liquid CO_2.

Consequently, the results of the drilling survey on the western part and the eastern part of the Shar Chuluut Mountain are probably detected the surrounding mineralization of the polymetallic type mineralization or the porphyry copper type mineralization and indicate the potential that such mineralizations exist under the mountain.

PART III CONCLUSIONS AND RECOMMENDATIONS

CHAPTER 1　CONCLUSIONS

Based on the results of a geological mapping and a geophysical survey (IP electric survey) carried out in the Erdenet SE area, Under/Shand area and the Mogoin gol area during the second phase, the following conclusions are summarized below at each area.

1-1 Erdenet SE area

Geology is composed of the lower Permian volcanic rocks, the quaternary sediment rocks, late Permian granitic rocks, Selenge complex, and dykes. K-Ar age of the granodiorite of the granitic rocks in the Selenge complex indicates 196Ma, early Jurassic. Diorite is adakitic rock which indicates the same feature as the granodiorite observed in the Erdenet mine in the Selenge complex.

The main geological structures are the NE-SW direction of the dykes and the NS and NE-SW directions of the fault structures. The NW-SE trending faults are considered developed along the river in the southern part of the area.

The mineral showings observed are the white silicification alteration zones with quartz veins in the northeastern part of the area. This alteration zone is formed by the acid hydrothermal alteration composed of quartz, plagioclase, K-feldspar, kaolin and sericite. Ore grade is low.

Alterations are composed of quartz-K-feldspar-sericite-(kaolin), quartz-sericite-(kaolin), quartz-sericite-andalusite-(kaolin), sericite-chlorite-epidote, chlorite-epidote and chlorite but the alteration zone related to the large scale mineralization was not observed. Single element and multi element factor analysis of the rock geochemistry did not catch geochemical anomalies related to the mineralizations neither.

Prospective mineralizations in the Erdenet SE area were not observed. It is estimated though the adakitic diorite which can be suitable for the igneous rock related to the formation of the Erdenet deposit is distributed in the area, there is no mineralization accompanied by the porphyry copper-molybdenum deposit.

As a result of the geophysical surveys (IP electric method), the high to medium resistivity continues into the deeper zone in the diorite to granodiorite of the Triassic to Jurassic Selenge complex. Low resistivity indicates the low possibility for the alterations and low chargeability indicate the low possibility for the mineralizations. The dacite to rhyolitic tuff of Permian to Triassic volcanic rocks indicates the high resistivity continuing into the deeper zone, but it has low possibility for the mineralization with no anomaly of the low resistivity and high chargeability. The low resistivity is distributed in the shallow part of the quaternary which covers almost areas.

The low airborne magnetic anomaly detected last year is recognized to be caused by the adakitic diorite, but it is scarcely possible that the there is the igneous intrusion accompanied with mineralization due to less IP effect.

The mineralization related to the porphyry copper-molybdenum deposit was not detected in the area by a geological mapping and a geophysical survey. Therefore, it is considered to be not necessary to continue further explorations.

1-2 Under/Shand area

Geology is composed of the late Permian volcanic rocks, the quaternary sediment rocks, the Selenge complex intrusion, the late Permian granitic rocks, and dykes in this area. Ages of the granodiorite (γ δ 1P2-T1s) and the granodiorite porphyry (γ δ π 2P2-T1s) indicate 235 Ma (medium Triassic; T3) and 239 Ma (medium Triassic; T3) respectively.

Main geological structures are the NW-SE, the NS and the NE-SW trending faults. The NW-SE trending potential fracture zones are estimated in the southern part of the area judging from the distributions of the syenite porphyry (ξ π 2P2-T1s) which arrange to the NW-SE direction. The NW-SE trending lineaments are predominantly interpreted in the southern part of the area and the NS and the NE-SW trending lineaments are dominant in the northern part from the satellite images. The Under mineral showing is located on the NS trending lineament and the Shand mineral showing exists on the cross junction of the NS and the NW-SE trending lineaments.

In the center of the acidic alteration zone in the Under mineral showing, the quartz-sericite alteration is distributed with sericitization outward. Mineral assembles was formed by an acidic hydrothermal alteration. The size of the mineralization is small which has 100m X 100m and the ore grades indicate low values, 0.002%Cu, less than 0.001%Mo, 0.003%Pb, less than 0.001%Zn and 0.83%Fe.

The Shand mineral showing is a blind deposit covered by the quaternary sediments. Mineral assembles is the sericite-chlorite around the showing and is broadly distributed. It is probable that this alteration minerals assemblage indicates a part of the alteration zone related to the porphyry copper-molybdenum deposit in the Erdenet mine.

The greenish oxidized coppers of the filmy malachite and azurite were observed in the potassium metasomatized medium-grained granodiorite and the maximum ore grades indicate 0.119%Cu, 0.036%Pb, 0.116%Zn and 24 ppm Ag. The pyrite dissemination zone, which is mainly composed of limonites, accompanied with the white silicification zone was observed in the western central part of the area. Quartz, K-feldspar, biotite, alunite, andalusite and kaolin are present in the central part of the mineralization and chloritization is outward. Spotty azurite and chalcopyrite, disseminated pyrite, geothite, hematite and limonite were observed as ore minerals. Ore grades are 0.001 to 0.014%Cu, less than 0.001 to 0.003%Mo, 0.003 to 0.005%Pb, less than 0.001 to 0.002%Zn and 0.40 to 8.55%Fe.

As a result of geophysical surveys, the medium IP anomaly which had high resistivity and low metal factor was detected in the Under mineral showing of the Under/Shand_1 area. IP anomaly

overlapped by small low resistivity, the high chargeability and the high metal factor was detected in the Shand mineral showing of the Under/Shand_3 area, and the mineralizations of this showing were intersected by previous performed seventeen drills.

Therefore, it is considered to be not necessary to continue an exploration program in the Under and the Shand mineral showings in the Under/Shand area. On the other hand, it is recommended that carrying out a geophysical surveys (IP electric method) and a semi-detailed geological mapping in order to understand and delineate mineralizations.

1-3 Mogoin gol area

Geology in this area is composed of upper Permian alkali volcanic rocks, upper Triassic to lower Jurassic volcanic rocks, Permian to Triassic granites, Jurassic dykes, dykes and quaternary. K-Ar ages of the diorite and the rhyolitic porphyry indicate 208 Ma and 210Ma respectively, the late Triassic ages (T3). These ages are close to the radiometric ages, 190 Ma to 210 Ma, of the sericites from the Erdenet mine. The diorite and the rhyolitic porphyry taken for the K-Ar measurements are adakitic. Adakitic rocks have been recently reported as contributable rocks for porphyry copper-molybdenum deposits.

The area is regionally located in the cross junction of the EW trending faults and the NW-SE trending faults. The main faults have predominantly NNW-SSE, NW-SE and EW direction in the northern part, NW-SE and EW direction in the central part and NE-SW and EW direction in the southern part. As the Erdenet deposit is known to be in the junction of the NW-SE and the EW trending structure zones, the white silicification zone in the Mogoin gol area is almost same structure controlled as the Erdenet ore deposit.

The mineralization zones, silicified zone with the oxidized copper minerals, are confirmed around and in the southern part of Mt. Shar Chuluut. The alteration zoning is assembled to be the quartz or quartz-sericite zone in the center and the sericite-chlorite and chlorite zone outward in the north alteration zone. This alteration zoning is the same type as that of the Erdenet deposit. The center part of the alteration zoning in the south white silicification zone is the quartz-sericite alteration zone at where biotite, topaz and andalusite were observed. There is no alteration zone observed outside them. These alteration features are generally observed in the epithermal acidic alteration zone of high sulfidation system which develops in the upper part of mineralizations of porphyry copper-molybdenum deposits.

The north white silicification zone has 1.2km NS direction and 2km EW direction. The south white silicification zone accompanied with the secondary silicified rock has small alteration zone of 800m NS direction and over 1400m EW direction. The magnetite zone was formed by liparite and diorite intrusions as another alteration zone. In the white silicification zone azurite and malachite occur as coating and spotty. The maximum ore grades in the mineralization points are low as

0.026%Cu, 0.001%Mo, 0.021%Pb, 0.004%Zn and 12.72%Fe. The maximum ore grades in the mineralization points of the south white silicification zone are also low as 0.009%Cu, less than 0.001%Mo, 0.006%Pb and 0.002%Zn like the north white silicification zone. The ore grades in the magnetite zone are low.

Statistics of rock chemical analytical data indicated three factors related to the mineralization such as Factor 2 (Mo: the north white silicification zone), Factor 4 (Au-(Ag-Ni): the north white silicification zone, rhyolitic porphyry and the southern part of the area) and Factor 5 (Hg-Cu: the north white silicification zone and the south white silicification zone). High factor scores are confirmed in the north white silicification zone. Analytical values of Mo, Au, Ag, Ni, Hg and Cu are relatively high. The results of the rock chemical analyses are also suggested to be the zone of element leaching.

Results of geological mapping indicate that it is highly potential to host porphyry copper-molybdenum deposits in the north and south white silicification zones and exists at relatively deeper zone. Especially, at the center and around Mt Shar Chuluut in the north white silicification zone is distributed and alteration zoning same as that of the Erdenet deposit was observed. Relatively high geochemical anomalies were also detected though low analytical value. Small magnetic anomalies were detected. IP survey detected large IP anomaly zone overlapped by low resistivity, high chargeability and high metal factor at the center of Mt Shar Chuluut.

Based on the results of the geological survey and geophysical survey of phase I and II, the drilling survey composed of MJME-M1 hole of 501.80m in depth and MJME-M2 hole of 500.20m in depth were conducted at the western and eastern rims of the north silicified zone and detected the surrounding mineralization of polymetallic type and porphyry copper type mineralizations including ore minerals of pyrite, chalcopyrite, sphalerite and galena.

Accordingly, a drilling program is recommended in the north white silicification zone. It is also recommended to widen the IP electric survey area to the eastern side of the second phase survey area as high chargeability increases and continue to the eastern deeper zone, and to continue an exploration in order to understand IP structures related to the mineralizations and construct the mineralization model.

CHAPTER 2　RECOMMENDATIONS FOR THE PHASE Ⅲ

As the results of geological mappings and geophysical surveys, the following programs are recommended for the phase III.

(1) Mogoin gol area

The white silicified zones were distributed at the center of and around Mt. Shar Chuluut and the same alteration zoning as the Erdenet deposit was detected. Although the values of chemical analysis are low, relatively high geochemical anomalies were detected on the silicified zone. The low airborne magnetic anomalies and low rock magnetizations were also detected. As the results of IP electric surveys, the large anomaly overlapped by low resistivity, high chargeability and high metal factor was detected at the center of Mt Shar Chuluut. Therefore, it is high potential for the porphyry copper-molybdenum deposit in the area, and it is recommended to conduct drills in the silicified zone as shown in Fig.I-5-1.　If the results of the drilling survey will be good, it is also recommended to widen the IP electric survey area to the eastern side of the second phase survey area and continue to the exploration in order to understand IP structures related to the mineralization as high chargeability increases and continues to the eastern deeper zone and to construct the mineralization model in more detail.

It is recommended to conduct a soil geochemical prospecting for the third phase project area to clarify the geochemical features related to the mineralization of the porphyry copper-molybdenum deposit same as the Erdenet ore deposit. Soils are preferable to be taken by a grid sampling using the IP electric survey lines.

(2) Under/ Shand area

The ores composed of filmy malachite and azurite was observed in the K-metasomatized medium grained granodiorite outside the northwestern part of the Under/Shand_3 area (0.119%Cu, 0.036%Pb, 0.116%Zn and 24ppmAg). The pyrite dissemination zone in the white silicification zone was confirmed in the central western part of the area.

It will be necessary to confirm and understand mineralizations by a geophysical survey (IP electric method) and the semi-detailed geological mapping on the pyrite dissemination zone in the northwestern part of the Under/Shand_3 area and the central eastern part of the Under/ Shand area. If this program leads good results, drills should be followed. However, the exploration priority in the area for phase III is low compare with the other areas as the Zuukhiin gol area, etc..

(3) Zuukhiin gol area

The results of the first phase program indicate that the low airborne magnetic anomalies were detected in the Zuukhiin gol area. The Zuukhiin gol mineral showing is regionally located in the cross junction of the NW-SE and the NE-SW trending fault zones. The sericite-chlorite zone same as the Erdenet deposit is distributed in the central part of the showing. Analytical values of copper indicate 50 to 11,740 ppm in this showing. Several factors related to the element behavior for the porphyry copper-molybdenum deposit are detected, and factor scores are high values. Previous drills detected the mineralizations continuing to over 300m in depth. At the previous program, the exploration activities were abandoned because of its low grade. However, it is estimated to be possible to the mining development with the recent SX-EW technology if the oxidized resources grading 0.3%Cu were distributed. It is desired to reevaluate the deeper zone to understand the mineralization at the deeper zone with a geological mapping, a geochemical prospecting, an IP electric surveys and drills.

(4) Another area

As the results of the previous data analysis, a geological mapping, an airborne survey for the first phase and a geological mapping and a geophysical prospecting for the second phase, it is confirmed that porphyry copper-molybdenum deposits are related to the adakitic plutonic rocks of the Erdenet complex and are located on the low magnetic anomaly in high magnetic zone. Therefore, it is recommended for the phase three that the target generation by comparison airborne geophysics results with existing geologic maps would be necessary for selecting potential areas and Khujiriin gol area in which should be carried out a program including a geological mapping, a geophysical prospecting (IP electric method) and drills at the potential areas to host ore deposits.

REFERENCES

Reference

Dejidmaa G. and Naito K. (1998): Previous studies on the Erdenetiin-Ovoo porphyry copper-molybdenum deposit, Mongolia. Bull. Geol. Surv. Japan, Vol. 49(6), p.299-308.

Gavrilova, S. P., Maximyk, I. E., Orolmaa, D. (1989) : The molybdenum deposits Erdenetiin ovoo, Mongolian People's Republic, Publication of IMGRE, Moscow, 40 p. (in Russian).

Geological Survey of Japan and Geological Survey of Mongolia(1996) : Research and Developments of Mineral Resources in Mongolia, 139P., ITIT Rep. 91-1-3.

Gerel, O. (1998) Ohanerozoic felsic magmatism and related mineralization in Mongolia, Bull. Geol. Surv. Japan, Vol.49(6), p.239-348.

Jargalsaihan, D., Kazmer, M., Baras, Z. and Sanjaadori, D. (1996) Guide to the geology and mineral resources of Mongolia, Geological Exploration, Consulting and Services Co. Ltd., 329.

Jargalan Sereenen and Murao Satoshi (1998): Fluorite deposits in Mongolia: an outline, Bulletin of the Geological Survey of Japan, 49, 6,309-318,(Geological Survey of Japan)

Jargalan Sereenen and Murao Satoshi (1998): Preliminary study on the characteristics of Tsagaan tsakhir uul gold deposit, Bayankhongor, southern Mongolia, Bulletin of the Geological Survey of Japan,49,6,291-298,(Geological Survey of Japan)

JICA and MMAJ (2001): Report on geological survey in the central north area, Mongolia.

Kishimoto Fumio (1979a) : Development of porphyry copper deposit in Mongolia、Chishitsu News, no.299, 49-55.

Kishimoto Fumio (1979b) : Discovery of new ore deposits in Mongolia、Chishitsu News, no.299, 56-57.

Kishimoto Fumio (1984) : On the earth of Gobi, Mongolia、Chishitsu News, no.357, 47-51.

Kurimoto Shiro (1997) : Visiting Bayankhongor in Mongolian glasslands, Chishitsu News, no.509, 49-58.

Murao Satoshi, Dorjgotov, Danjindorjiin and Tseden Tsagaanbilegiin (1998): K-Ar dating of granitoids and hydrothermal micas from the northern part of Kherlen Depression, Mongolia, Bulletin of the Geological Survey of Japan, 49,6,249-255, (Geological Survey of Japan)

Naito Kazuki and Sudo Sadahisha (1999) : Visiting Erdenet Mine, Mongolia、Chishitsu News, no.534, 19-30.

Nukushima Renzo (1998) A manual of Romanization of Mongolian geographical terms, Bulletin of the Geological Survey of Japan, 49, 6, 319-340, (Geological Survey of Japan)

Pearce, J. A., Harris, B.B.W. and Tindle, A.G. (1984): Trace element discrimination diagrams for the tectonic interpretation of granitic rock, Journal of Petrology, Vol. 25, Part 4, 956-983.

Richard H. Sillitoe (1995) : Exploration of porphyry copper lithocaps, PACRIM, 527-532.

Sato Takeo (1991) : Travel to Mongolia、Chishitsu News, no.438, 39-51.Satoshi Kanisawa (1999) :

Igneous activity in Mongolia, Chishitsu News, no.534, 31-40.

Takahashi Y., Arakawa Y., Oyungerel S. and Naito K. (2000): Geochronological data of granitoid in the Bayankhongor area, central, Bulletin of the Geological Survey of Japan, 51, 5,157-174, (Geological Survey of Japan)

Takahashi Yuhei (1999): Geological research works in, Bulletin of the Geological Survey of Japan, 50, 4,279-289, (Geological Survey of Japan)

Takahashi Yuhei, Oyungerel Sambuu, Naito Kazuki, Delgersogt Baljinnyamiin (1998): The granitoid series in Bayankhongor area, central Mongolia, Bulletin of the Geological Survey of Japan,49,1,25-32, (Geological Survey of Japan)

Takahashi Yuhei, Oyungerel Sambuu, Naito Kazuki and Delgersogt Baljinnyamiin (1998): Mineralogical characteristics of feldsparts of the granitoids in Bayankhongor area, central Mongolia,Bulletin of the Geological Survey of Japan,49,8,439-446,(Geological Survey of Japan)

Teraoka Y., Suzuki M., Tungalag F., Ichinnorov N. and Sakamaki Y. (1996) Tectonic framework of the Bayankhongor area, Bulletin of the Geological Survey of Japan, 47, 9, 447-455, (Geological Survey of Japan)

Tsagaanbilegiin Tseden, Satoshi Murao and Dangindorijiin Dorjgotov (1992): Introduction to geology of Mongolia, Bulletin of the Geological Survey of Japan,43,12, 735-744,(Geological Survey of Japan)

Tseden Tsagaanbilegiin, Murao Satoshi, Dorjgotov Dangindorjiin (1992):Introduction to Geology of Mongolia, Bulletin of the Geological Survey of Japan, 43, 12, 735-744, (Geological Survey of Japan)

Tseden Tsagaanbilegiin, Murao Satoshi, Baatarhuyag Abirmediin, Altantsetseg Dambiin and Oyunchimeg Chagnaadorjiin (1998): A note on newly found ore fields in Govi-Altai area, southern Mongolia, Bulletin of the Geological Survey of Japan, 49, 12, 633-638, (Geological Survey of Japan)

LIST OF FIGURES AND TABLES

List of figures

List of tables

APPENDICES